TECHNISCHE UNIVERSITÄT MÜNCHEN

Fakultät für Chemie

Lehrstuhl für Biotechnologie

Regulation of the molecular chaperone BiP by its co-chaperones

Christina Utta Nickels

Vollständiger Abdruck der von der Fakultät für Chemie der Technischen Universität München zur Erlangung des akademischen Grades eines Doktors der Naturwissenschaften (Dr. rer. nat.) genehmigten Dissertation.

Vorsitzender: Prof. Dr. Bernd Reif

Prüfer der Dissertation:

1. Prof. Dr. Johannes Buchner
2. Prof. Dr. Matthias J. Feige

Die Dissertation wurde am 29.04.2019 bei der Technischen Universität München eingereicht und durch die Fakultät für Chemie am 05.06.2019 angenommen.

Für meine Eltern

Index

Abstract

BiP, the mammalian Hsp70 chaperone in the ER, has an important function in protein homeostasis and thus in the cellular stress response. The ATP-dependent chaperone cycle of BiP is regulated by co-chaperones. In this thesis, the co-chaperones ERdj3 as well as Bap and Grp170 were investigated in detail. The purified proteins were characterized with regard to their stability, structure and functionality. It was shown that ERdj3 is a homotetramer that can stimulate BiP's ATPase activity as well as decrease its ability for nucleotide exchange. The NEFs Grp170 and Bap usually promote this nucleotide exchange. The latter has been characterized in detail in this thesis. Bap has been shown to not only stimulate the nucleotide release but also stimulates BiP's ATPase activity. For this stimulation, the N-terminal domain of Bap is necessary which also acts as a pseudo substrate of BiP. This has also been confirmed by anisotropy chase experiments. Finally, mutations of Bap that lead to the rare autosomal recessive disease MSS have been investigated. Interestingly, the disease phenotype does not require a complete loss of Bap function but as for some mutants only a slight impairment was observed.

Kurzfassung

Das Hsp70 Chaperon BiP aus dem endoplasmatischen Retikulum spielt eine entscheidende Rolle in der Protein Homöostasis und der Stressantwort der Zelle. Der ATP abhängige Zyklus von BiP wird von verschiedenen Co-Chaperonen reguliert. In dieser Doktorarbeit wurden das Co-Chaperone ERdj3 und die zwei Nukleotidaustauschfaktoren Bap und Grp170 genauer untersucht. Die gereinigten Proteine wurden hinsichtlich ihrer Stabilität, Struktur und Funktionalität untersucht. Es konnte gezeigt werden, dass ERdj3 als Tetramer vorliegt und die ATPase Aktivität von BiP zwar stimuliert, gleichzeitig aber den Nukleotidaustausch hemmt. Beim Nukleotidaustauschfaktor Bap konnte gezeigt werden, dass er nicht nur den Nukleotidaustausch sondern auch die ATPase Aktivität von BiP stimulieren kann. Für diese Stimulation ist der ungefaltete N-terminus des Proteins wichtig, welcher als Pseudosubstrat an die Substratbindedomäne von BiP bindet. Letztlich wurde untersucht, wie sich Mutationen, die mit der Erbkrankheit MSS in Verbindung gebracht werden, auf die Funktion von Bap auswirken.

Abbreviations

Abbreviation	Description
aa	Amino acid
AUC	Analytical ultracentrifugation
Bap	Also Sil1; BiP-associated protein (human, UniProt ID: Q9H173)
BiP	Binding immunoglobulin protein (from mouse, UniProt ID: P20029)
CD	Circular dichroism
CH1	First constant domain of antibody heavy chain (here: CH1 1GAF)
CL	Constant domain of antibody light chain (here: CL 1GAF)
DOL	Degree of labeling
ER	Endoplasmic reticulum
ERAD	ER-associated degradation
FUV	Far UV (ultraviolet light ranging from ~180 nm – 260 nm)
GdmCl	Guanidinium chloride
Grp170	170 kDa glucose-regulated protein (UniProt ID: Q9Y4L1)
Grp94	94 kDa glucose-regulated protein (UniProt ID: P14625)
H/DX	Hydrogen–deuterium exchange
IB	Inclusion body
JDP	J-domain containing protein
kDa	Kilodalton
LDH	Lactate dehydrogenase
MALS	Multi angle light scattering
MS	Mass spectrometry
MSS	Marinesco-Sjögren syndrome (OMIM ID: 248800)
NADH	Reduced nicotinamide adenine dinucleotide (oxidized: NAD^+/H^+)
NBD	Nucleotide binding domain
NEF	Nucleotide exchange factor
PDI	Protein disulfide isomerase

Abbreviation	Description
PEP	Phosphoenolpyruvate
PK	Pyruvate kinase
RT	Room temperature
S200	Superdex 200 size exclusion column (16/60)
SBD	Substrate binding domain
SDS-PAGE	Sodiumdodecylsulfate polyacrylamide gelelectrophorese
SEC	Size exclusion chromatography
TT	Thermal transition
UPR	Unfolded protein response
wt	Wildtype
JDP	J domain containing protein

1. Introduction

1.1. Protein folding

Proteins are responsible for most biological functions in living organisms. They are synthesized on ribosomes (a process called translation) as an amino acid sequence (primary structure) before they start folding into mainly α-helical or β-sheet structures (secondary structure). To fulfil their function they must adopt a well-defined three-dimensional structure (tertiary structure) which occurs often spontaneously during or after translation. Studies by Anfinsen suggest that the three-dimensional structure of proteins is already encoded in their primary structure [1,2]. The spontaneous folding by randomly sampling all possible conformations would take too long [3]. Rather polypeptide chains explore a funnel-shaped potential energy surface while progressing towards their native structure [4]. Proteins need to find an optimum between their thermodynamic stability and the flexibility for fulfilling their biological function or only fold partially without a partner. The polypeptide chains move around the energy landscape towards the global minimum (See **Figure 1**).

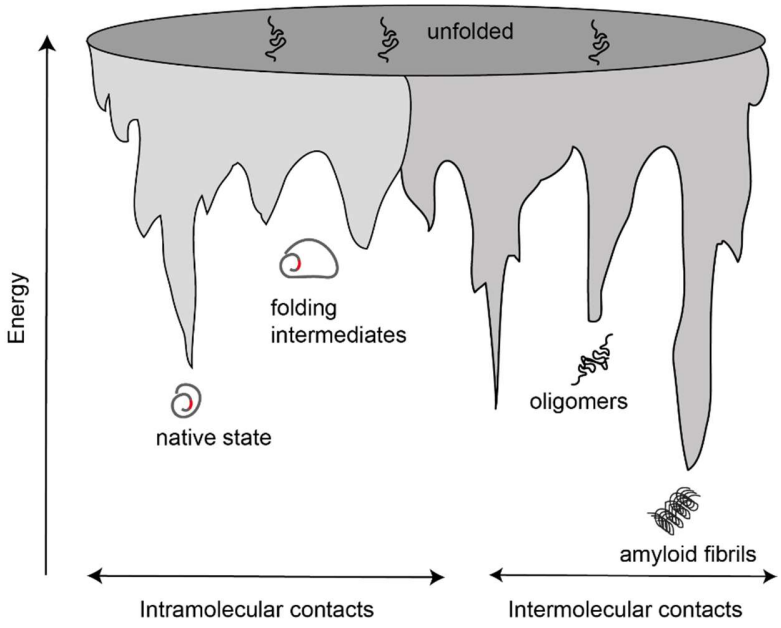

Figure 1: Energy landscape of protein folding (adapted from Hartl and Hayer-Hartl, 2009 [5]).

During this process stable intermediates can be formed, which represent local minima on the folding landscape. Sometimes kinetic barriers need to be crossed and proteins might be trapped in an intermediate state. This leads to misfolding of the proteins which is even amplified by the crowded cellular environment with macromolecule concentrations of around 0.3-0.4 g/ml in *E. coli* [6]. Usually hydrophobic amino acids are exposed to the solvent und can lead to aggregation of the proteins or even to the formation of amyloid-like fibrils. To prevent misfolding in the cell, molecular chaperones aid in folding and stabilizing proteins during and after translation.

1.2. Molecular chaperones

Molecular chaperones assist proteins in folding and prevent aggregation without being part of its final structure [7–9]. They are also involved in protein homeostasis and take part in the protein degradation machinery [10]. Molecular chaperones are conserved and many were first discovered in correlation to heat shock. Therefore many chaperones are also named heat shock proteins (Hsps) although many are constitutively expressed [11] and fulfill important functions in many other challenging situations for the cell, like redox changes or accumulation of unfolded proteins. Hsps are categorized by their molecular weight. Chaperones can act as holdases or foldases, but they can also have additional functions such as peptidyl-prolyl isomerization (PPIase) [12] or oxidoreductase function [13]. Many chaperones need nucleotide (ATP) to fulfill their cellular function (e.g. Hsp70, Hsp90), although ATP-independent chaperones exist and play an important role in protein homeostasis (e.g. small Hsps [14], trigger factor). Some classes of chaperones also provide a protected environment for the protein to fold like the GroEL/Hsp60 family [15]. Chaperones usually do not act alone, but other proteins affect their functionality. These proteins are referred to as co-chaperones. Molecular chaperones form networks in the cell which allow the transfer of the substrate to other members of the chaperone network [16].

1.3. Chaperones in the endoplasmatic reticulum

It is estimated that one third of all proteins synthesized in the cell are destined for integration in the membrane, secretion or transfer other organelles and therefore usually have to pass the endoplasmic reticulum (ER) [17]. These proteins carry an N-terminal signal sequence which interacts during synthesis with the signal recognition particle leading the ribosome to the ER membrane [18]. The protein is

synthesized directly into the ER lumen. Many folding steps and chaperones are necessary to secure the correct folding.

Proteins destined for the ER carry a retention motif, very often KDEL for luminal proteins or KKXX for transmembrane proteins [19]. Important chaperones in the ER are the calnexin/calreticulin system which detect N-linked glycans and unfolded regions [20] and prevents misfolded proteins from being exported to the Golgi apparatus. Heat shock proteins of the ER are the Hsp90 homolog Grp94 and the Hsp70 homolog BiP. Co-chaperones like J-domain proteins (JDP) and nucleotide exchange factors (NEFs), protein disulfide isomerase (PDI) and peptidylprolyl isomerases are also part of the chaperone systems in the ER [21,22]. These chaperones however, cannot exclude that the load of misfolded or unfolded proteins in the ER exceeds the chaperone capacity, which eventually lead to ER stress, activating the stress response in the cell.

1.4. Unfolded protein response (UPR)

When the capacity of chaperones in the ER and the load of unfolded or misfolded proteins is imbalanced, the unfolded protein response (UPR) is activated (**Figure 2**) [23]. It comprises three main steps, which are sensed by three different transmembrane proteins. The first step is reduction of the protein load by slowing down translation and translocation. This is mediated by the protein IRE1 (inositol-requiring protein 1) [24,25]. Upon ER stress it dimerizes and autophosphorylates its cytosolic domain [26,27] and promotes translation of the transcription factor XBP1. This transcription factor drives transcription of genes for the folding machinery like chaperones [28]. Monomeric IRE1 represses the UPR [29].

ATF6 (activating transcription factor 6) is the second sensor and responsible for upregulation of genes that code for the ER protein folding machinery and regulated proteolysis. PERK (protein kinase RNA like ER kinase) is an important factor to regulate translation by eventually inactivation a translation initiation factor (eIF2α) and therefore decreasing protein synthesis and reduce the ER protein load. If the unfolded protein load still exceeds the folding capacities of the ER, the last step is the cell death (**Figure 3**).

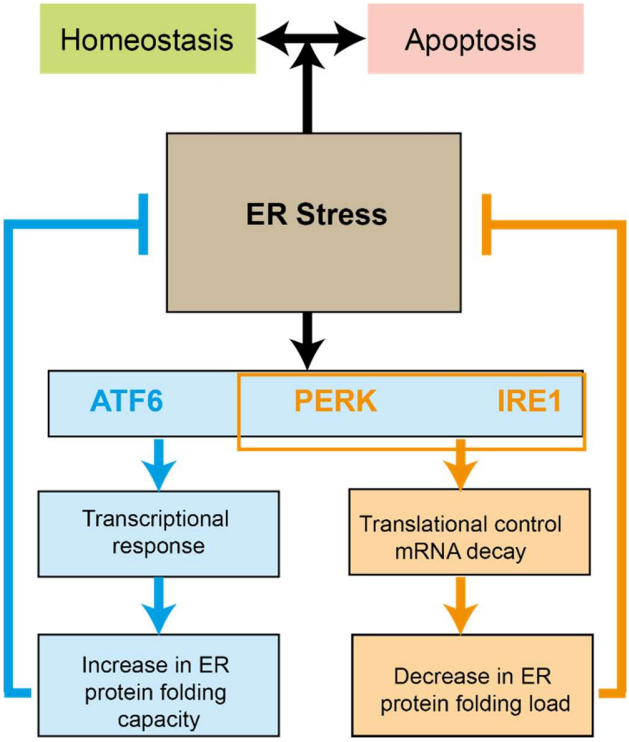

Figure 2: Diagram of the UPR signaling network adapted from Walter and Ron, 2011 [23]. ER stress leads to activation of ATF6, PERK and IRE1. Activation of all factors leads to a transcriptional control of factors that increase the ER folding capacity (blue). PERK and IRE1 also decrease the protein load in the ER via RIDD or eIF2α (orange). If the stress continues, cell death is activated.

How the load of unfolded proteins is sensed is still not entirely clear, but for IRE/PERK different models have been proposed [23,30]. Binding of unfolded proteins might lead to an oligomerization of the two protein domains [31]. It has also been suggested that BiP binds to the luminal domains and when it is recruited to unfolded proteins, the domains can interact [32]. Also direct binding to the unfolded protein like C_H1 has been suggested [33]. A combination of the two models is another option.

Targets of the UPR are also involved in autophagy and in the ER-associated protein degradation (ERAD), a process where ER proteins are degraded by the proteasome in the cytosol [34–36]. Therefore, ERAD and UPR-induced autophagy are also ways to lower the load of unfolded proteins in the ER.

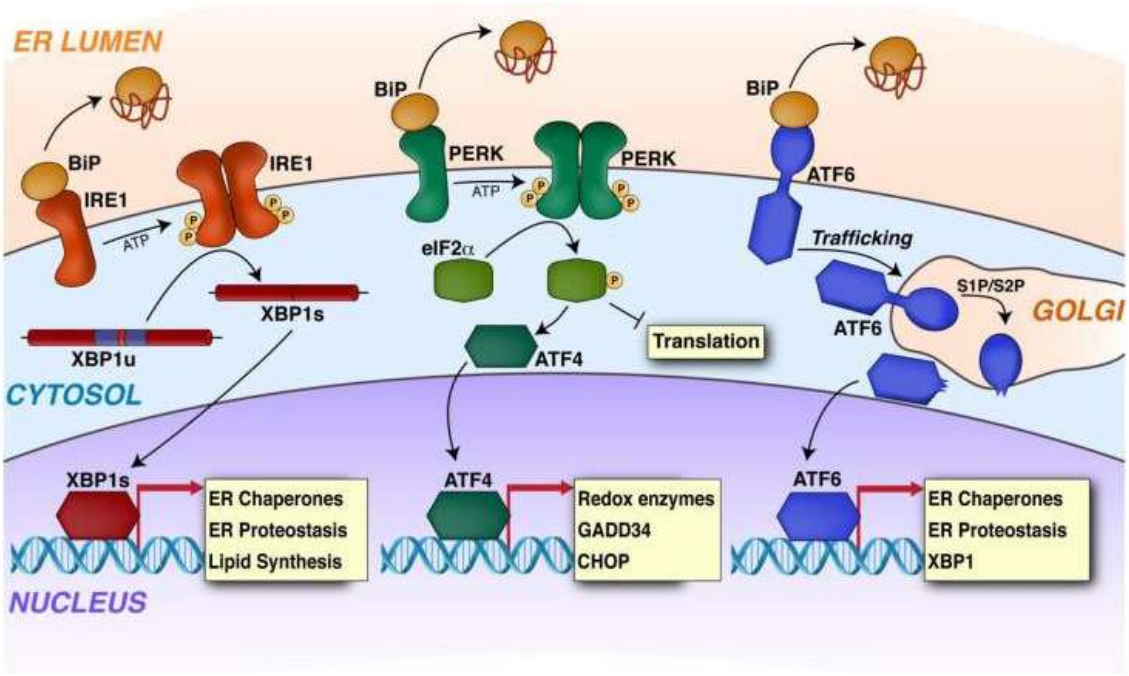

Figure 3: Downstream signaling of the three branches of unfolded protein response taken from Plate and Wiseman, 2017 [30]. ER stress activates IRE1 dimerization and eventually transcription of of genes involved in protein homeostasis. PERK activation leads to translational regulation via eIF2α and activation of transcription of important redox enzymes. Proteolytic cleavage of ATF6 activates it and leads to transcription of genes important for ER proteostasis.

1.5. Hsp70 and heavy chain-binding protein (BiP)

Hsp70 chaperones are involved in de novo folding as well as refolding, translocation and degradation. They can also bind to partially folded proteins [37]. Hsp70s comprises a nucleotide binding domain (NBD) connected via a flexible linker with a substrate binding domain (SBD) with a α-helical lid part at its C-terminal end. The Hsp70 chaperone cycle is ATP-dependent and regulated by co-chaperones (see **Table 1**).

This cycle is regulated by nucleotide exchange factors (NEFs), like Hsp110 proteins or BAG proteins and Hsp40 co-chaperones called J-domain proteins (JDPs). In bacteria, the Hsp70 system consists of DnaK with the NEF GrpE and the Hsp40 DnaJ.

Table 1: BiP and its interaction partners in the mammalian ER as summarized in Melnyk et al., 2015 [22].

Interaction partner	Protein examples
Hsp40-type chaperone	ERdj1-7
Nucleotide exchange factors	Grp170, Bap
UPR signal transducers	IRE1, IRE2, ATF6, PERK
Sec proteins	Sec61α1, Sec61β, Sec61γ, Sec62
Chaperones	BiP, Grp94, Calnexin, Calreticulin
Co-chaperones	Sig-1R, HspA5BP1

In the ER only one Hsp70 chaperone is present which is called BiP (binding immunoglobulin protein) [38] or Grp78 (glucose regulated protein)[39]. It can bind to the SEC61 translocon [40,41] and is an important UPR transducer [42,43]. BiP comprises the N-terminal NBD which contains the ATPase site and the C-terminal SBD containing the β-sandwich domain where the substrate binds and the flexible α-helical lid (see **Figure 4**A [44]).

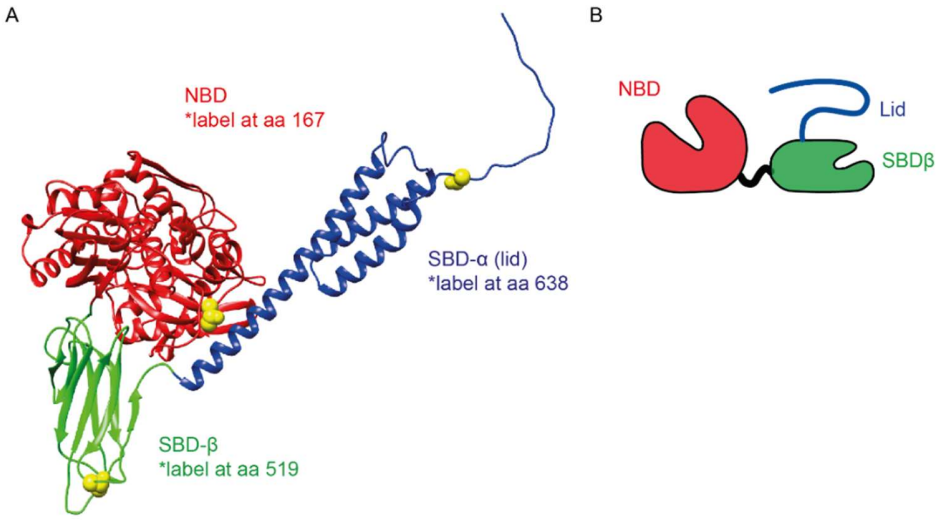

Figure 4: Structure of BiP. A) Murine BiP modelled on the crystal structure of human BiP (PDB: 5E84) using Chimera [45,46]. The NBD (red) with the labeling position 167 (yellow). The SBDβ subunit (green) with the labeling position 519 (yellow). The SBD-lid subunit (blue) and the labeling position 638 (yellow). B) Schematic structure of BiP with the same colors as in A).

BiP activity and availability in the ER is strongly regulated. In the absence of stress, BiP is ADP-ribosylated at two Arg residues in the SBD [47,48] and it might also be phosphorylated [49]. Recently it has been shown, that BiP also has AMPylation sites and forms pools of oligomeric BiP [50–52]. Depending on the nucleotide status and substrate availability, BiP forms dimers and higher oligomers but only monomeric BiP binds to substrate [49,53]. Therefore oligomeric BiP might be a storage pool and in case of need BiP gets recruited back to its active form [54]. In the ATP state, BiP has a low protein affinity with high on and off rates for the substrate [55,56]. In this state, the NBD is closed and the SBD is open. In the ADP state, BiP exhibits a high affinity for protein and a slow exchange. Single molecule experiments revealed that the NBD and SBD are in a dynamic distance distribution, where the NBD and SBD are more separated than in the ATP state, where the domains are close together [57]. The ATP status is communicated to the SBD via the NBD and might be similar to the communication in DnaK since important residues for this communication are conserved in the two Hsp70 chaperones [58,59]. The flexible linker between the two domains plays a role in the domain communication [60–62]. A simple chaperone cycle of BiP can be seen in **Figure 5**.

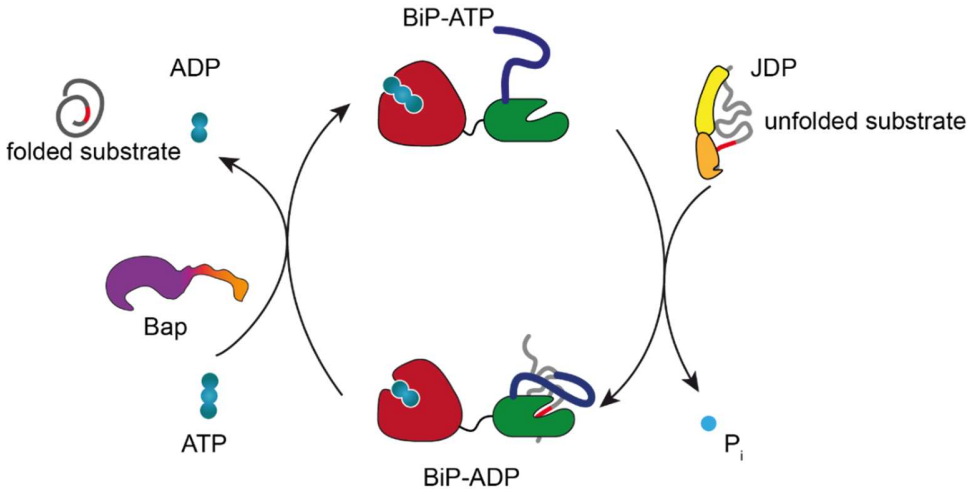

Figure 5: Nucleotide-dependent chaperone cycle of BiP. The NBD and SBD are in close proximity in the ATP state with the lid open. Substrate affinity is low. JDPs can transport unfolded protein substrate to BiP and hydrolyzation of ATP to ADP is increased by the co-chaperone, which then increases the substrate affinity. NBD and SBD are more distant and the linker is more exposed. Upon nucleotide exchange with the help of Bap, the substrate is released and a new cycle can start.

In the ATP state, the Lid domain is open and the NBD and SBD are separated through the flexible linker region. Substrates are transported to BiP by JDPs and upon ATP hydrolysis, the substrate is bound

by BiP leading to a closing of the lid and a more docked domain architecture. Nucleotide exchange leads to substrate release and a more open conformation of BiP. The cycle can start again [63].

BiP itself has a low intrinsic ATPase rate [64,65]. It has been shown that peptides stimulate the ATPase activity [66,67] and alter its oligomeric state but it is very unlikely that BiP indeed interacts with peptide substrates in the ER. Protein substrate can decelerate the ATPase rate [64]. Although tools exist to predict BiP substrates [68–71], BiP is able to recognize many different polypeptides with no obvious sequence similarity which is important for its role as a general chaperone in the ER. BiP can bind to patches of 5-7 preferably hydrophobic residues [66,72] and on average, every 40 amino acids a potential BiP binding site is predicted [66,69], although the hydrophobic cores are usually buried in the folded protein. Additionally, binding sites of different Hsp70 chaperones show variations in their specificity. While both, DnaK and BiP prefer leucine-rich peptides, only BiP accepts tryptophanes in its binding site [57,71,73,74]. Known or predicted binding sites seem to be located in hydrophobic regions that are usually buried in the protein but also parts of the peptide chain take up their final conformation late in the folding pathway [75], like interfaces between heavy and light chain in antibodies [76].

1.6. J-domain proteins (JDP)

J-domain proteins (JDP) are important co-chaperones for Hsp70 and describe a large and diverse class of proteins with 41 JDPs in the human system [77]. All JDPs harbor the J domain, which comprises four α-helices containing a highly conserved His-Pro-Asp motif (HPD) between helix II and III. This HPD motif is essential to stimulate BiP's ATPase activity and mutation of His to Glu (HPD→QPD) leads to the abolishment of ATPase stimulation [77].

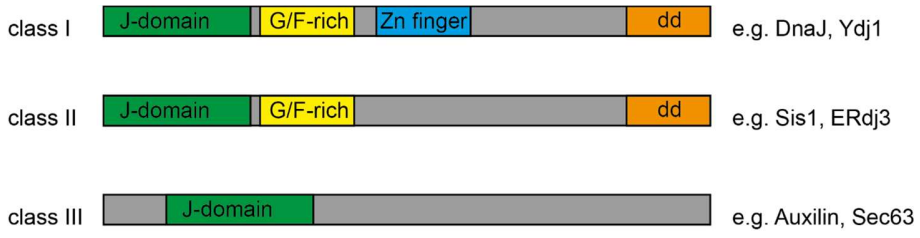

Figure 6: Domain organization of JDPs adapted from Tamadaddi and Sahi, 2016 [78]. Class I proteins are DnaJ-like and comprise the J-domain with the HPD motif as well as a Gly and Phe rich domain followed by a CXXCXGXG type cysteine-rich zinc-finger domain and a C terminal dimerization domain (dd). Class II proteins lack the zinc-finger domain and class II JDPs are the most diverse class and only share the J-domain with the other JDPs.

JDPs are structurally classified into class I, II and III. Class I proteins share similarity to DnaJ, the JDP of *E.coli*. The proteins comprise an N-terminal J domain, a Gly/Phe-rich region, a zinc finger motif and a C-terminal region, which is important for client binding. Class II proteins lack the zinc finger domain and class III proteins do not fit in either of the other two classes. In the ER, seven JDPs (ERdj1-7) are present distributed in the lumen and membrane of the ER.

Table 2: Concentration of BiP and its co-factors in the ER measured in rough microsomes [22].

Protein	**concentration in ER**
BiP	5 μM
ERdj3	0.29 μM
Bap	0.005 μM
Grp170	0.6 μM

ERdj3 is a highly abundant ER luminal class I protein and binds to numerous proteins in the ER [79]. It has an approximate concentration (measured in rough microsomes, see **Table 2**) of 0.29 μM [22,80,81]. ERdj3 is upregulated upon stress and is able to stimulate BiP's ATPase activity and stabilize substrate interaction [76,82,83]. This interaction takes place in the ATP state, where NBD and SBD are docked [84]. In the ATP state ERdj3 only transiently interacts with BiP [76], induces ATP hydrolysis and binds stably to the ADP conformation of BiP as it has been shown for other JDPs [85]. Besides regulating folding and degradation of secretory proteins like immunoglobulin heavy and light chains, it is also involved in regulating ER permeability and protein translocation by interacting with Sec61 translocon [86,87]. Interestingly ERdj3 lacks the ER retention signal (KDEL) and can be detected outside the cell after ER stress independent from BiP [88,89]. It is known that JDPs have dimerization sites and that dimerization is important for their function in vivo [90]. ERdj3 can also assemble in higher oligomers in the presence of aggregates [91]. A representation of the domain architecture and the modeled structure [92] can be seen in **Figure 7**.

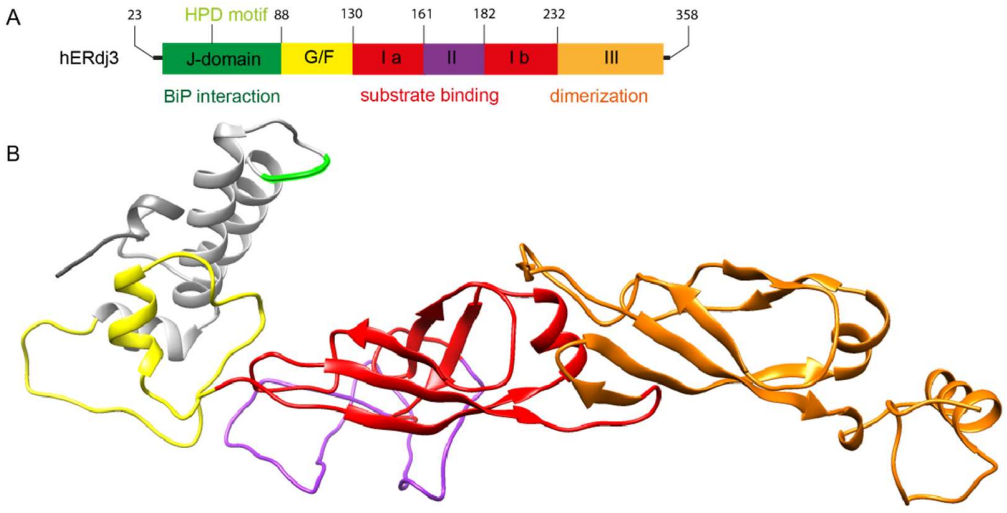

Figure 7: Secondary and tertiary structure prediction by the online tool Phyre2. A) Schematic representation of the ERdj3 protein used in this thesis. J-domain containing the HPD motif is depicted in green, a G/F rich flexible domain in yellow, substrate binding domains (I) in red are separated by a cysteine rich domain (II) (purple) and the potential dimerization domain (III) in orange (adapted from Chen et al., 2017). B) Modeled structure of ERdj3 by Phyre2. The colors are similar to A).

For ERdj3 it was assumed for a long time that it dimerizes [90,94], but it has been recently shown, that ERdj3 functions as a tetramer [93].

1.7. Nucleotide exchange factors of BiP

The Hsp70 chaperone cycle is strongly regulated by ATP binding and release. Besides different co-chaperones that can modulate the substrate binding and ATPase activity, nucleotide exchange factors play a crucial role for resetting the ATPase cycle. In the bacterial Hsp70 system (DnaK), the nucleotide exchange factor GrpE is essential to re-enter the folding cycle [95,96]. In the eukaryotic Hsp70 system, several groups of NEFs exist that exhibit different modes of nucleotide exchange.

The most prominent example are the BAG (Bcl-2 associated athanogene) family proteins where six different family members exist in humans [97–99]. Two other NEFs are the Grp170/Hsp110 family and the Sil1/HspBP1 family which are also present in the ER. In the ER nucleotide exchange seems to play a special role as a rate limiting step, because of the high Ca2+ concentrations which lead to an increased affinity of BiP to ADP [100].

In yeast it was shown that double knockout of the two proteins Lhs1 (yeast orthologue of Grp170) and Sil1 (yeast orthologue of Bap) are lethal and this lethality was connected to the yeast BiP named Kar2 [101]. They both bind preferably to BiP in the ADP state. BiP concentrations in the ER are determined from rough microsomes to be around 5 µM [22,80,81], whereas Grp170 is 10-fold less abundant with a concentration of about 0.6 µM and Bap being 1000-fold less abundant with 0.005 µM. The ratios stay similar if the intact ER is taken into consideration [80]. These strong differences in protein abundance in the ER suggests specialized roles of the NEFs in the ER.

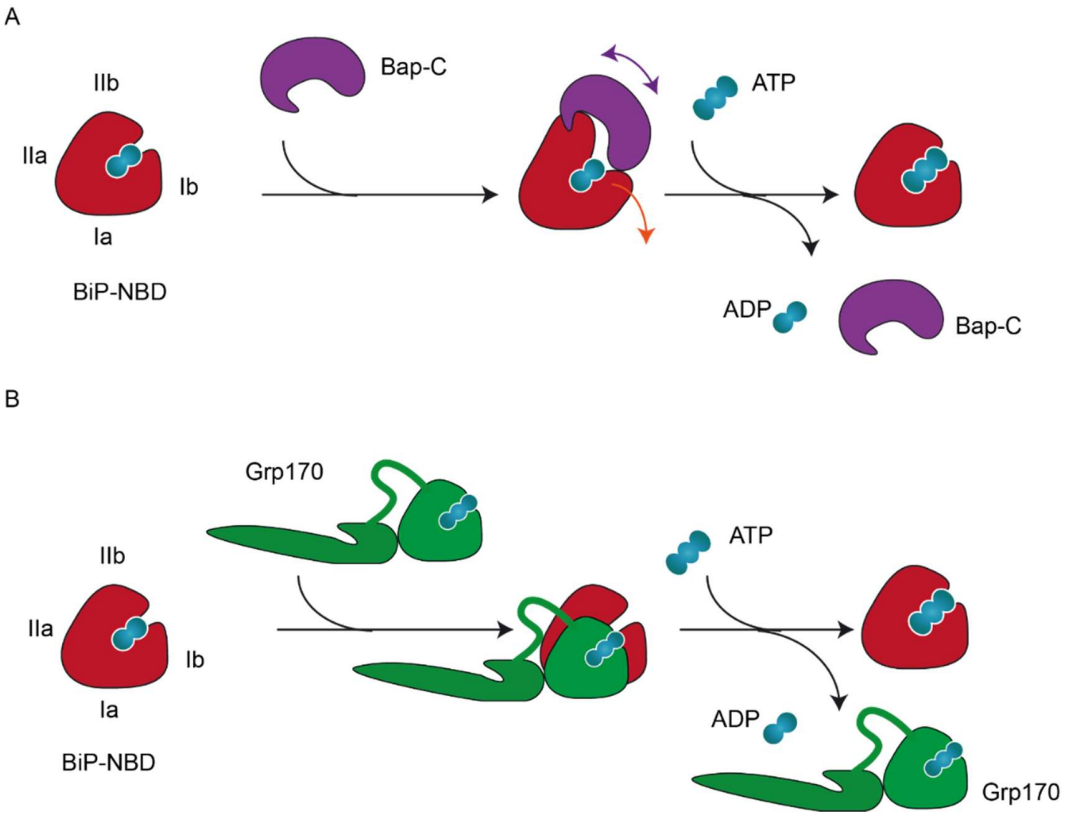

Figure 8: Nucleotide exchange by Bap and Grp170 (adapted from Behnke et al., 2015 [100]). A) Bap binds to the ADP-bound NBD of BiP and tilts lobe Ib and IIb outwards. This destabilizes the NBD and leads to ADP release. B) The mechanism of ADP exchange by Grp170 is still under investigation. Grp170 binds to the ADP-bound NBD of BiP. This destabilizes the BiP-NBD and leads to ADP release.

Nucleotide exchange mechanism differ between Bap and Grp170 and can be seen in **Figure 8**. Bap is binding to BiP's NBD mainly with its armadillo repeats. Thereby lobe IIb and Ib rotate away from the bound nucleotide, which eventually leads to the nucleotide release. Nucleotide exchange for Grp170 is not completely dissolved but it is supposed to be similar to cytosolic Hsp110 by binding to BiP's NBD

and opening it at lobe II [102]. It is assumed that Grp170 needs to bind ATP [103–105] to fulfil its function as a NEF. Also, Bap and Grp170 do not interact with each other and bind to BiP by exclusive interaction suggesting a competition for BiP binding [100,106].

Glucose-regulated protein 170 kDa (Grp170) is assigned to the family of large Hsp70s [107,108] and has a NBD that is similar to the Hsp70 family but shows great divergence in its C-terminal domain with a C-terminal extension and insertions in the SBD [109]. It exhibits a higher affinity for ATP than BiP [110]. Grp170 can bind directly to client proteins, but it is supposed that they are kept in a refolding competent state [111,112]. The substrate interaction is yet to be understand, but different from BiP it seems to bind substrate with domains that are unique to large Hsp70s [100,111]. It is highly glycosylated and also exhibits chaperone activity [112,113]. The role of the glycosylation is not completely resolved since overexpressed proteins in *E. coli* also seem to fulfil important functions of Grp170 [52].

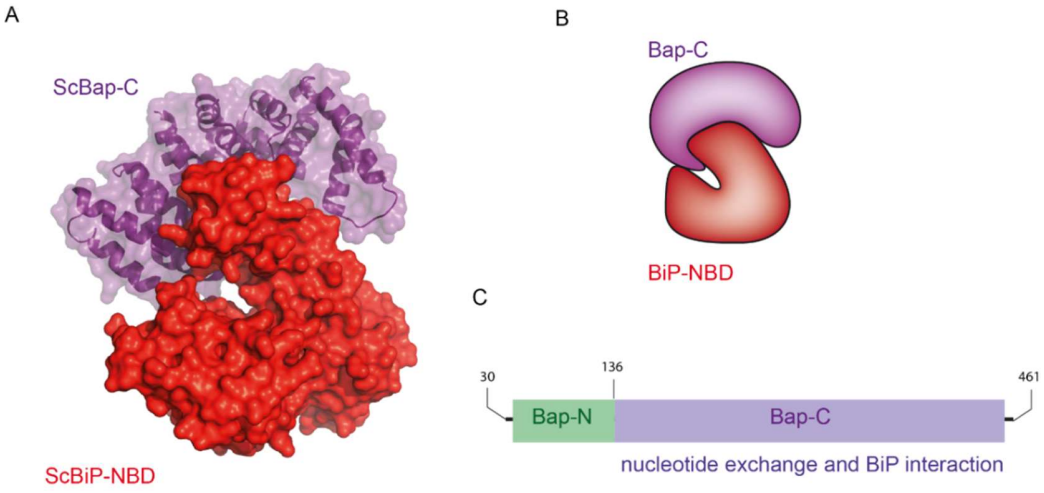

Figure 9: Structure of Bap. A) Crystal structure of the C-terminal domain of yeast Bap/Sil1 (purple) in complex with the yeast BiP (Kar2) nucleotide binding domain (red) adapted from Yan et al., 2011 [114]; PDB-ID: 3QML. B) Schematic representation of Bap binding to BiP-NBD. C) Human Bap construct used in this thesis (sequence from UniProt ID: Q9H173).

Bap (BiP-associated Protein, Sil1) was the first NEF discovered for BiP [115]. It was shown to accelerate the ATPase activity of BiP and nucleotide exchange [115]. A crystal structure of the yeast protein (ScSil1) shows a structural similarity to the cytosolic HspBP1 with a potentially unstructured N-terminal domain and an 16 α-helix containing C-terminal domain forming four armadillo-like repeats (**Figure 9** A and B) [114,116]. These armadillo repeats are important for the NEF activity since they cause lobe IIb and lobe Ib of BiP-NBD to rotate and therefore promote ADP release from BiP-NBD.

Although the domain architecture is similar to HspBP1, interaction sites with Hsp70 differ strongly between the two homologs suggesting a different mode of nucleotide exchange [114]. In addition, scSil1 and human Bap differ strongly in their sequence with just ~15% sequence homology. Retention of proteins in the ER is usually secured by a KDEL sequence at the C terminus of the proteins. Bap has a different sequence namely KELR which is not as strong as a retrieval signal but is mainly important for the protein stability [117]. Retention of Bap in the ER seems to be prevalent due to its BiP interaction [100].

Mutations in Bap are associated with an autosomal-recessive disorder called Marinesco-Sjögren syndrome (MSS OMIM-ID 248800)[118]. The disease was first described in a Rumanian family [119]. Later an autosomal recessive inheritance pattern for this disease was described [120] before it was mapped to the chromosome 5q31. The mutations found in patients are frame shifts, in-frame deletions, change of splice sites to premature stop codons in the Sil1 gene. As diverse as the found mutations is the patient phenotype. Although the symptoms start early in childhood they differ from patient to patient and the disease is usually characterized by cataracts, myopathy and delayed motor milestones as well as hypotonia and cerebellar atrophy [117,121,122].

2. Material and Methods

Methods are derived from standard protocols developed at the chair of biotechnology, Technische Universität München.

2.1. Material

2.1.1. Chemicals

Preparation of buffers and solutions were made in double-distilled water (ddH_2O). Chemicals were purchased in *pro analysi* (p.a.) grade. Buffers were sterile filtered and degassed.

Chemical	Supplier
^{13}C-Glucose	Cambridge Isotope Laboratories
$^{15}NH_4Cl$ (ammonium chloride, nitrogen 15 isotope)	Cambridge Isotope Laboratories
2-Mercaptoethanol	Merck
5,5'-Dithiobis(2-nitrobenzoic acid) (DTNB)	Merck
Acetic acid	Roth
Acetonitrile	Merck
Acrylamide/Bisacrylamide solution 38:2 (40% w:v)	Serva
Agar Agar	Serva
Agarose	Serva
Ammonium chloride (NH_4Cl)	Merck
Ammonium persulfate (APS)	Roth
Ampicillin sodium salt	Roth
Bromophenol blue	Serva
Calcium chloride ($CaCl_2$)	Merck
Coomassie Blue R	Serva
Coomassie Brilliant Blue R-250	Serva
Copper (II) chloride ($CuCl_2$)	Merck

Chemical	Supplier
Deoxynucleoside triphosphates (dNTPs)	NEB
Deuterium oxide (D_2O)	Merck
Dimethyl sulfoxide (DMSO)	NEB
Dithiothreitol (DTT)	Roth
EDTA	Merck
Ethanol	Merck
Formic acid	Merck
Glucose	Merck
Glutathione, oxidized (GSSG)	Merck
Glutathione, reduced (GSH)	Merck
Glycerol	Roth
Glycine	Roth
Guanidinium chloride (GdmCl)	Merck
HEPES	Merck
Hydrochloric acid (HCl) 32%	Merck
Iron (III) chloride ($FeCl_3$)	Merck
Isopropanol	Merck
Isopropyl β-d-1-thiogalaktopyranoside (IPTG)	Serva
Kanamycin sulfate	Roth
L-Arginine	Merck
LB medium	Serva
Magnesium sulfate ($MgSO_4$)	Merck
Manganese (II) chloride	Merck
Potassium chloride (KCl)	Roth
Potassium phosphate, monobasic (KH_2PO_4)	Merck
Protease inhibitor Mix G, HP	Serva
Sodium azide (NaN_3)	Merck

Chemical	Supplier
Sodium chloride (NaCl)	Merck
Sodium dodecylsulfate (SDS)	Serva
Sodium hydroxide (NaOH)	Merck
Sodium phosphate, dibasic (Na_2HPO_4 * 2 H_2O)	Merck
Sodium phosphate, monobasic (NaH_2PO_4 * 2 H_2O)	Merck
Stain G	Merck
Tetraethylethylendiamin (TEMED)	Roth
Thiamin-HCl	Merck
Tris	Roth
Tris(2-carboxyethyl)phosphine hydrochloride (TCEP)	Merck
Triton X-100	Merck
Urea	Merck
Zinc chloride ($ZnCl_2$)	Merck

2.1.2. Buffers

Molecular Biology and protein biochemistry

Buffer name	Substance	concentration
TAE	Tris/acetate, pH 8.0 EDTA	2 M 50 mM
DNA loading dye	Glycerol Tris/HCl , pH 8.0 Orange G Xylencyanol	50 % (v/v) 10 mM 0.2 % (w/v) 0.2 % (w/v)
SDS separating gel buffer (4x)	Tris/HCl, pH 8.8 SDS	1.5 M 0.8 % (w/v)

Buffer name	Substance	concentration
SDS stacking gel buffer (2x)	Tris/HCl, pH 6.8	0.25 M
	SDS	0.4 % (w/v)
SDS-PAGE running buffer (10x)	Tris/HCl, pH 8.0	0.25 M
	Glycine	2 M
	SDS	1 % (w/v)
Laemmli sample loading buffer (5x)	Tris/HCl, pH 6.8	0.3 M
	SDS	10 % (w/v)
	Glycerol	50 % (v/v)
	2-Mercaptoethanol	5 % (v/v)
	Bromophenol blue	0.05 % (w/v)
Fairbanks A	2-Propanol	25 % (v/v)
	Acetic acid	10 % (v/v)
	Coomassie Blue R	0.05 % (w/v)
Fairbanks D	Acetic acid	10 % (v/v)

Protein purification and assay buffers

Buffer name	Substance	concentration	
PBS	NaCl	137	mM
	KCl	2,7	mM
	Na_2HPO_4	10	mM
	KH_2PO_4	2	mM
	pH 7.4		
HKM	HEPES (pH 7.5)	50	mM
	KCl	150	mM
	$MgCl_2$	10	mM

Buffer name	**Substance**	**concentration**	
HAKM	HEPES (pH 7.5)	20	mM
	NH_4Cl	1	M
	KCl	30	mM
	$MgCl_2$	10	mM
BiP-Buffer A	HEPES (pH 7.5)	50	mM
	NaCl	400	mM
	Imidazole	20	mM
BiP-Buffer B	HEPES (pH 7.5)	50	mM
	Imidazole	1	M
TEV protease digest buffer	HEPES (pH 7.5)	50	mM
	KCl	100	mM
	Imidazole	20	mM
Bap-Buffer A	HEPES (pH 7.5)	50	mM
	NaCl	400	mM
	Imidazole	20	mM
	Glycerol	10%	
Bap-Buffer B	HEPES (pH 7.5)	50	mM
	Imidazole	1	M
	Glycerol	10 %	
Bap-Low Salt	HEPES (pH 7.5)	50	mM
	$MgCl_2$	10	mM
	Glycerol	10%	
Bap-High Salt	HEPES (pH 7.5)	50	mM
	KCl	1	M
	$MgCl_2$	10	mM
	Glycerol	10 %	

Buffer name	Substance	concentration	
J3-Buffer A	HEPES (pH 7.5)	50	mM
	NaCl	400	mM
	Imidazole	20	mM
J3-Buffer B	HEPES (pH 7.5)	50	mM
	NaCl	400	mM
	Imidazole	1	M
Grp170-Buffer1	Tris –HCl (pH 7.5)	50	mM
	NaCl	500	mM
	MgCl2	1	mM
	Glycerol	10 %	
Grp170-Buffer2	HEPES (pH 7.5)	50	mM
	NaCl	300	mM
	Imidazole	30	mM
	Glycerol	10 %	
Grp170-Buffer3	HEPES (pH 7.5)	50	mM
	NaCl	300	mM
	Imidazole	250	mM
	Glycerol	10 %	
Ulp1 buffer	Tris-HCl (pH 8)	25	mM
	Igepal (NP-40)	1 %	
	NaCl	250	mM
	DTT	500	µM
	Glycerol	50 %	

2.1.3. Plasmids

Below the plasmids used in this thesis and the mutations they contain are outlined. Amino acid numbers are according to UniProt.

Construct	Plasmid	Description	Origin
mBiP wt	pProEx	E20-L655	Moritz Marcinowski
BiP-NBD-167C	pProEx	E20-V420 C42S T167C	Mathias Rosam
BiP-Δlid	pProEx	E20-R533	Mathias Rosam
BiP 167C-519C	pProEx	E20-L655 C42S T167C C421S T519C	Moritz Marcinowski
BiP-Δlid 167C-519C	pProEx	E20-R533 C42S T167C C421S T519C	Mathias Rosam
BiP 167C-638C	pProEx	E20-L655 C42S T167C C421S S638C	Moritz Marcinowski

Construct	Plasmid	Description	Origin
BiP 519C-638C	pProEx	E20-L655 C42S C421S T519C S638C	Moritz Marcinowski
BiP-SBD	pProEx	D419-G640	Moritz Marcinowski
Bap wt	pSUMO	L30-R461	Christina Nickels
Bap-C	pSUMO	136-R461	Christina Nickels
Bap-N	pSUMO	L30-L135	Christina Nickels
Bap-N S31C	pSUMO	L30-L135 S31C	Christina Nickels
Bap-FRET	pSUMO	L30-R461 C42S C408S	Janine Hochmair, Christina Nickels
Bap-MSS1	pSUMO	L30-R461 V231del I232del	Christina Nickels
Bap-MSS2	pSUMO	L30-R461 G312R	Christina Nickels
Bap-MSS3	pSUMO	L30-437 Q438X	Christina Nickels
Bap-S31C	pSUMO	L30-R461 S31C	Christina Nickels
hERdj3	pSUMO	G23-Y358	Christina Nickels
hGrp170	pSUMO	L33-L999	Claes Andreasson, David Ron
Ulp1	pET28	403-621	Alexander Bepperling

2.1.4. Primers

Primer	Direction	T_a (°C)	sequence
Sumo_BAP	fwd	60	CAGAGAACAGATTGGTGGATCCCTCAGTCATCAGAACCTG
Sumo_BAP	rev	60	CAGTGGTGGTGGTGGTGGTGCTCATCTCAGCTCCTTCAG
Sumo_BAPNdom	rev	60	CAGTGGTGGTGGTGGTGGTGCCTATCACAGTGCACTCTTG
Sumo_BAP_DN	fwd	60	CAGAGAACAGATTGGTGGATCCGCAAAATTCAAGGAGGGG
BAP_C294S	fwd	61	CTGTTTGCACTGTCCTCCCTGCTG
BAP_C294S	rev	61	CAGCAGGGAGGACAGTGCAAACAG
BAP_C408S	fwd	64	CTGACCACCTCCCGGGACCGC
BAP_C408S	rev	64	GCGGTCCCGGGAGGTGGTCAG
hERdj3_SUMO	fwd	59	CAGAGAACAGATTGGTGGATCCGGACGAGATTTCTATAAGATCTTG
hERdj3_SUMO	rev	59	CAGTGGTGGTGGTGGTGGTGCTCGAGTCAATATCCTTGCAGTCC
Bap S31C	fwd	56	GATCCGTCGACTCTCTGCCATCAGAACCTGAAG
Bap S31C	rev	56	CTTCAGGTTCTGATGGCAGAGAGTCGACGGATC

2.1.5. Peptides

Peptides used in this Dissertation are marked with an *. The other peptides were used in experiments that are not described in this dissertation or performed by Mathias Rosam [123].

Peptide Name	Sequence (N to C)
*1	Ac-MASTKGPSVFPLAPS-NH2
*4	Ac-TKGPSVFPLAPSSKS-NH2
*8	Ac-SVFPLAPSSKSTSGG-NH2
*44	Ac-SGALTSGVHTFPAVL-NH2
*48	Ac-TSGVHTFPAVLQSSG-NH2
*52	Ac-HTFPAVLQSSGLYSL-NH2
333	Ac-PPRFSGSKDVARNRG-NH2

Peptide Name	Sequence (N to C)
8>S2	Ac-EFALTNP-NH2
*9>S3	Ac-KEFALTN-NH2
*10>S5	Ac-FALTNPE-NH2
*11>S9	Ac-LTNPEKS-NH2
IA1	Ac-PGHPPRF-NH2
IA2	Ac-GPCSERR-NH2
IA3	Ac-PQVPPRF-NH2
IA4	Ac-KDVARNR-NH2
IA5	Ac-QPEDEAM-NH2
IA6	Ac-MGARSSE-NH2
IA7	Ac-HPIETLV-NH2
IA8	Ac-PMAEGGG-NH2
IA9	Ac-FMDVYQR-NH2
IA10	Ac-PPRFLLR-NH2
*Pep5	Ac-HVRLNLQ-NH2
*Pep8new	Ac-GQAVPAG-NH2
*NB1	Ac-SSTKETE-NH2
NB2	Ac-TKAEEEL-NH2
J-chain1	Ac-RIIVPLN-NH2
J-chain4	Ac-TTMVPLR-NH2
J-chain2	Ac-TAVVPLVY-NH2
J-chain3	Ac-RNFVYH-NH2
Tp-BiP	Ac-PTLYNVSLT-NH2

2.1.6. Bacterial strains

All media were sterilized by using a laboratory autoclave at 121°C for 20 minutes. Kanamycin (35 mg/ml) and IPTG stock solutions (1M) were sterile filtered (0.22 µM) and stored at -20°C.

Strain	**Genotype**	**Origin**
E. coli XL1blue	*recA1 endA1 gyrA96 thi-1 hsdR17 supE44 relA1 lac*	Stratagene (LaJolla, USA)
E. coli BL21-Codon+ (DE3)-RIL	F– *ompT hsdS*(rB– mB–) *dcm*+ Tetr *gal endA* Hte (*argU proL* Cam^R)	Stratagene (LaJolla, USA)
E. coli SHuffle	F´ *lac*, *pro*, *lacI*^{q} / *Δ(ara-leu)7697 araD139 fhuA2 lacZ::T7 gene1 Δ(phoA)PvuII phoR ahpC* galE (or U) galK λatt*::pNEB3-r1-*cDsbC* (Spec^R, *lacI*^{q}) *ΔtrxB rpsL150*(Str^R) *Δgor Δ(malF)3*	New England Bioloabs (Ipswich, USA)
E. coli HB101	F$^-$ *thi-1 hsdS20*(rB$^-$ mB$^-$) *supE44 recA13 ara-14 leuB6 proA2 lacY1 galK2 rpsL20*(*StrR*) *xyl-5 mtl-1*	Promega (Madison, USA)

2.1.7. Reagents and Kits

Reagent/Kit	**Manufacturer**
PeqGold 1kb ladder	PeqLab (Erlangen, Germany)
Low Range molecular weight marker	Serva (Heidelberg, Germany)
Gel filtrations standard	BioRad (Hercules, USA)
Wizard Plus SV Mini-Prep DNA purification	Promega (Madison, USA)
Wizard SV Gel and PCR Clean-up System	Promega (Madison, USA)

2.1.8. Enzymes

Enzyme	Manufacturer
DpnI	New England Biolabs (Ipswich, USA)
α-Chymotrypsin	Sigma-Aldrich (St. Louis, USA)
Other restriction enzymes	New England Biolabs (Ipswich, USA)
Phusion Polymerase	New England Biolabs (Ipswich, USA)
T4 DNA Polymerase	New England Biolabs (Ipswich, USA)
T4 DNA Ligase	New England Biolabs (Ipswich, USA)
DNaseI	Roche (Mannheim, Germany)
Pyruvate Kinase (PK)	Roche (Mannheim, Germany)
L-Lacate dehydrogenase (LDH)	Roche (Mannheim, Germany)
Ulp1 (SUMO Protease)	Christina Nickels

2.1.9. Labels

Label and crosslinkers	Manufacturer
Atto 488 maleimide	AttoTec (Siegen, Germany)
Atto 532 maleimide	AttoTec (Siegen, Germany)
Atto 647 maleimide	AttoTec (Siegen, Germany)
Lucifer yellow iodoacetamide	Invitrogen (Carlsbad, USA)

2.1.10. Columns

Column	Manufacturer
HisTrap Fast Flow (5 ml)	GE Healthcare (Freiburg, Germany)
PD-10 Desalting Columns	GE Healthcare (Freiburg, Germany)
Q Sepharose Fast Flow (self-packed)	GE Healthcare (Freiburg, Germany)
Resource Q (5 ml)	GE Healthcare (Freiburg, Germany)

Column	Manufacturer
HiLoad Superdex 75 Prep Grade (26/60) or (16/60)	GE Healthcare (Freiburg, Germany)
Highload Superdex 200 Prep Grade (26/60) or (16/60)	GE Healthcare (Freiburg, Germany)
Superdex 200 HR (10/300GL)	GE Healthcare (Freiburg, Germany)
TSK G3000PW HPLC gel filtration	Tosoh Bioscience (Yamaguchi, Japan)

2.1.11. Equipment

Device	Origin
Analytical Ultracentrifuge	
XL-A equipped with absorbance and fluorescence detections system	Beckman Coulter (Krefeld, Germany) and AVIV biomedical (Lakewood, USA)
Centrifuges	
Avanti J25 with Rotor JA-10, JA-25.50 und JLA 16	Beckman Coulter (Vienna, Austria)
Optima XL-A (equipped with FDS)	
Optima XL-I	Beckman Coulter (Lakewood, USA)
Rotina 46R	Beckman Coulter (Lakewood, USA)
Rotina 420R	Hettich (Tuttlingen, Germany)
Universal 320R	Hettich (Tuttlingen, Germany)
Benchtop centrifuge 5418	Hettich (Tuttlingen, Germany)
Benchtop centrifuge Mikro R200	Eppendorf (Hamburg, Germany)
	Hettich (Tuttlingen, Germany)
Chromatography systems	
ÄKTA Pure	GE Healthcare (Freiburg, Germany)
ÄKTA Purifier	GE Healthcare (Freiburg, Germany)
ÄKTA Explorer	GE Healthcare (Freiburg, Germany)
ÄKTA FPLC	GE Healthcare (Freiburg, Germany)
FPLC system	Pharmacia Biotech (Uppsala, Sweden)

Shimadzu Prominence HPLC system	Shimadzu (Munich, Germany)
Superloops (various volumes)	GE Healthcare (Freiburg, Germany)
Spectroscopic instruments	
J710 (with PFD-350S Peltier device)	Jasco (Großumstadt, Germany)
J715 (with PTC 348 WI Peltier device)	Jasco (Großumstadt, Germany)
Varian Cary 50/100 Bio UV–Vis spectrophotometer	Varian (Palo Alto, USA)
Jasco FP-8500 FDP spectrofluorimeter with polarizers	Jasco (Großumstadt, Germany)
FluoroMaxIII spectrofluorimeter with polarizers FluoroMax-4	Jobin Yvon (Edison, USA)
Nanodrop ND-1000 UV–Vis spectrophotometer	Jobin Yvon (München, Germany) Peqlab (Erlangen, Germany)
Temperature controlled incubator	
Digital heat block	VWR (Darmstadt, Germany)
Eppendorf-Thermomixer	Eppendorf (Hamburg, Germany)
TB1 Thermoblock	Biometra (Göttingen, Germany)
Gel electrophoresis and blotting	
Hoefer Mighty Small II dual gel caster	GE Healthcare (Freiburg, Germany)
Pharmacia EPS 3500, 301, 1001 power supply	GE Healthcare (Freiburg, Germany)
Biodoc II	Biometra (Göttingen, Germany)
ImageQuant 300	GE Healthcare (Freiburg, Germany)
Image Scanner III	GE Healthcare (Freiburg, Germany)
Additional Equipment	
Membrane vacuum pump	Sartorius (Göttingen, Germany)
Autoclave Varioclav EP-Z	H+P (Oberschleißheim, Germany)
Quartz Cuvettes	Hellma (Müllheim, Germany)
pH-Meter 538 MultiCal	WTW (Weilheim, Germany)

Cell Disruption Apparatus Basic Z	Constant Systems (Warrick, UK)
CL 1000 UV Crosslinker	UVP, Upland, USA
pH meter	WTW (Weilheim, Germany)
Power amplifiers EPS 3500, 3501 and 1001	GE Healthcare (Freiburg, Germany)
Homogeniser Heidolph DIAX 900	Heidolph (Staufen, Germany)
Incubator	New Brunswick Scientific (Nürtingen, Germany)
Thermal cycler MJ Mini 48 well	Biorad (München, Germany)
Ultra filtration cell 8050	Merck-Millipore (Darmstadt, Germany)
Amicon Ultra Centrifugal Filters	Merck-Millipore (Darmstadt, Germany)
Ultraflex II MALDI ToF/ToF	Bruker Daltonics (Bremen, Germany)
Vortex MS2	IKA (Staufen, Germany)
X-ray film processor Optimax TR	MS Laborgeräte (Dielheim, Germany)
Zeba Spin Desalting Columns	Thermo Fisher Scientific

2.1.12. Software, databases and web-based tools

SedFit	Peter Schuck
OriginPro 2018b	OriginLab Corporation
Adobe Illustrator	Adobe Inc.
CDNN	Gerald Böhm
ProtParam	https://web.expasy.org/protparam/
Pymol	Schrödinger, DeLano Scientific LLC
Chimera	UCSF
Serial Cloner	Franck Perez
PsiPred	http://bioinf.cs.ucl.ac.uk/psipred/
FoldIndex	https://fold.weizmann.ac.il/fldbin/findex
iupred	https://iupred2a.elte.hu/

Epson TT8 Launch Silver Fast	Epson
ASTRA 5.3.4	Wyatt Technology, Dernbach, Germany
UniProt	https://www.uniprot.org
RCSB Protein Data Bank (PDB-ID)	https://www.rcsb.org
DynamX 3.0	Waters
Phyre2	http://www.sbg.bio.ic.ac.uk/phyre2
GENtle	Magnus Manske
PLGS and DynamX	Waters.com

2.2. Methods

2.2.1. Molecular biology

DNA isolation

All cloned constructs were amplified in 5 ml liquid *E. coli* culture with appropriate antibiotic. The DNA was isolated using the Wizard Plus SV Mini-Prep kit, according to the manufacturer's manual. DNA concentration was determined using a Nanodrop spectrophotometer and DNA was stored at -20 °C. DNA sequence was verified by sequencing at GATC Biotech (Konstanz, Germany).

Agarose gel electrophoresis

DNA was separated using 1% agarose gels (w/v) with 1:50000 DNA stain G in TAE buffer. The gels were run at 120 V for 30 min. PCR products or gel extraction was purified with the Wizard SV Gel and PCR Clean-up Kit.

Polymerase chain reaction

To amplify DNA fragments the polymerase chain reaction (PCR) was performed using Phusion Polymerase with the buffers provided by the manufacturer. The following standard protocol was performed for the PCR.

DNA template	1 µl
5 x Phusion buffer HF	10 µl
Primer fwd + rev (100 pmol/µl)	2.5 µl
dNTPs (100 mM)	1 µl
Phusion Polymerase	0.5 µl
Nuclease free water	*ad.* 50 µl

PCR reaction was performed using a thermocycler with the following reaction protocol.

Step	Temperature	Time	
Initial denaturation	95 °C	2 min	
Denaturation	95 °C	1 min	Repeat 30 times
Primer annealing	40 -70 °C (see primer list)	45 s	
Amplification	72 °C	30 s /1000 bp	
Final amplification	72 °C	5 min	
storage	4 °C	forever	

SLIC cloning

Sequence and ligation independent cloning (SLIC) was used for cloning constructs into the pSUMO or pSUMO pro vector. The vector was linearized by restriction digest with BsaI for pSUMO pro or XhoI and BamHI for pSUMO. The PCR of the insert was performed as described with the specific annealing and elongation times. Vector and insert were purified using the Wizard SV Gel and PCR Clean-up System. A 10 µl assembly mix was pipetted as described below and incubated for 2.5 min at room temperature. To stop the reaction, the assembly is put on ice for at least 10 min and directly transformed into XL1 blue competent cells.

SLIC assembly mix
100 ng digested vector
insert (ratio vector:insert 1:2 - 1:10)
1x NEB cut smart buffer
1x BSA
0.6 U T4 Polymerase

Site directed mutagenesis

Single point mutations were incorporated using the QuickChange protocol by Stratagene with small modifications. After DNA amplification, the PCR product was digested in the reaction buffer using DpnI

enzyme for 1 h at 37 °C and heat inactivated for 20 min at 60 °C. The digested PCR product was purified and directly transformed into competent cells.

Transformation

For transformation, 100 µl competent *E. coli* cells (XL1 blue for vector preparation, BL21-De3 for overexpression) were incubated 10 min on ice with 50 ng vector DNA or 10 µl ligation reaction/QuickChange reaction. Heat shock was performed at 42 °C for 45 s and the cells were transferred to ice for another 5 min. 1 ml LB media was added to the transformed cells and the cells were allowed to grow for 1 h at 37 °C. The cells were plated out on LB Agar with the appropriate antibiotic and incubated overnight at 37 °C. Single colonies were picked for overnight cultures to check for the right clone or start overexpression.

2.2.2. Protein biochemistry

a) Protein expression

For expression of Bap proteins and BiP, the vector was transformed into BL21-DE3 cells; for ERdj3 the vector was transformed into SHuffle cells according to manufacturer's protocol and an overnight culture was inoculated. For ERdj3, LB media with the appropriate antibiotic was inoculated to an OD_{600} of 0.1 and grown at 30 °C until an OD_{600} of 0.6-0.8 and then induced with 0.5 mM IPTG and grown over night. For the other proteins, fresh LB media with appropriate antibiotic was inoculated to an OD_{600} of 0.1 and grown at 37 °C until an OD_{600} of 0.6-0.8 was reached. Induction was performed with 1 mM IPTG for BiP or 0.5 mM IPTG for the other proteins. Bap and Grp170 containing cells were cooled to 16 °C before induction with IPTG and grown over night at 16-18 °C. Cells were harvested by centrifugation at 8000 x g for 15 min at 4 °C after 3 h for BiP or after 18 h for the other proteins.

b) Cell disruption

After harvesting, cells were homogenized in the buffer used for the first step of purification or in IB buffer using a Heidolph DIAX 900 homogenizer. Usually DNase and protease inhibitor HP were added. For protein purification, the cells were disrupted using a pressure-operated cell disruption apparatus

Basic Z at 1.9 kbar and the cell debris was removed by centrifugation at 50,000 x g for at least 30 min at 4 °C.

For test expressions, the cells were disrupted in the buffer used for the first step of the purification using ultrasound. 10 µl of the complete lysate were mixed with 90 µl H_2O and 25 µl Laemmli. 200 µl supernatant were mixed with 50 µl Laemmli and 15 µl of the prepared solutions were loaded on a SDS-Gel.

c) Protein purification

Some protein purification protocols were established during this thesis. Therefore exact purification protocols can be found in the results section. Fractions to pool and the purity of the proteins were tested via SDS-PAGE. All proteins were frozen in liquid N_2 and stored at -80 °C. Protein concentration was determined by UV spectroscopy and the extinction coefficient was calculated by ProtParam. Ulp1 SUMO Protease was purified by nickel affinity chromatography and gel filtration and stored in the Ulp1 buffer according to a protocol described by A. Bepperling.

Purification of BiP

Centrifuged protein lysate was applied on a pre-equilibrated 5 ml His-Trap column and washed with 100 ml BiP-Buffer A and eluted on a 50 ml gradient of 0-100 % BiP-Buffer B. Flow speed was 4 ml/min. The fractions containing BiP were pooled and 100 µl TEV protease (~100 µM) was added before dialysis overnight at 4 °C in TEV protease digest buffer. The filtered protein solution was applied on a pre-equilibrated His-Trap column. The flow-through of loading and wash was collected and the fractions containing cleaved BiP were concentrated in a Milipore Amicon 30k MWCO to 10 ml, filtered and applied on a Superdex 200 (26/60) column and eluted in HKM. Fractions containing pure BiP protein were concentrated and frozen.

Purification of ERdj3

Protein lysate containing ERdj3 was applied on a 5 ml His-Trap column in J3-BufferA and eluted with a gradient from 0-100% J3-Buffer B with a 4 ml/min flow rate. Fractions containing the protein were mixed with Ulp1 and dialyzed for at least 4 h against Buffer A to cleave off the SUMO tag. The cleaved

ERdj3 was again applied on a His-Trap column and the flow-through from load and wash was collected, concentrated and applied on a Superdex 200 (26/60) column and eluted in HAKM buffer. Fractions containing the pure protein were concentrated and stored at -80 °C.

Purification of BAP and its mutants

The protein lysate was applied to a 5 ml His-Trap column in Bap-Buffer A and the column was washed with 50 ml of buffer A with a flow rate of 4 ml/min. The bound protein was again washed with buffer A supplemented with 10 mM ATP at a flow rate of 1 ml/min. After another washing step in 50 ml buffer A, the protein was eluted in 100 % Bap-Buffer B with 4 ml/min flow rate. The eluted protein was applied on a Q-Sepharose column and eluted in 100 % Bap-High Salt. Fractions containing Bap were pooled and digested for at least 2 h with Ulp1 Sumo-protease at 4 °C. The cut protein was applied to a 5 ml His-Trap column and the unbound fractions were collected and strongly diluted to Bap-Low Salt buffer. The protein solution was applied on a ResQ in Bap-Low Salt and is eluted in a gradient of 100 ml from 0-100% in Bap-High Salt buffer with a flow rate of 5 ml/min. Fractions containing Bap with no DnaK impurities were applied to a Superdex 200 (16/60) column and eluted in HKM buffer. Pure fractions of Bap were pooled and concentrated in a Milipore Amicon 10k MWCO.

The Bap-N purification was performed as described for Bap wt by His-Trap purification with subsequent SUMO cleavage by the Sumo-Protease Ulp1. Another His-Trap run was performed to remove the uncleaved Bap, the SUMO tag and the Ulp1 protease. Afterwards size exclusion chromatography with a Superdex 200 (26/60) column was performed in HKM buffer.

Purification of Grp170

The cells were lysed in Grp170-Buffer1 and the lysate was loaded on a 5 ml His-Trap column in Grp170-Buffer2. The bound protein was washed with 50 ml in Buffer2 and 50 ml of Buffer2 supplemented with 10 mM ATP at a flow rate of 4 ml/min. Afterwards the bound protein was washed in Buffer2 before wash in 100 ml Grp170-Buffer2. The proteins bound were eluted in Grp170-Buffer3 and dialyzed with Ulp1 Sumo-protease over night at 4 °C against Grp170-Buffer2. The cut protein was applied to a His-Trap column (in Grp170-Buffer2) and the unbound fractions are collected and

concentrated to 5 ml in a Milipore Amicon 30k MWCO. Protein solution was applied to a Superdex 200 (16/60) column in HKM and fractions containing Grp170 protein were pooled and concentrated.

d) SDS-Polyacrylamide gel electrophoresis (SDS-PAGE)

SDS-PAGE was used to examine the size and purity of proteins or the homogeneity of the samples and was performed as described [124]. Depending on the expected protein size 18 % (mainly antibody domains and SLC proteins), 15 % (Bap, Erdj3) or 12.5 % (BiP). A 5 % stacking gel was casted on top to concentrate the samples. Gels were casted and polymerization was induced using ammonium persulfate (10 % w/v) and TEMED.

Samples for SDS-PAGE were mixed with Laemmli buffer containing 5 % β-Mercaptoethanol, heated to 95 °C for 5 min and centrifuged at 14,000 x g for 5 min before loading into the pockets on the stacking gel. Gels were run at a current of 35 mA per gel for around 50 min. Gels were stained using warm Fairbanks A solution for 15 min followed by a destaining step in Fairbanks D for about 30 min until the bands were clearly visible and background was removed.

e) Protein labeling

Proteins were labeled at cysteines using maleimide chemistry and Atto dyes. The different BiP mutants were labeled using the protocol described by Mathias Rosam [123]. Briefly, the protein was reduced using 200-fold excess of TCEP for 1 h at room temperature and after TCEP removal by diafiltration in an Amicon Ultra-0.5, the proteins were labeled for 2-3 h in a 1:2 ratio of the respective Atto label. Free label was removed by diafiltration in an Amicon Ultra-0.5 until the flow-through was clear and the degree of labeling was determined by UV-Vis absorption spectroscopy using the following formula:

$$DOL = \frac{A_{dye} \times \varepsilon_{protein}}{(A_{protein} - A_{dye} \times CF_{dye}) \times \varepsilon_{dye}}$$

Here, A_{dye} represents the measured absorbance of the dye at its maximum, A_{proten} is the absorbance measured at 280 nm, $\varepsilon_{protein}$ is the molar extinction coefficient of the protein at 280 nm, CF_{dye} is the correction factor at 280 nm and ε_{dye} is the molar extinction coefficient of the dye at its absorotion maximum. Bap was labeled using a protocol described by Janine Hochmair [125].

f) Ellman assay

To determine the concentration of accessibly sulfhydryl groups as in cysteines that do not form disulfide bonds, an Ellman assay was performed as described [126,127]. The reaction was performed with 90 µg/ml final protein concentration in 0.1 M Tris buffer. Ellmans reagent (5,5-dithiobis-2-nitrobenzoate, DTNB) was dissolved in 100 mM K_2HPO_4 and 1 mM EDTA (pH 8). 300 µM of Ellmans reagent was added to the protein sample and incubated for 1 h at room temperature. The reaction of DTNB with free thiol groups eventually results in TNB^{2-} salt, which is responsible for the yellow coloring of the sample. The absorption was measured at $\lambda = 412$ nm and the concentration of TNB2- was calculated with the extinction coefficient of $\varepsilon = 14159\ M^{-1}cm^{-1}$, which is equivalent to the free thiol groups in the solution.

g) Limited proteolysis

The tested proteins were diluted to 15 µM in 100 mM Tris, 100 mM NaCl, 10 mM CaCl (pH 7-8). α-Chymotrypsin was dissolved in a 1 mM HCl solution to 25 µg/ml. For BiP and Bap, 15 µM of each protein was pre-incubated for 20 min. Samples were incubated with α-Chymotrypsin at 5:1 (wt/wt; Protein:αChymotrypsin) ratio at RT the reaction was stopped by adding 15.5 µl of the sample with 2 mM PMSF. Samples were diluted with Laemmli-buffer containing β-ME and analyzed by SDS-PAGE on a 4-20% SERVAGel™ TG PRiME™ 12 sample well gel for 90 min according to the manufacturer's protocol.

h) Circular Dichroism (CD) spectroscopy

Determination of secondary structure was performed using circular dichroism [128]. All CD spectra were recorded using a Jasco J-715 or J-720 spectropolarimeter equipped with a temperature controller. Instrument settings were as below:

Parameter	**Setting**
Sensitivity	Standard (100 mdeg)
Wavelength range	260-190 nm
Data pitch	0.1 nm
Scanning speed	30 nm/min
Response	4 s
Band width	1 nm

Samples were measured using quartz cuvettes with a path length of 1 mm, 0.5 mm or 0.2 mm. Proteins were usually concentrated at 0.5 mg/ml. The proteins were diluted to the desired concentration using PBS buffer. Spectra were usually recorded at 20 °C with 10 accumulations and were normalized to the mean residue ellipticity by the following formula.

$$[\Theta]_{MRW,\lambda} = \frac{\Theta_\lambda \times \frac{M}{N_{aa} - 1}}{c \times d}$$

Θ is the measured ellipticity at a specific wavelength and M the molecular mass of the protein in Da. N_{aa} is the number of amino acids, c the concentration of the protein in mg/ml and d the pathlength of the cuvette in cm.

Thermal stability was measured in the 1 mm cuvette at 222 nm with a heating rate of 30 °C per hour. The obtained melting curve was fitted with the Boltzmann function as described below.

$$y = \frac{A_1 - A_2}{1 + e^{(x - x_0)/t}} + A_2$$

With A_1 as the initial value, A_2 as the final value and t as time constant. The calculated midpoint x_0 of the function describes the state, where half of the protein is already unfolded and is referred to as the melting temperature T_m in this work.

i) Fluorescence spectroscopy

Unfolding of proteins leads to a change in tryptophane (and to a lesser extent tyrosine and phenylalanine) fluorescence which can be detected by fluorescence spectroscopy. For the GdmCl-induced unfolding, 1 µM protein samples were incubated over night at 20 °C with different concentrations of GdmCl. Measurements were carried out in a FluoroMaxIV fluorimeter (Horiba Jobin-Yvon) at 20 °C in a 1 cm quartz cuvette. Exitation was at 280 nm and the spectra were recorded for 20 s at 300-450 nm with the slits set to 5 nm. Single step unfolding was fitted with a Boltzmann Fit described in 2.2.2 g.

j) Analytical ultracentrifugation

All AUC runs were performed with Pamina Kazman or Philipp Schmidt (Technische Universität München, Germany) using a Beckman ProteomLab XL-A ultracentrifuge equipped with an absorbance and fluorescence detector. Centrifugation was carried out in the storage buffer of the protein at 42,000 rpm at 20 °C. Absorbance measurements were performed with the concentrations indicated in the text. Absorbance at 280 nm was measured and the concentration was set to an absorbance of 0.8. Fluorescence experiments were usually performed using 500 nM of labelled protein and unlabeled protein was titrated or added in a at least 10-fold excess. The obtained data was analyzed using SedFit with a model-free continuous Svedberg distribution model c(S) [129,130].

k) Single molecule FRET

Single molecule FRET experiments were performed and evaluated as described before [131] using a combination of multiparameter fluorescence detection and pulsed interleaved excitation (MFD-PIE). The reaction buffer was HKM and 1 µM Atto488-labeled BiP was incubated for 15 min at 37 °C with nucleotide and/or co-chaperone and then further diluted to < 70 pM whereas the incubation partners were kept constant. The experiments were performed by Ganesh Agam from the Nanosystems Initiative Munich and Center for Nanoscience at the Ludwig Maximilians University in Munich in the laboratories of Don Lamb.

l) Anisotropy measurements

Anisotropy was measured at a Jasco FP-8500 spectrofluorimeter equipped with polarizers at 37 °C if not stated otherwise. For detecting substrate association and dissociation, competition experiments were performed. All measurements were performed in a 1 cm quartz cuvette. 1 µM labeled substrate (usually 1 µM Lucifer Yellow (Ly) labeled HTFPAVLGSC) was incubated with 1 mM ADP for 10 min to reach a stable baseline. 15 µM BiP was added and the association was followed for around 2,000 s until there was no further signal change detectable. After reaching steady-state, unlabeled substrate was added in excess (for peptides usually 150-fold excess, proteins 20-fold excess) and the dissociation was again followed. Excitation wavelength for Ly was set to 428 nm with a bandwith of 5 nm and association was followed at 525 nm with a bandwith of 10 nm. Sensitivity was set to "high" and the time interval was set to 1 s. The

kinetic parameters were fitted with a single exponential model. Displacement efficiency is calculated by division of the amplitude of the displacement against the amplitude of the binding of HTFPAVL-Ly to BiP.

m) Maldi-TOF MS

The molecular weight analysis of impurities in protein batches and crosslink bands between BiP and BAP were performed on a Brunker Ultraflex-2 Maldi-TOF/TOF mass spectrometer according to the standard protocol used at the chair of Biotechnology, Technische Universität München. A Zip Tip preparation was performed according to the manufacturer's protocol (Millipore). The α-Cyano-4-hydroxycinnamic acid (HCCA)- matrix was dissolved in 0.1% TCA, 80% acetonitrile and 20% ddH2O. Proteins were spotted in the matrix solution and were analyzed after evaporation of the solvent.

n) Steady-state ATPase assays

The ATPase activity of BiP and the influence of cochaperones or substrates were determined by employing an ATP-regenerating system [132]. The coupled reactions of ATP hydrolysis (1), ADP phosphorylation (2), and NADH oxidation (3) allow experimental conditions without limiting ATP concentrations and inhibitory ADP accumulation. Phosphoenolpyruvate (PEP) and ADP react with the enzyme pyruvate kinase (PK) to ATP and pyruvate. Pyruvate is used to produce lactate with the help of the enzyme lactate dehydrogenase (LDH) and by oxidizing NADH/H to NAD^+.

$$ATP + H_2O \longrightarrow ADP + P_i \quad (1)$$

$$ADP + PEP \longrightarrow ATP + Pyruvate \quad (2)$$

$$Pyruvate + NADH/H^+ \longrightarrow Lactate + NAD^+ \quad (3)$$

$$PEP + NADH/H^+ \longrightarrow P_i + Lactate + NAD^+$$

During these reactions, the linear decrease in NADH was followed by monitoring the absorbance at 340 nm over time. The k_{cat} of the ATP hydrolysis can be calculated with the following formula:

$$k_{cat} = \frac{m}{\varepsilon_{NADH,340nm} \times d \times c_{ATPase}}$$

The molar extinction coefficient of NADH at 340 nm is $\varepsilon_{NADH,340nm}$ = 6200 $M^{-1}cm^{-1}$, a path length of the used quartz cuvette of d= 1 cm was used, and a concentration of the ATPase (usually BiP) c_{ATPase}= 2 µM. The linear slope is m.

The ATPase measurements were carried out in a Varian Cary 50/100 Bio UV–Vis spectrophotometer in HKM buffer at 37 °C. A 2x premix was prepared as described below which can already contain the ATPase in the measurement.

Component	**stock uM**	**end (2x) uM**	**Original**
Buffer (ul)			5581.3
PEP 100 mM (ul)	100000	4000	240.0
NADH 50 mM (ul)	50000	400	48.0
LDH (U/min)	2750	20	43.6
PK (U/min)	2000	4	12.0
BiP 358uM (ul)	319.6	4	75.1
Total (ul)			**6000.0**

After detection of a stable baseline for ~10 min, the hydrolysis reaction was started by adding 1 mM of ATP to a total sample volume of 150 µl and NADH decrease was monitored for 90 min.

o) H/DX MS

Hydrogen/Deuterium exchange mass spectrometry (H/DX-MS) was performed in an automated system equipped with a Leap PAL RTC, a ACQUITY M-Class UPLC (Waters), HDX manager and Synapt G2-S ESI-TOF mass spectrometer as described before [131]. Data was evaluated using the Waters Protein Lynx Global Server PLGS and DynamX as described [131]. 3 µl of 15 µM Bap or/and 45 µM BiP were analyzed at 0, 10, 60, 600, 1800 and 7200 s at 20 °C. Protein solutions were diluted 1:20 in 99.9 % D_2O containing HKM with 1 mM ADP and quenched upon addition of 1:1 200 mM KH_2PO_4, 200 mM Na_2HPO_4 (pH 2.3) at 1 °C.

p) Nucleotide exchange measurements

Nucleotide exchanged experiments were performed by Jochen Reinstein (Max-Planck Institute for Medical Reasearch in Heidelberg, Germany). Nucleotide exchange kinetics were measured on a BioLogic SFM 400/MOS 450 stopped flow instrument in single mixing configuration equipped with a 1.5 x 1.5 mm quartz cuvette (FC 15) at 20 °C in HKM buffer.

A complex of BiP with the fluorescent nucleotide analog C8-MABA-ADP was formed by incubation of 0.75 µM BiP with 5 µM C8-MABA-ADP (diluted to 0.3 µM and 2 µM in the final mixture in the cuvette). The dissociation of C8-MABA-ADP was monitored by chasing this complex in the absence and presence of different concentrations of Bap (up to 6 µM in the final mixture) and excess ADP (0.5 mM in the final mixture). The excitation wavelength was set to 365 nm, emission was monitored using a 420 nm long-pass filter. Slit width was 1 nm and 1000 data points were recorded in the first second followed by 2850 points in the second time window up to 60 s. Photomultiplier voltage was set to 650 V. The data was normalized between 0 and 1 and fitted with a single exponential fit with linear slope as can be seen in the following equation:

$$y = A * e^{-kx} + mx + B$$

With A as the initial value of the exponential fit, k as rate coefficient, m as the slope and B as the offset of the linear slope.

q) SEC-MALS and HPLC measurements

HPLC measurements were performed using a Shimadzu Prominence HPLC system with a 0.5 ml/min flow rate. The HPLC runs were performed using a Superdex 200 HR (10/300GL) or a TSK3000 column. For HPLC measurements the column was equilibrated in the running buffer (usually HKM) and the BioRad protein standard was run as a reference. Proteins were diluted as described in the experiment and the UV/Vis detector was set to 280 nm and fluorescence was excited at 280 nm and detected at 350 nm.

For SEC-MALS a Shimadzu Prominence HPLC system equipped with a Wyatt Helios light scattering detector, the column used was equilibrated for at least 24 h prior to the measurements in the respective

buffer with 0.02% azide to get a stable baseline. Protein samples were diluted to 1 mg/ml and centrifuged for 10 minutes at 14,000 x g. Measurements were performed at room temperature with a flow rate of 0.4-0.6 ml/min. For the calibration of the light scattering detectors, the instrument and the column a 1 mg/ml BSA solution run was employed. Data evaluation was performed with ASTRA 5.3.4.

3. Results and Discussion

3.1. Protein purification

The following chapter gives an overview over the established purification protocols during this PhD. The protein purifications not mentioned in this chapter were already established and the protocols are in the Material and Methods section.

3.1.1. Bap proteins

Bap, as well as Bap-C and Bap-N, were cloned in a pET-SUMO vector with an N-terminal His-tag followed by a SUMO-tag for better solubility during overexpression (**Figure 10**) in BL21-DE3 cells. Expression at low temperatures (16 °C) and at low IPTG concentrations (0.5 mM) was necessary to obtain soluble protein. Induced bacterial pellets were stored at – 80 °C for up to 4 weeks. Bap-N was obtained almost exclusively in a soluble form under the conditions used for overexpression.

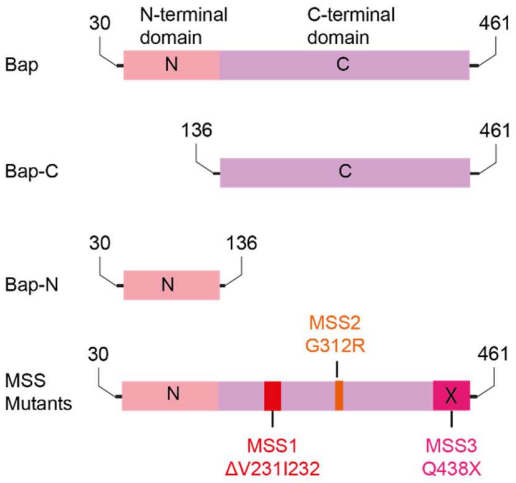

Figure 10: Constructs of Bap proteins used in this thesis. The N-terminal domain is depicted in pink, the C-terminal domain in purple. Sequences as in UniProt (ID Q9H173).

In a first step, the Bap purification was performed using a standard protocol including a His-Trap purification with subsequent cleavage by the Sumo-Protease Ulp1. Another His-Trap run was performed to remove the uncleaved Bap, the tags and the Ulp1 protease. Afterwards size exclusion chromatography with a Superdex 200 was performed in HKM buffer. This protocol worked well for Bap-N purification. However, purified Bap and Bap-C still contained impurities at a higher molecular weight. One protein

band of smaller size (~ 40 kDa) on SDS-PAGE gels is a degradation product of Bap, similar to the construct Bap-C. The band at 70 kDa is DnaK as determined by mass spectrometry (**Figure 11**).

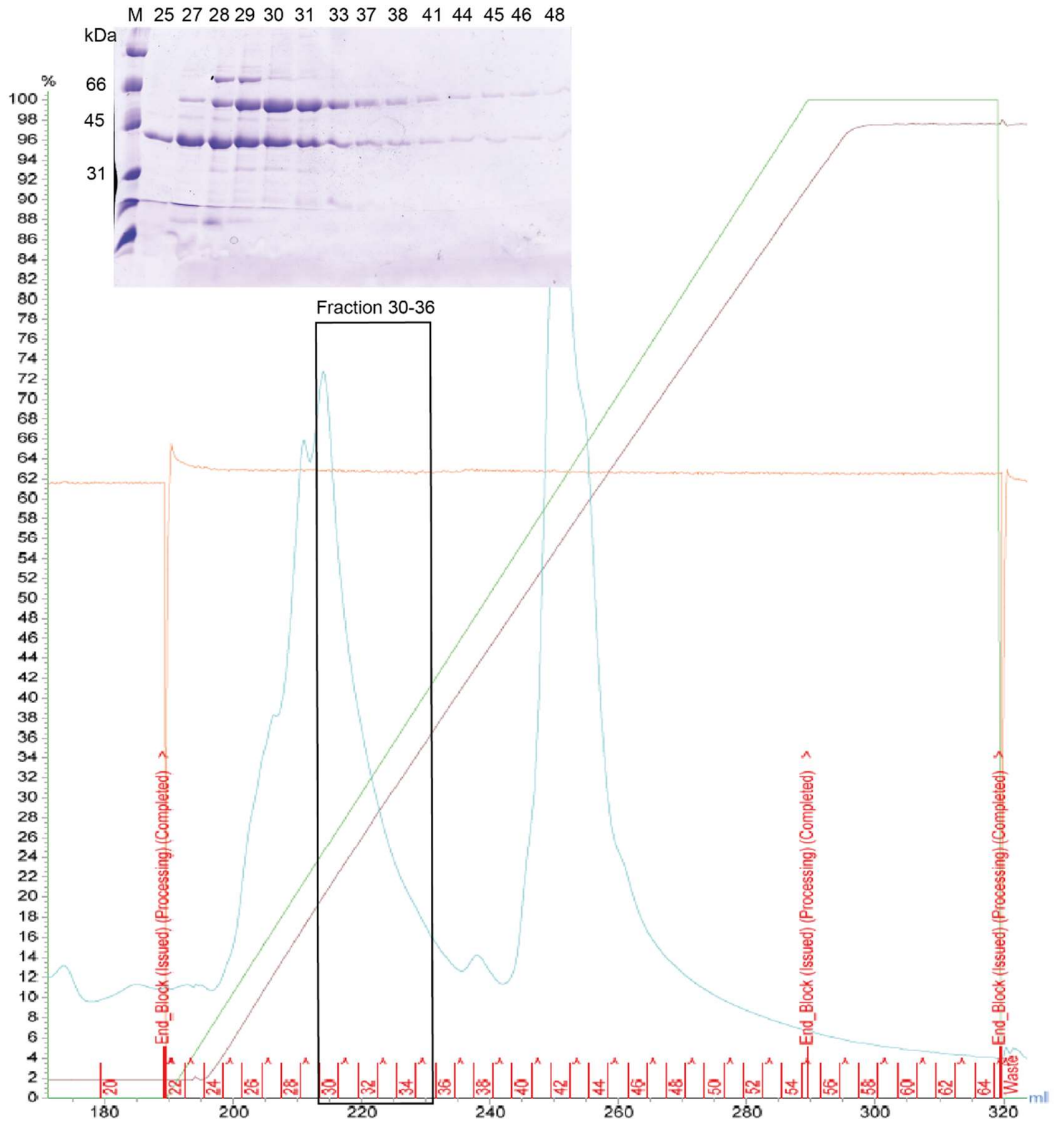

Figure 11: ResourceQ elution profile of Bap and SDS-PAGE gel. The fractions 30-36 at 22-40 % high salt buffer contained almost no impurities at 70 kDa and were pooled.

Purification of Bap was optimized to get rid of DnaK impurities, since DnaK distorts the results of diverse measurements performed in this thesis. Whether these impurities are the result of misfolded Bap binding as a substrate to DnaK, or Bap being a co-factor for DnaK has yet to be resolved. Therefore another column was introduced and after the second His-Trap column. After a dialysis step in low salt buffer, a ResourceQ run was performed (**Figure 11**). This resulted in pure protein (**Figure 13**). The

schematic purification protocol can be seen in **Figure 12** A. The purification yield is very much dependent on the time span of purification. To receive optimal results, the purification was performed in two days. Purification yielded around 0.5 – 1 mg per L of media. The protein was stable when concentrating with an *Amicon* Ultra Centrifugal Filters up to a protein concentration of 120 µM. The full purification protocol can be seen in 2.2.2 c.

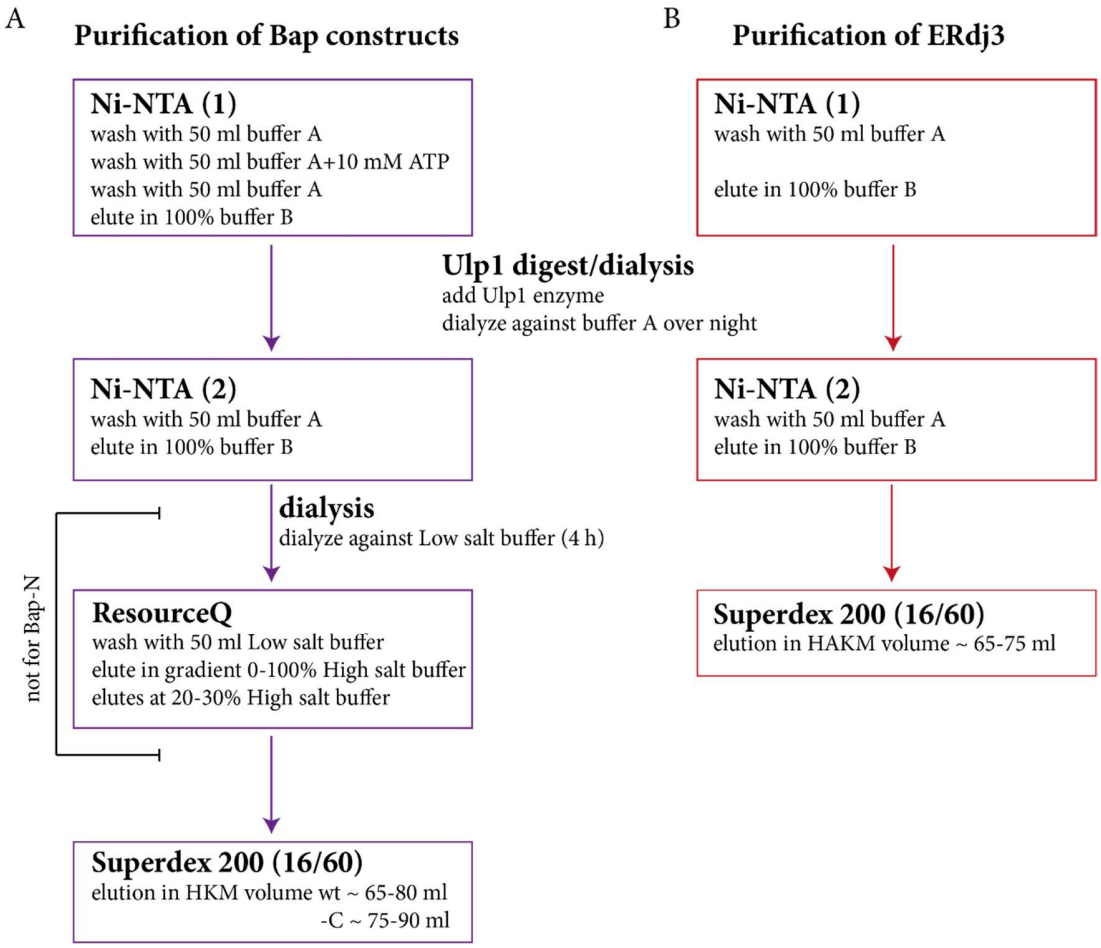

Figure 12: Schematic purification protocol. A) Bap proteins and B) ERdj3 purification. All purifications were performed on ÄKTA Pure or Purifier FPLC systems with the buffers described in 2.1.2.

For Bap-C no degradation band was visible, however, DnaK impurities were also obtained. Therefore, purification of Bap-C was performed as Bap wt. Bap-C yielded ~1 mg pure protein per L of media and was stable upon concentration up to concentrations of 160 µM. The stability of this protein was enhanced compared to old expression and purification protocols [123]. All other Bap constructs were purified as the wt protein, however, purification efficiencies and stability varied between the mutants.

3.1.2. ERdj3

ERdj3 contains four cysteines that are supposed to form two disulfide bonds, although it is still not clear, which cysteines react with each other [133,134]. Since expression in *E. coli* occurs in a reducing environment, disulfide bond formation is usually difficult to obtain. This is the reason why ERdj3 was previously purified by refolding [135]. An alternative expression strain is *E. coli* SHuffle cells, which is designed to allow disulfide bond formation in the *E. coli* cytosol [136]. To avoid refolding of ERdj3, human ERdj3 (UniProt ID Q9UBS4; I264V) was cloned in the pET-SUMO vector and overexpressed in the *E. coli* SHuffle strain. Overexpression at 30 °C with 0.5 mM IPTG overnight yielded a low amount of soluble protein and inclusion bodies (IB).

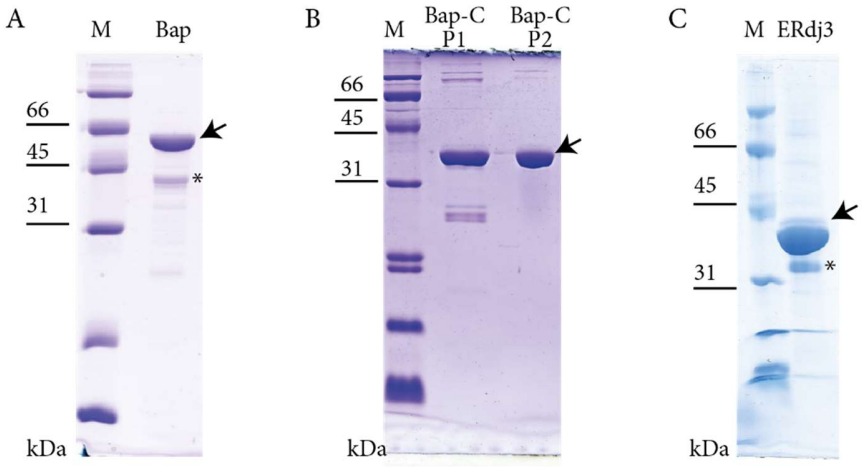

Figure 13: Example of 12.5% or 15 % SDS-PAGE gels of the purified proteins A) Bap wt, B) Bap-C or C) ERdj3. As marker (M) the low molecular weight standard by Biorad was used. Arrrows mark the purified protein, the asterisk * marks degradation products as verified by MS.

For purification, the lysate was run over a His-Trap column and afterwards the His- and SUMO-tag were cleaved with the SUMO-Protease Ulp1 over night during dialysis in Buffer A-j3. Another His-Trap run separated the untagged protein from its SUMO-tagged form. Afterwards size exclusion chromatography on a Superdex 200 was run in HAKM buffer. The schematic protocol can be seen in **Figure 12** B. The obtained protein was stable up to concentrations of 200 µM in the high salt buffer HAKM, yielding ~ 2 mg per L culture (**Figure 13**). The purification protocol is also in the 2.2.2 c). After purifiying ERdj3, an Ellman assay was performed to test for oxidation of the internal disulfide bridges [127].

No free cysteines were detected with the Ellman assay under native conditions. If ERdj3 was reduced using 200 µM TCEP, the Ellman assay showed a yellow color and free thiols were detected.

3.1.3. Discussion

Bap and ERdj3 were expressed in their native form and purified using a solubility tag. The stability of the protein was as expected from previous purifications or even better, as in the case Bap-C [123,135]. With the old refolding protocol of Bap-C, the protein precipitated at 37 °C, whereas the natively expressed Bap-C is as stable as Bap. This is also in line with publications that state that scBap-C is stable [114]. Further optimization concerning the storage buffer or other columns might be performed. ERdj3 storage buffer with high salt concentrations stabilizes the protein. Storage or experiments in other buffers destabilize ERdj3, which can be seen by strong precipitation of the protein after several hours.

3.2. Characterization of the proteins

To test the correct folding of the proteins, CD spectra were collected as described for all the constructs. To test the stability of the proteins, thermal unfolding experiments were performed and monitored by CD spectroscopy. Also chemical unfolding experiments were performed using GdmCl and the tryptophan fluorescence was monitored in a Fluorometer. Dimerization and aggregation status was analyzed using SEC-HPLC and AUC.

3.2.1. BiP

The structure of murine BiP was modelled on the available crystal structure of human BiP (PDB: 5E84 [44] (**Figure 4** A)). The NBD mainly consists of α-helical structures whereas the SBD is predominantly composed of β-sheets (SBD-β) and the C-terminal lid consisting mainly of α-helices. For some experiments, the protein was labeled and the labeling positions are visible in **Figure 4** A.

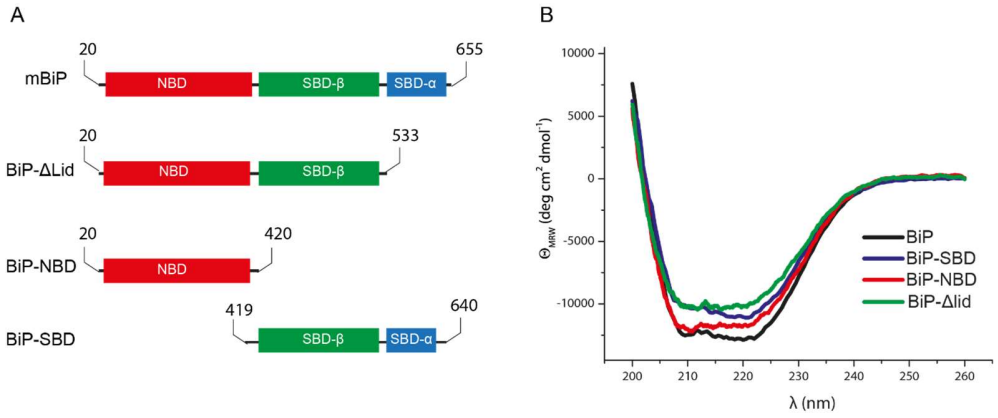

Figure 14: BiP constructs in this thesis. A) Schematic domain structure of constructs used in this thesis and B) FUV CD-spectra for the BiP constructs measured at 25 °C in a 1 mm CD cuvette with concentrations of 0.5 mg/ml.

Four main constructs of BiP were used in this work (**Figure 14** A) and their FUV-CD spectra can be seen in **Figure 14** B. BiP shows an α-helical overall structure with minima at around 222 nm and 212 nm. For the NBD alone, a α-helical structure is observed. For the BiP-SBD the picture is different and the spectrum shows a mixture of α-helix and β-sheet with a broadened maximum at around 220 nm. A construct of BiP without the C-terminal lid again gives a similar picture as BiP wt. To test the stability of the protein constructs, thermal transition experiments were performed (**Figure 15**). The melting temperature T_m here is defined as the inflection point (x_0) in the Boltzmann equation.

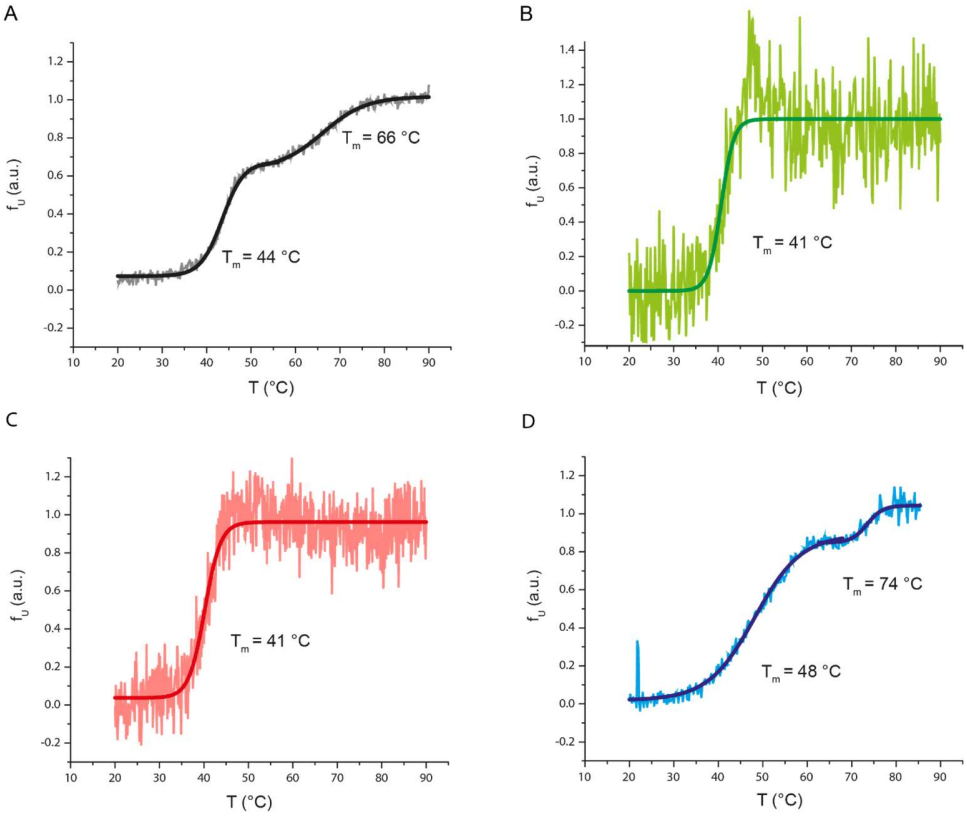

Figure 15: Thermal transition data of BiP and its different constructs measured at 222 nm. A) Thermal transition of BiP wt. The data was twice fitted with a Boltzmann fit. B) Thermal transition of BiP-Δlid. The data showed a single denaturation step. C) Thermal transition of BiP-NBD shows a one-step unfolding. D) Thermal transition of BiP-SBD shows a two-step unfolding.

For all protein constructs unfolding starts at around 35-40 °C and the T_m can be seen in **Figure 15**. For BiP at least two transitions were detectable at around 44 °C and 66 °C (**Figure 15** A). BiP-Δlid and BiP-NBD show a more noisy spectrum and the denaturation seems to occur in only one step (**Figure 15** B and C, respectively). The transition is steep and the protein is fully denatured at around 50 °C. For BiP-Δlid a melting temperature of 41 °C was obtained and BiP-NBD denatured at 40 °C. For the BiP-SBD again at least two melting points can be obtained at 48 °C and 74 °C (**Figure 15** D).

3.2.2. Bap

Structure and Stability

Bap and Bap-C secondary structure and stability were analyzed using CD spectroscopy. Both proteins exhibit a mainly α-helical secondary structure with the characteristic minima at 208 and 222 nm

(**Figure 16** A). This is in line with already published structures of Bap orthologs from other species [114]. The minimum at 208 nm seems to be even more pronounced in the Bap-C constructs. This might be due to the missing N-terminal domain. The isolated N-terminal domain of Bap (Bap-N) shows a spectrum typical for random coil with a minimum at 195 nm, although the maximum at 212 nm is not visible.

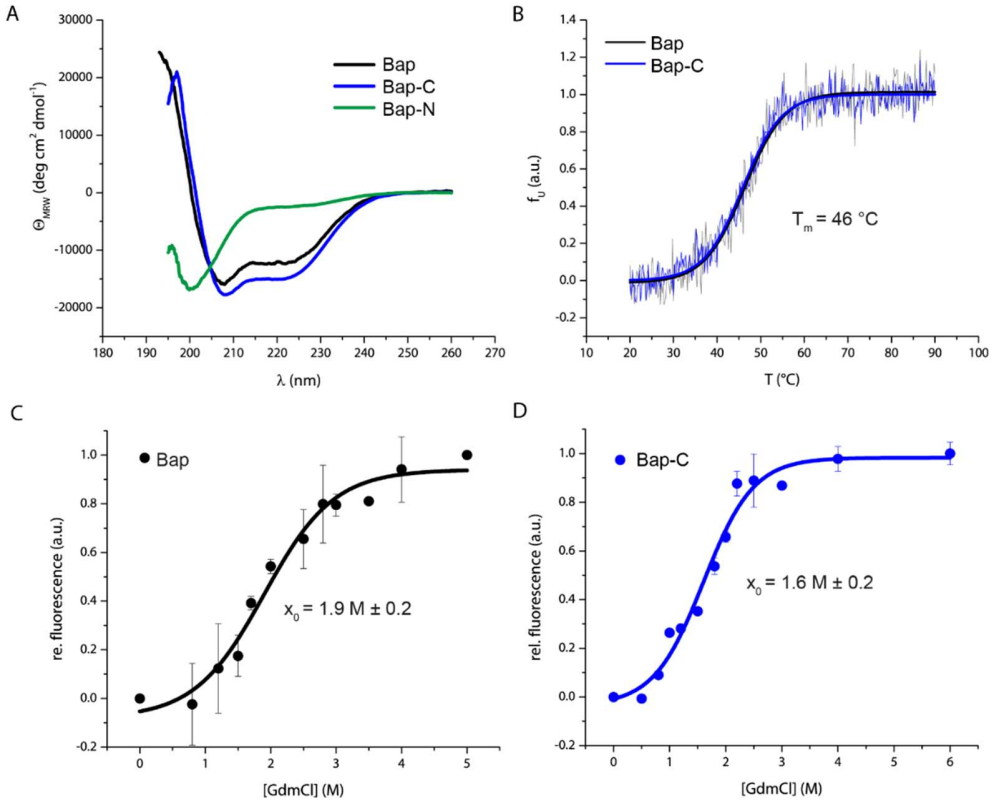

Figure 16: Structural data and stability measurements of Bap and Bap-C. A) FUV-CD spectra of Bap, Bap-C and Bap-N measured at 25 °C in HKM in a 1 mm CD cuvette with concentrations of 0.5 mg/ml (black, blue and green). B) Thermal transition of Bap and Bap-C measured by CD spectroscopy at 222 nm, normalized and fitted with a Boltzmann fit. C)+D) Fluorescence measurements at Ex=280 nm and Em=350 nm in presence of different concentrations of GdmCl for C) Bap and D) Bap-C. The resulting values were fitted using a Boltzmann Fit.

Thermal denaturation of Bap monitored by CD spectroscopy showed a simple unfolding which can be fitted with a Boltzmann equation. For both curves unfolding starts at around 25 °C and complete unfolding is observable above 60 °C (**Figure 16** B). The melting temperature T_m is around 46 °C for both Bap and Bap-C. Due to its unfolded character, no thermal transition could be obtained for Bap-N. Bap and Bap-C were also tested for their chemical stability. Therefore the proteins are mixed with increasing concentrations of the denaturant GdmCl and the change in tryptophan fluorescence was measured. Both proteins show already unfolding upon addition of low concentrations of GdmCl and are completely

unfolded at a concentration of about 3 M GdmCl (**Figure 16** C and D). The data points were again fitted with a Boltzmann fit and the stability was determined as the inflection point of the curve. This leads to values of 1.9 M GdmCl for Bap and 1.6 M GdmCl for Bap-C.

Dimerization studies

To test the dimerization state of the Bap proteins, different methods were used. Previous published results [114] suggest that the yeast homolog (ScBap) forms dimers, whereas the truncated version Bap-C is only present as a monomer.

First, SEC-HPLC measurements were performed in HKM buffer using a S200 size exclusion column and 60 µM Bap, Bap-C and Bap-N (**Figure 17** A). The proteins eluted in a single peak. However, a small shoulder is visible for Bap at the same retention time as Bap-C. Size determination using a SEC standard showed a size for Bap of 80 kDa (monomer size as calculated from ProtParam: 49 kDa) for the retention time of 28.3 min. The size of Bap-C was calculated to be 50 kDa (monomer size as calculated from ProtParam: 37 kDa) for the retention time of 30.5 min. Bap-N has a retention time of 33.2 min, which corresponds to a size of 22 kDa (monomer size as calculated from ProtParam: 12 kDa). These values are in between dimers or monomers and therefore the SEC-HPLC measurements could not solve the question, whether the proteins correspond to a monomer or a dimer.

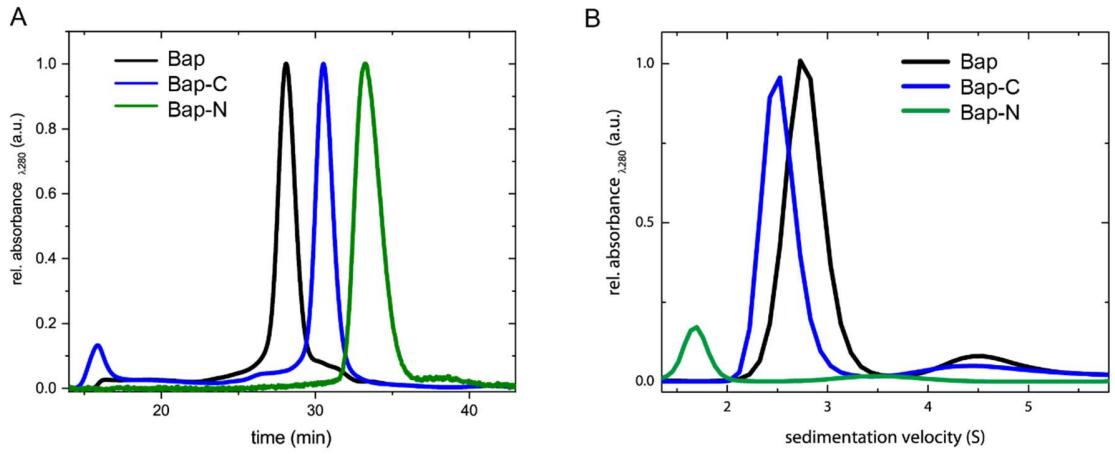

Figure 17: Dimerization studies of Bap and Bap-C in HKM. A) Normalized SEC-HPLC runs on a Superdex 200 column. Retention time for 60 µM Bap is 28.3 min with a shoulder at 30.5 min (black line). Retention time for 60 µM Bap-C is 30.5 min (blue line). Retention time for 20 µM Bap-N is 33.2 min. B) AUC-SV experiments at a concentration of 0.7 mg/ml Bap (black line), 0.5 mg/ml Bap-C (blue line) and 0.6 mg/ml Bap-N (green line). Tryptophan absorption was determined at an excitation wavelength of λ=280 nm.

To resolve the question of dimerization, AUC measurements were performed using the intrinsic tryptophan fluorescence of the proteins for detection. All constructs show mainly a single peak in the AUC measurements evaluated by SedFit (**Figure 17** B). Bap exhibits a sedimentation velocity of around 2.9 S, which corresponds to a size of ~ 45 kDa. A very small peak is also visible at 4.8 S, with a size of 103 kDa. Bap-C shows one peak at 2.6 S, corresponding to a protein size of ~ 35 kDa. Bap-N has a sedimentation velocity of about 1.8 S, corresponding to a size of 14 kDa.

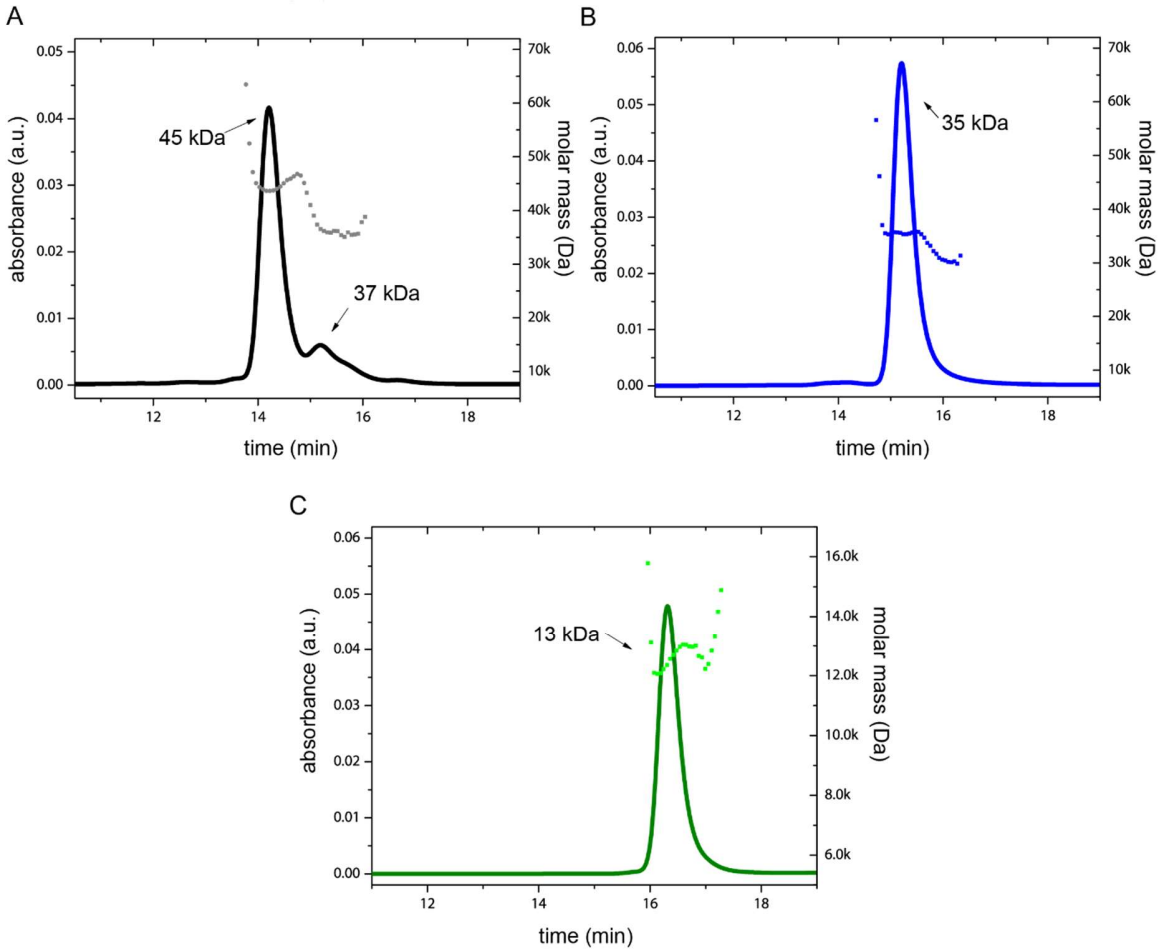

Figure 18: Size analysis of Bap constructs with SEC-MALS experiments performed at protein concentrations of 1 mg/ml on a TSK G3000PW. A) Bap eluted between 13.8 and 14.9 min and a molar mass of 45 kDa was measured. An additional peak at a retention time between 14.9 min and 16.4 min has a molar mass of 37 kDa. B) Bap-C eluted in one peak between 14.6 and 16.3 min and has a molar mass of 35 kDa. C) Bap-N eluted in one peak at the retention time 16.3 min and has a molar mass of 13 kDa.

To confirm the AUC results, SEC-MALS measurements were performed using a TSK G3000PW column and HKM buffer. Bap eluted in two peaks (**Figure 18** A). The main peak has a size of

approximately 45 kDa, the small peak has a size of 37 kDa. Bap-C only shows one peak with a size of approximately 35 kDa (**Figure 18** B). Thus both proteins Bap and Bap-C are monomeric. Bap-N also elutes as a monomer with a size of 13 kDa (**Figure 18** C).

3.2.3. Erdj3

Structure and stability

To test the structure and stability of the natively purified ERdj3, CD spectroscopy was performed and can be seen in **Figure 19**.

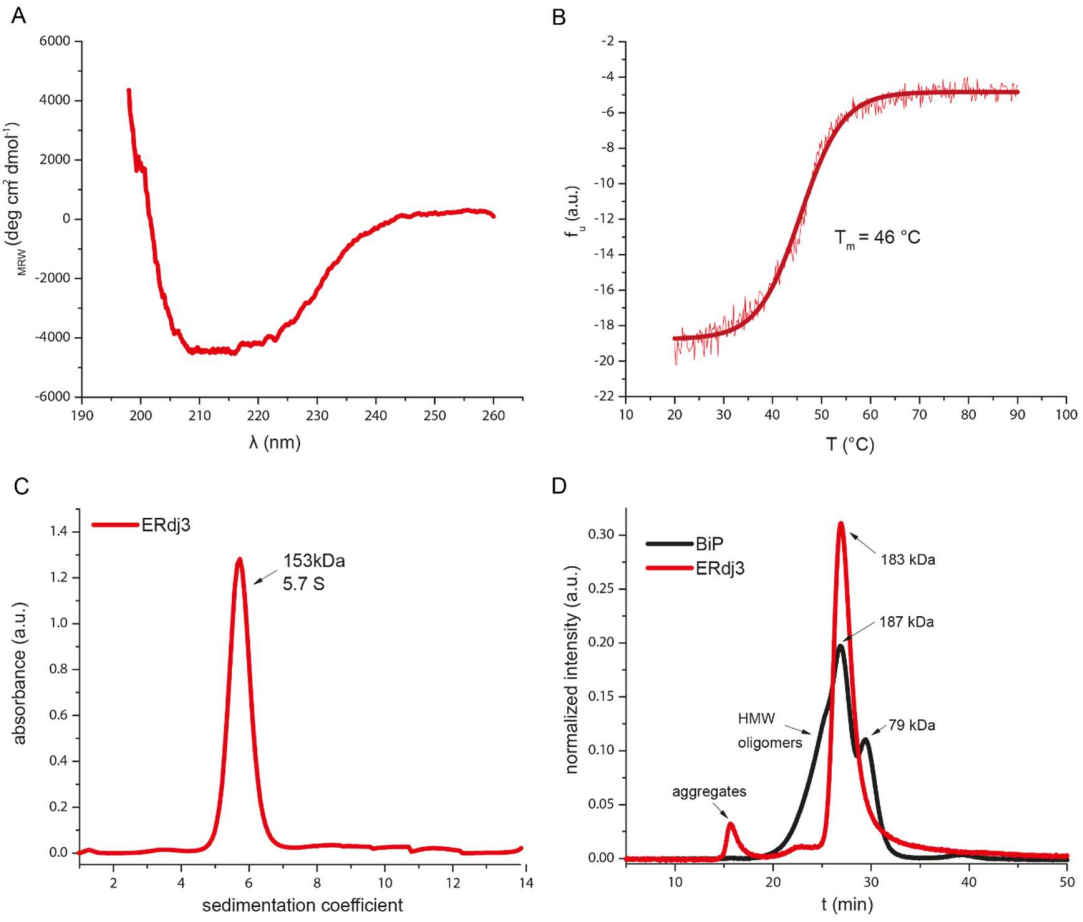

Figure 19: Structural analysis of hERdj3 protein. A) FUV-CD spectra of 0.65 mg/ml ERdj3 in PBS measured in a 0.2 mm cuvette. B) Thermal denaturation of 0.5 mg/ml ERdj3 measured in the CD spectroscopy at 222 nm in 1 mm cuvette in HKM buffer. The obtained melting curve was fitted with the Boltzmann fit. C) Analytical ultracentrifugation of ERdj3 using the absorption at 280 nm. Data was evaluated using SedFit. D) HPLC analysis of 10 µM BiP or ERdj3 on a S200 column in HKM buffer.

The FUV spectra of ERdj3 displayed a folded structure which seems to be a mixture of α-helices and β-sheets with a broad minimum between 208 and 218 nm (**Figure 19** A). Structural prediction using the K2d algorithm on the Dichroweb platform [137–139] suggests a 51 % random coil structure with about 19 % α-helices and 30 % β-sheets.This result is also supported by the secondary structure prediction tool Phyre2 (**Figure 7**, **Figure 20** [92]). There, it is assumed that about 21 % of the protein are α-helices and 28 % are β-sheets. The model of ERdj3 by Phyre2 can be seen in **Figure 7**. The protein also seems to be stable, as it unfolds upon thermal denaturation starting at 30 °C and with a melting temperature of 46 °C. The unfolding can be fitted with a Boltzmann fit (**Figure 19** B). The quarternary structure of ERdj3 was investigated using analytical ultracentrifugation and SEC-HPLC measurements. In AUC measurements, one single species was obtained at a sedimentation coefficient of about 5.7 S (**Figure 19** C). SedFit analysis resulted in a value of 153 kDa for the 5.7 S species which fits very well to an ERdj3 tetramer.

SEC-HPLC measurements of BiP show the known distribution of monomers, dimers and higher molecular weight oligomers (**Figure 19** D). Comparison with an HPLC standard revealed that the monomer peak of BiP is ~73 kDa as expected. It represents 25 % of the species seen in SEC-HPLC. The dimer peak with a calculated size of about 187 kDa is about 45 %. Higher molecular weight oligomers are ~30 % of the species as calculated by integration. For ERdj3 one single species with about 80 % of signal intensity was observed whereas the rest seems to form aggregates. The retention time of about 26.9 min fits the retention time of the BiP dimer. The calculated size of the protein eluting in this peak is 183 kDa, which would again fit a tetrameric ERdj3 protein.

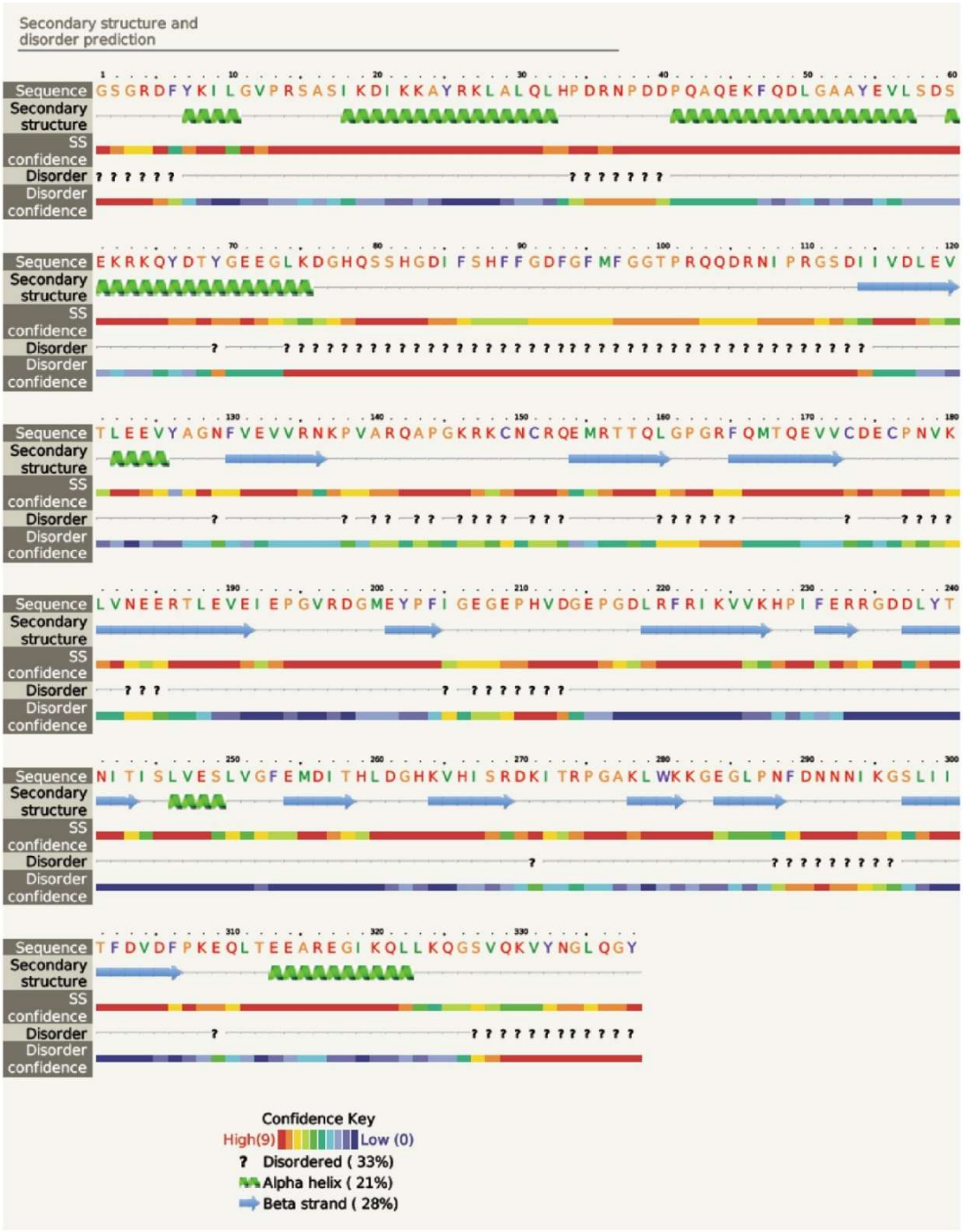

Figure 20: Secondary structure prediction of human ERdj3 using Phyre2.

3.2.4. Grp170

Grp170 is a NEF for BiP and belongs to the group of Hsp110 chaperones. To characterize the protein, FUV-CD spectroscopy was performed. Grp170 shows an α-helical CD spectrum with a stronger minimum at 208 nm (**Figure 21** A, C).

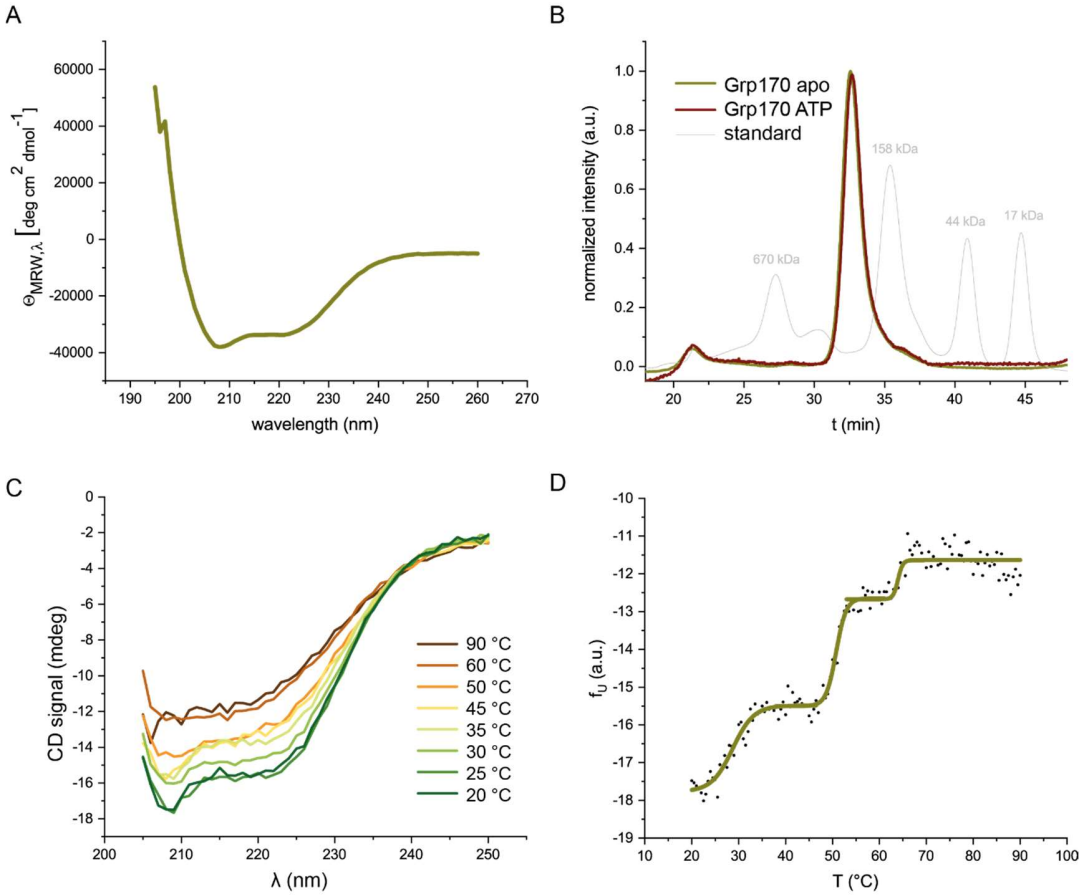

Figure 21: Characterization of Grp170. A) FUV-CD spectra of Grp170 at 20 °C in a 1 mm cuvette at 0.5 mg/ml concentration in HKM. B) SEC-HPLC run of 10 µM Grp170 on S200 column. C) FUV CD spectra of Grp170 at different temperatures. (D) Thermal unfolding of Grp170 at 208 nm at the same conditions used for FUV-CD.

Grp170 unfolds in three steps with the first one occurring around 30 °C, the second step ~ 50 °C and a third at ~ 65 °C (**Figure 21** C, D). On SEC-HPLC, it elutes as a single species with a retention time of around 32 min (**Figure 21** B). Some higher oligomers can be detected at shorter retention times independent of the nucleotide status. Reducing the concentration in the SEC-HPLC run still leads to elution as a single peak with a retention time of around 32 min.

3.2.5. Discussion

BiP wt shows a predominantly α-helical CD spectrum with two minima at 208 and 222 nm. This is a typical spectrum for a protein consisting mainly of α-helices. This is in line with the published crystal structure [44] where the NBD is a mixture of α-helices and β-sheets whereas the SBD consist of an β-sheet part and a lid consisting of α-helices. Therefore, SBD alone has a broad minimum around 220 nm. This is in line with a mixture of α-helices and β-sheets, which exhibit a minimum at 218 nm. The CD spectrum of the Δ-lid mutant is similar to that of the wt. The two thermal transitions for the wt were expected [123,135,140] and represent the unfolding of the different domains of BiP [140]. Interestingly, Grp170 shows three unfolding transitions at 208 nm. BiP-NBD and BiP-Δlid alone exhibit a one-phase transition at around 40 °C whereas the BiP-SBD has two transition. One explanation is the unfolding of the individual domains, which differ significantly in their thermal stabilities and lead to the characteristic transition. However, BiP-Δlid, which also has two domains has a one-fold transition. Another conclusion is that the BiP-SBD with lid can bind itself as substrate and therefore stabilize the protein in a holdase manner. BiP binding to itself via its SBD has been shown previously and is an important factor for oligomerization of BiP and as a storage form [141]. Only upon full unfolding of the protein at more than 60 °C the rest of the protein fully unfolds (**Figure 15**).

The Bap constructs Bap wt and Bap-C are very similar in structure and stability (**Figure 16**). These results are in agreement with results obtained by Mathias Rosam [123] for these proteins, although the expression and purification protocol were different. The unfolded N-terminal domain does not have a measureable influence on the stability, although the secondary structure is slightly affected.

Some NEFs of Hsp70 chaperones show dimer or oligomer formation which is associated with their functionality [109]. However, for Bap no data on quarternary structure was available so far, although it has been discussed for the yeast homolog [114]. The dimerization behavior of Bap is different than expected from published results for yeast Bap, where dimerization for the full length protein was detected but not for the C-terminal part [114]. Here, SEC-HPLC and AUC data (**Figure 17**) only gave one peak for Bap and Bap-C. Taking together, it can be concluded that, different from the results by Yan et al., 2001 [114], both Bap and Bap-C are only present as monomers. The shoulder, detectable for Bap wt in the SEC-HPLC measurement (**Figure 17**) might correspond to the degradation product, which is visible in SDS gels for

purified Bap wt and has approximately the size of Bap-C (**Figure 13**). The degradation of Bap is also described in the literature [114] and can be also seen in the SEC-MALS measurements as a small peak with the size of 37 kDa **(Figure 17**). As judged from the dynamics revealed in the HDX data obtained for Bap (**Figure 25**), it might be possible that Bap is cleaved by proteases at the aa VVIET motif (aa 175-180) which leads to a fragment with a weight of around 32 kDa, which is the approximate size of the product visible on SDS-PAGE gels and in SEC-HPLC.

Grp170 exhibits nine predicted glycosylation sites [100]. Bacterial expressed Grp170 is not glycosylated but it has been published that it is still able to stimulate ADP release from BiP in a concentration-dependent manner [52].Regarding dimerization, Grp170 also showed an unexpected behavior. It elutes as a single species in the SEC-HPLC experiments that probably corresponds to a monomer as it cannot be changed by addition of nucleotide or reducing the concentration on the column. This is unexpected since BiP or other Hsp70s which have a strong structural similarity to Grp170 show oligomerization in a concentration- and nucleotide-dependent manner.

ERdj3 contains α-helices in its J-domain (**Figure 20**, **Figure 7** grey/green) and in the dimerization domain (orange), whereas the substrate binding domain contains mainly β-sheets. This is in line with the FUV-CD spectrum **(Figure 19** A) and the predictions performed (**Figure 20**). Most Type II Hsp40 co-chaperones, like DnaJ or Hdj1dimerize and crystal structures of these dimers are available [142,143]. It has been shown that ERdj3 functions as a dimer or a multiple of a dimer [76,90]. Comparing AUC, SEC-MALS and SEC-HPLC data of ERdj3, we can conclude that human ERdj3 indeed is a tetramer in solution. (**Figure 19**). This is in line with recent publications, where ERdj3 has also been found as a tetramer in AUC and SEC-HPLC experiments [93] and negative stain EM structures suggest that ERdj3 is a dimer of dimers forming a ring with the J-domains in the middle [93].

3.3. Interplay of BiP and its co-factors

3.3.1. ATPase rate of different BiP mutants

The functional cycle of Hsp70 chaperones is highly dependent on ATP binding and hydrolysis [144]. Different co-factors play an important role in controlling this cycle. J-domain containing proteins are known to accelerate the ATP hydrolysis but also nucleotide exchange factors are critical for the chaperones to be able to cycle between the different nucleotide states. However, different Hsp70 chaperones exhibit different ATP hydrolysis rates and are stimulated by different co-factors [145]. Using a steady state ATPase assay, different mutants of BiP and DnaK were tested for their ability to hydrolyse ATP in absence of any co-chaperones (**Figure 22**).

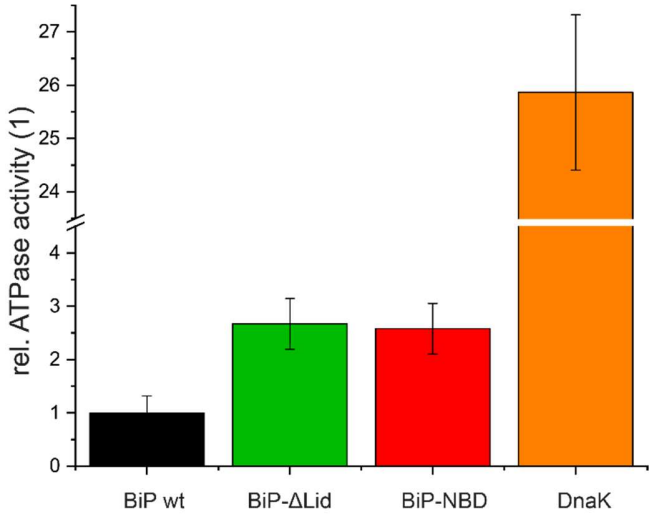

Figure 22: Steady state ATPase assay performed at 37 °C with 2 µM of the respective chaperone. The values for BiP were set to 1 (black) and can be directly compared to the lidless mutant (green), the nucleotide binding domain (red) and the bacterial Hsp70 chaperone DnaK (orange). The assay was measured at least in triplicates.

The k_{cat} values used for **Figure 22** are shown in **Table 3**. The k_{cat} values for wildtype BiP in this assay were around 0.2 min^{-1} and the value was set to 1, to make it easier to compare the data. Both mutants of BiP tested (BiP-Δlid in green and BiP-NBD in red) show an increased ATPase rate. This can be also seen in the k_{cat} values obtained in this experiment. Here, BiP-Δlid and BiP-NBD hava a k_{cat} of around 0.5 min^{-1}. The *E. coli* Hsp70 DnaK shows the highest ATPase rate which is ~ 26-fold higher than that of BiP and a k_{cat} value of around 5 min^{-1}.

Table 3: Steady state ATPase assay performed with 2 µM of chaperone. Depicted are the ATPase assay-derived k_{cat} values of ATP hydrolysis.

Protein	k_{cat} (min^{-1})
BiP	0.20 ± 0.08
BiP- Δlid	0.54 ± 0.18
BiP-NBD	0.52 ± 0.10
DnaK	5.30 ± 0.30

3.3.2. Grp170 interacts with BiP

To test the interaction of Grp170 with BiP, an AUC experiment was performed. 0.6 µM Atto488-labelled BiP-167C was mixed with 5 µM of Grp170 in the apo state (**Figure 23**).

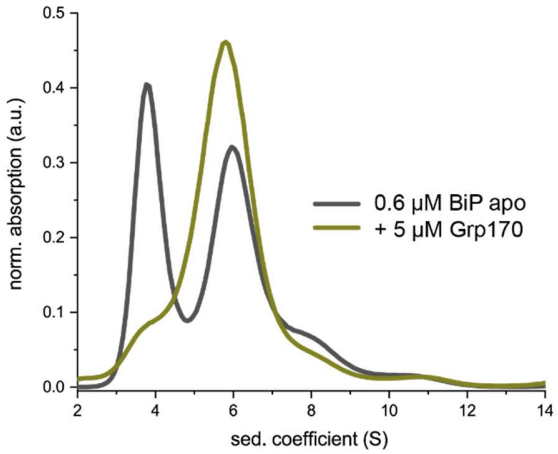

Figure 23: AUC run with 0.6 µM Atto488-labeled BiP (167C) and 5 µM Grp170 in the apo state.

BiP alone forms monomers at around 3.9 S, dimers and higher oligomers in the apo state. Addition of Grp170 shifts the peak to around 6.4 S, probably being the complex of BiP and Grp170, whereas the monomer peak at 3.9 S almost vanishes completely except for a little shoulder at 3.9 S.

3.3.3. *Bap interacts with BiP*

To verify the interaction between BiP and Bap and to calculate K_d values for this interaction, AUC measurements were performed. To rule out an effect of the labeling position for the Atto488 dye, two titrations with different labels on BiP were performed and evaluated (**Figure 24**).

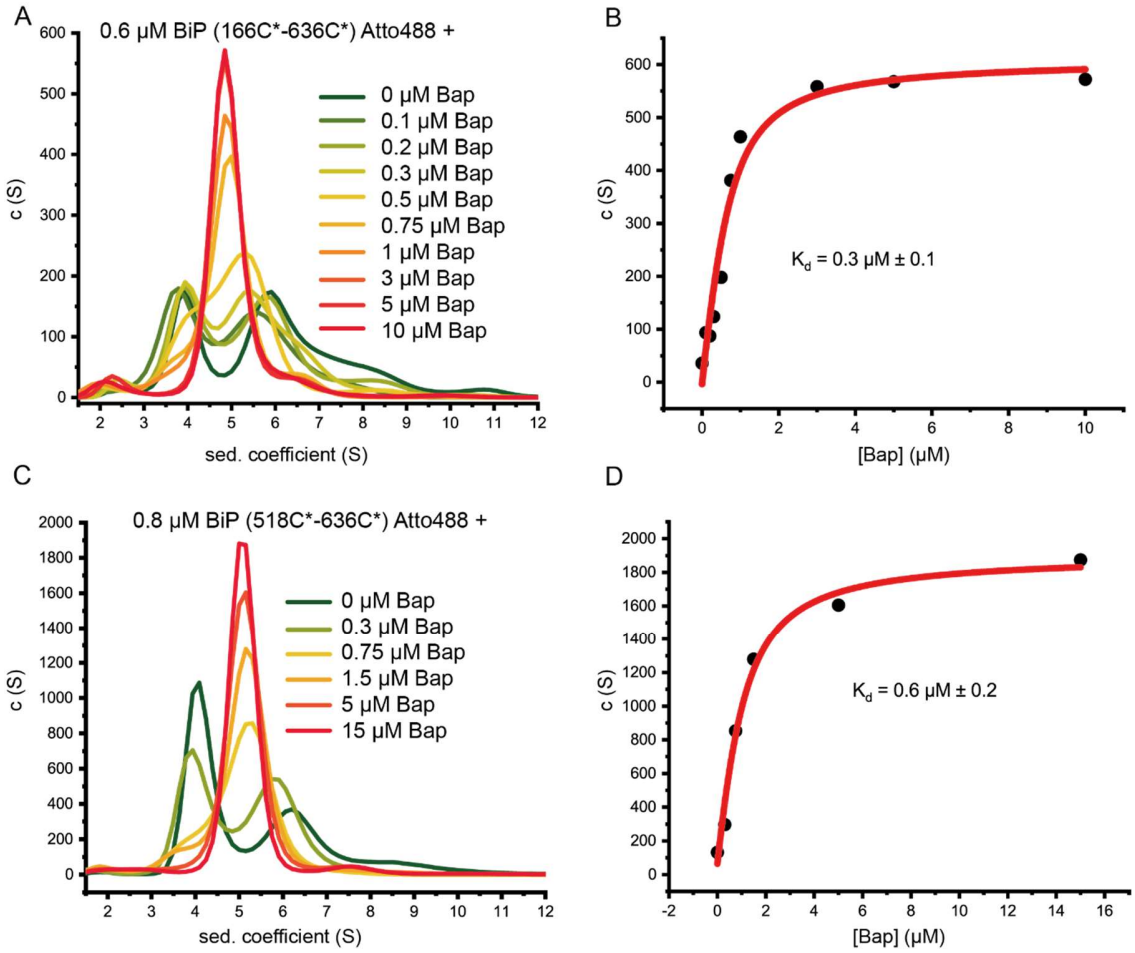

Figure 24: AUC titration of Atto488-labeled BiP and Bap without nucleotide. A) BiP labeled at position 167 and 638 and addition of Bap in increasing concentrations (green to red). C(S) value at 4.8 S lead to B) measurement points for measuring the K_d of the interaction. C) BiP labeled at position 519 and 638 and addition of Bap in increasing concentrations (green to red). C(S) value at 5.2 S lead to D) measurement points for measuring the K_d of the interaction.

The AUC runs were performed under apo conditions and binding of Bap leads to a signal increase at around 5 S which correlates with a size of 120 kDa and is between the monomer and the dimer peak of BiP. This size is the complex of the BiP monomer binding to Bap. Plotting the c(S) values and the concentration of Bap allows to determine the K_d value. The K_d is 0.3 µM (BiP 167C-638C) or 0.6 µM (BiP

519C-638C) (**Figure 24** A,B and C, D respectively). Thus, the labeling position does not seem to have an effect on the calculated K_d. Furthermore the value is similar to the K_d reported in the AMP-PNP state [123].

To investigate the interaction of Bap with BiP and its effect on Bap protein stability, H/DX-MS measurements were performed. This method detects the exchange of hydrogen atoms bound to heteroatoms in the protein against deuterium. The resulting mass shift of the peptides is detected by mass spectrometry. First, Bap alone was investigated (**Figure 25** A, **Figure 26**).

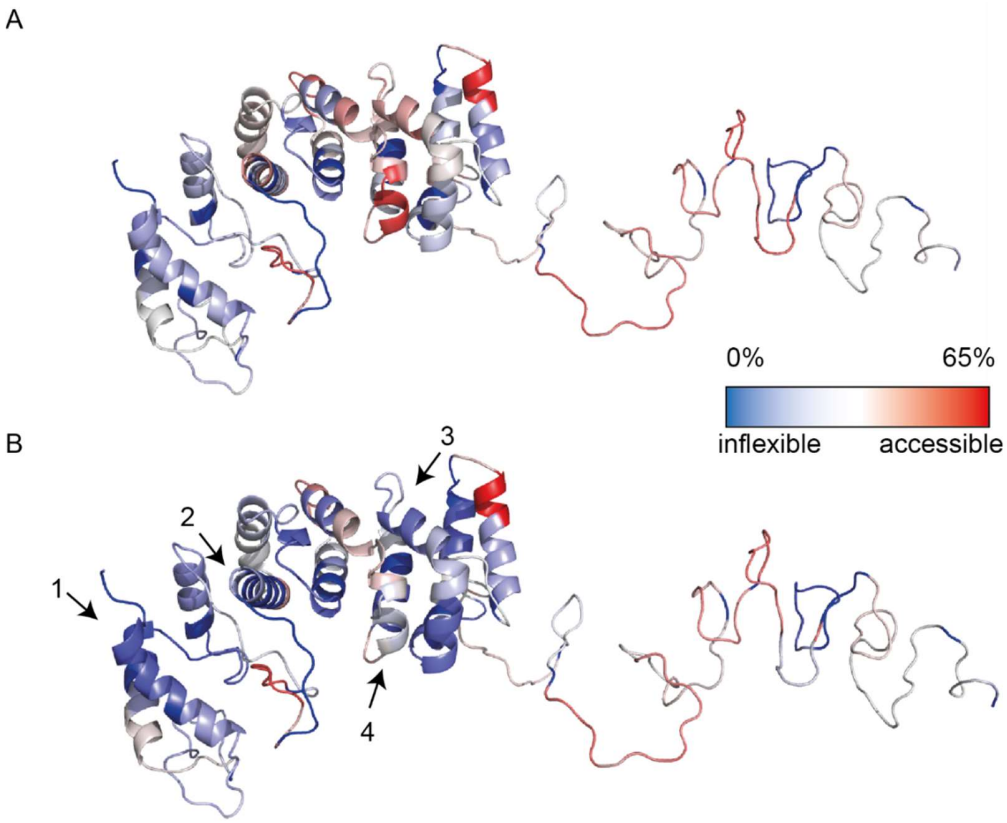

Figure 25: HDX data of Bap in the presence or absence of BiP with 1 mM ADP mapped on the modelled structure of hBap after 30 min. A) B-values on structure for Bap alone or B) in complex with BiP. Black arrows show areas with a difference in HDX of Bap alone and in complex with BiP. Corresponding heat maps are depicted in **Figure 26**.

The red color indicates areas, where a strong exchange is detected and where the protein seems to be flexible and therefore also easily accessible for hydrogen exchange. This means that also proteases might easily attack at these positions. Areas in blue show almost no hydrogen exchange and are therefore very inflexible areas.

If Bap is pre-incubated with BiP and then the H/DX-MS is performed, it gives a hint on the areas that are important for binding. It can be clearly seen, that addition of BiP has an effect on the flexibility and accessibility of Bap, since regions with increased exchange are observed (**Figure 25** B). Except for some areas with no change like the first helix in the C-terminal domain, Bap shows less hydrogen exchange and is therefore less flexible when BiP is bound. The mainly unfolded N-terminal domain shows no big difference when bound to BiP but in the C-terminal region four major areas (**Figure 25** B, black arrows) exhibit a strong decrease in flexibility upon interaction with BiP. Arrow 1 is the very C terminus of Bap that is also known to be important for Bap stability and functionality [117]. Region 2-4 are in the armadillo repeat region, where the NEF function of Bap is located.

To have a better overview for hydrogen exchange over time, a heat map was prepared from the H/DX-MS data (**Figure 26**). Here, hydrogen exchange over time can be seen and the differences between Bap alone and in complex with BiP are also visible. Regions that have high deuterium uptake are in yellow and correspond to the regions that are red in the structural data. The N-terminal domain seems to be more flexible compared to the rest of the protein independent of BiP binding. At amino acids R187-V231, L273-T318 and E375-L405, regions with a strong exchange over time are visible. The aa R187-V231 are in the first armadillo-like repeat (ARM1). L273-T318 are in Helix 8-10 and are just between ARM2 and ARM3. E375-L405 is at Helix 14 and 15 which is part of ARM4.

To complement the H/DX measurements, limited proteolysis was performed with BiP and Bap. A stabilizing effect of binding to BiP can also be seen by limited proteolysis with the protease α-Chymotrypsin. This protease has a molecular weight of around 25 kDa and catalyzes hydrolysis of peptide bonds on the C-terminal side of the amino acids Tyr, Phe, Trp and Leu.

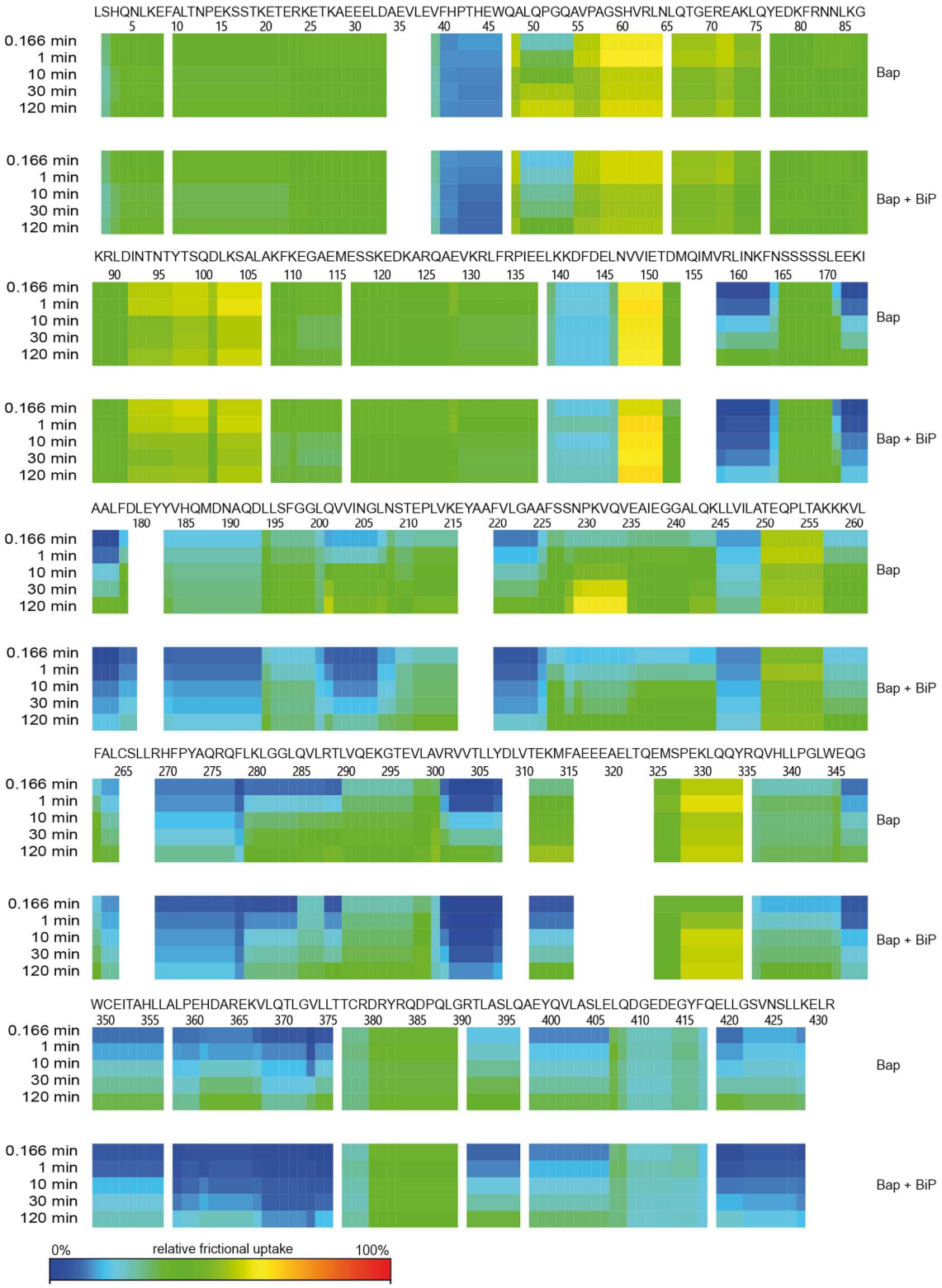

Figure 26: Heat map of H/DX measurements performed with Bap and BiP and Bap over time.

Chymotrypsin autolyses into fragments of 7 and 10 kDa, which can be seen on the gel. BiP gets rapidly degraded in many smaller fragments that stay mostly stable over 90 min (**Figure 27** A).

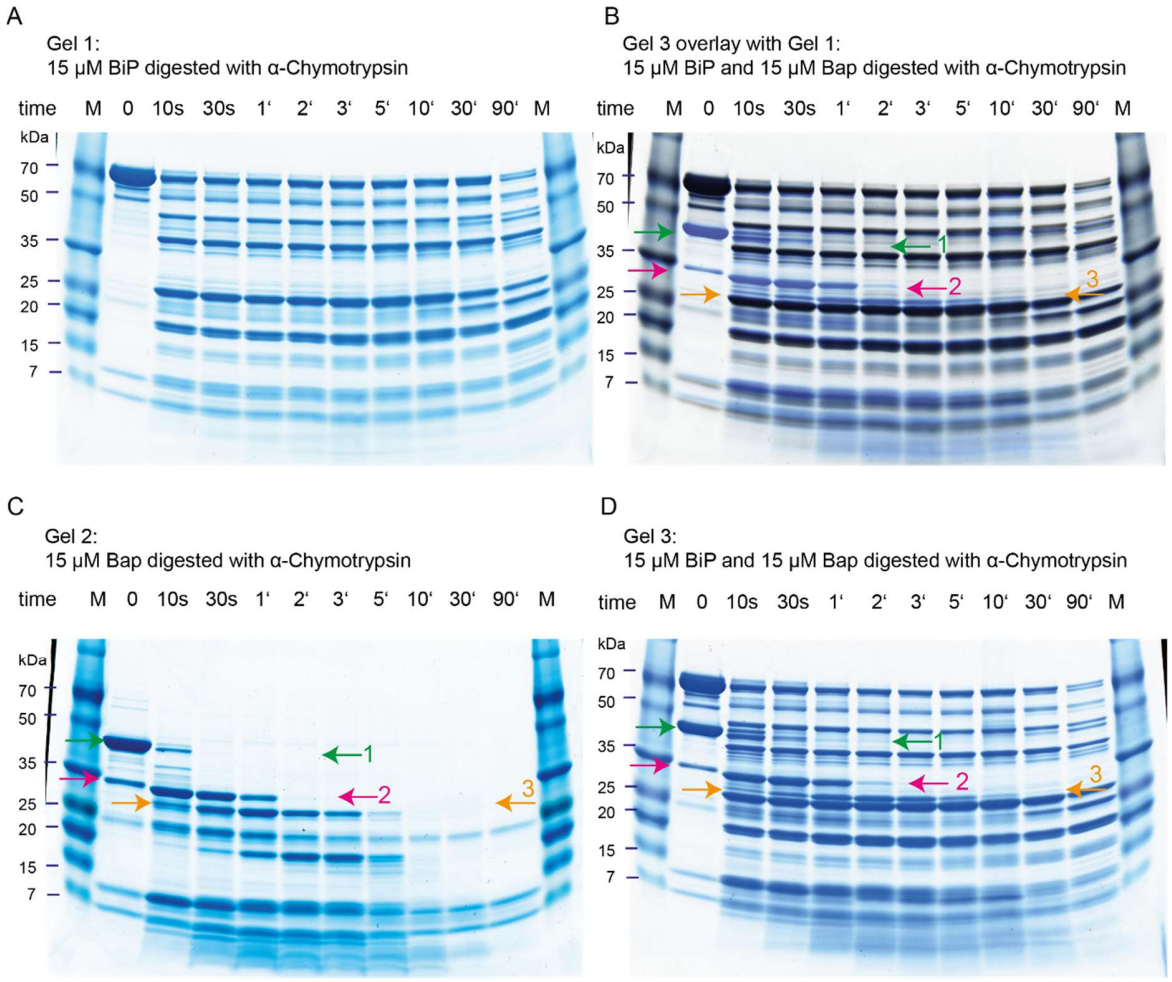

Figure 27: Limited proteolysis with α-Chymotrypsin in a 1:5 ratio at room temperature. A) Limited proteolysis of 15 µM BiP B) and D) Limited proteolysis of 15µM BiP and 15 µM Bap each. B) The Gel depicted in A) is overlayed on D) and in black to see the bands from Bap digestion which can be compared to C) limited proteolysis of 15 µM Bap. The different species that occur during digestion are marked with arrows in green (species 1), magenta (species 2) and orange (species 3).

This strong fragmentation makes it difficult to detect the single bands of Bap in the combined gel (**Figure 27** D). Bap alone is rapidly degraded by chymotrypsin and is overall far less stable than BiP, since the intact protein is already completely cut after 30 s (**Figure 27** C). The rest of the smaller fragments of Bap is degraded after 5 min. Digestion of Bap and BiP leads to a complex picture. However, some bands of the degradation of Bap can be followed over time and clearly distinguished from the BiP degradation

products (**Figure 27** B, bands in blue and marked with arrows). Species 1 (green arrows) is already completely degraded after 30 s but is stabilized by BiP until approximately 3 min. Species 2 (magenta arrow) is already visible after purification of Bap and can be detected upon chymotrypsin digestion for 1 min before it gets fully degraded. This species is also stabilized 1 min longer by BiP. Species 3 (orange arrows) is formed after 10 s, has a strong band at 1 min and then it diminishes until it is fully degraded at around 5 min. Upon interaction with BiP, this band is stable for 30 min. These results suggest that the interaction of BiP with Bap stabilizes the latter against degradation with chymotrypsin by influencing its flexibility.

3.3.4. Bap is a NEF for BiP

Bap is described as a nucleotide exchange factor for BiP. To test this, BiP was pre-incubated with MABA-labeled ADP and different concentrations of Bap. Upon addition of high amounts of unlabeled ADP, the nucleotide exchange was measured by a chase setup in a the stopped-flow instrument (**Figure 28**).

The data was best fit with a single exponential fit with a linear slope to take photo bleaching into account. The linear slope in each curve is very similar with around 0.1. The rate constants for ADP release can be seen in **Table 4** with the accuracy of the fit in %.

BiP shows a k_{off} rate of around 0.11 s^{-1}. This rate can be increased by addition of both Bap and Bap-C in a concentration-dependent manner. Addition of 6 µM (20-fold excess) of Bap increases the off-rate by a factor of more than 2.5 (**Figure 28** A).

Bap-C increases the off rate even more than wt with a factor of ~ 4 for a 20-fold excess of Bap-C over BiP (**Figure 28** B). Stimulation of BiP by Bap-C shows the highest off rate measured in this setup (k_{off} = 0.48 s^{-1}). Bap-N did not show any effect on nucleotide release by BiP.

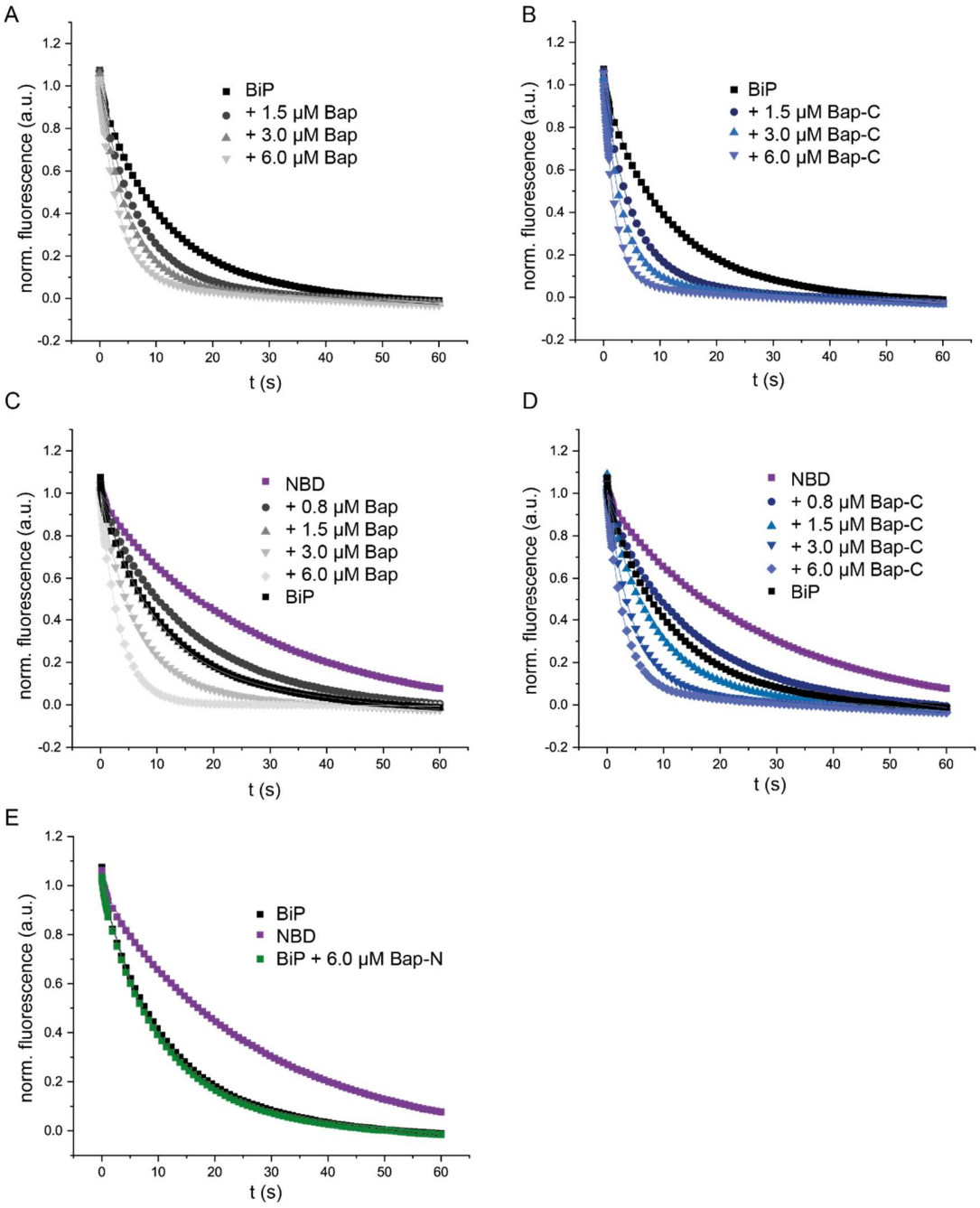

Figure 28: Nucleotide release from BiP or BiP-NBD in the presence of Bap proteins. BiP's ADP release alone or in presence of increasing concentrations of A) Bap and B) Bap-C. C) Nucleotide release from BiP-NBD with increasing concentrations of Bap and D) Bap-C. E) Comparison of ADP release from BiP, BiP-NBD and BiP+Bap-N. Addition of Bap-N to BiP showed no change in the release rate (black and green curve).

Table 4: Release rate k_{off} of MABA-ADP in stopped flow experiments in Figure 28 and Figure 47. Curves were fitted with a single exponential fit with a linear slope.

protein	k_{off} (s^{-1})	Deviation in %
0.3 µM BiP	0.11	2
+ 1.5 µM Bap	0.16	2
+ 3 µM Bap	0.21	1
+ 6 µM Bap	0.29	1
+ 1.5 µM Bap-C	0.20	1
+ 3 µM Bap-C	0.31	1
+ 6 µM Bap-C	0.48	1
+ 6 µM Bap-N	0.11	2
0.75 µM BiP + 15 µM ERdj3	0.03	3
0.75 µM BiP + 15 µM ERdj3 + 1.5 µM Bap	0.05	2
0.75 µM BiP + 15 µM ERdj3 + 3 µM Bap	0.06	1
0.75 µM BiP + 15 µM ERdj3 + 6 µM Bap	0.09	1
0.3 µM NBD	0.06	5
+ 0.8 µM Bap	0.09	2
+ 1.5 µM Bap	0.14	2
+ 3 µM Bap	0.23	1
+ 6 µM Bap	0.35	1
+ 0.8 µM Bap-C	0.08	3
+ 1.5 µM Bap-C	0.12	2
+ 3 µM Bap-C	0.17	1
+ 6 µM Bap-C	0.30	1

The NBD alone exhibits a 2-fold slower ADP release than BiP wt (**Figure 28** E, **Table 4**) but can be stimulated by both Bap and Bap-C to a higher extent than full-length protein. Addition of Bap in the

highest concentration measured stimulated BiP-NBD by a factor of almost 6 (**Figure 28** C), addition of Bap-C by a factor of 5 (**Figure 28** D). This k_{off} is similar to the stimulation of BiP by Bap.

3.3.5. Bap has a function additional to nucleotide exchange

Bap stimulates ATPase activity

The influence of both J-proteins and NEFs is known to also play an important role in the cycle of Hsp70 chaperones. Bap stimulates the ATPase rate of BiP [115,131]. To further investigate this, steady state ATPase assays were performed (**Figure 29**).

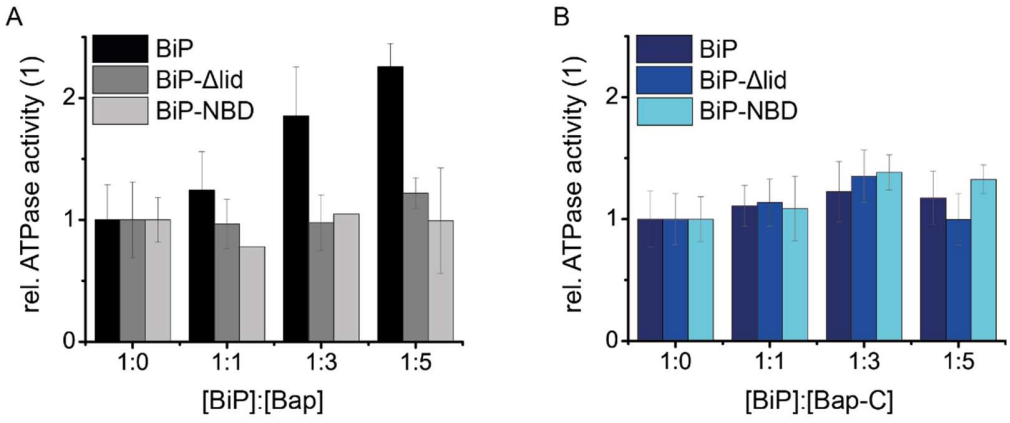

Figure 29: Steady state ATPase assay at 37 °C with 2 µM BiP, BiP- Δlid and BiP-NBD upon addition of A) Bap or B) Bap-C. The values for the ATP hydrolysis rate without co-factor were set to 1.

Since k_{cat} values of BiP vary with the age of the frozen protein, the time on ice and the amount of freeze and thaw cycles, the hydrolysis rate for BiP alone was normalized and set to 1 [123]. The effect of the addition of Bap or Bap-C is depicted in relation to the BiP ATPase rate (or BiP mutants). Bap or Bap-C alone do not show any ATP hydrolysis except for the autohydrolysis of ATP (**Figure 32** B, last two bars). Addition of Bap wt to BiP shows a concentration-dependent increase in BiP's ATPase activity (**Figure 29** A). Interestingly, addition of Bap to BiP mutants lacking the lid (BiP-Δlid, dark grey, and BiP-NBD, light grey) does not lead to a stimulation of ATP hydrolysis. Addition of Bap-C to BiP or its mutants also results in no stimulation of ATP hydrolysis (**Figure 32** B). Only Bap wt is able to stimulate ATP hydrolysis in BiP wt. ATP hydrolysis rate of BiP was not stimulated by Bap-N in the concentrations tested (**Figure 30**).

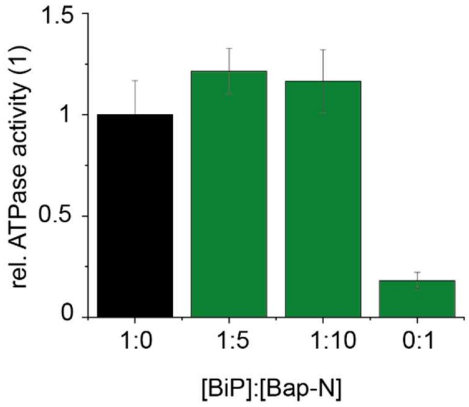

Figure 30: Steady state ATPase assay at 37 °C with 2 µM BiP and Bap-N. The values for the ATP hydrolysis rate without co-factor were set to 1 (black bar).

As described in 3.1.1, DnaK is usually co-purified with Bap and several columns are needed to get rid of these DnaK impurities. To investigate the influence of DnaK on Bap and vice versa, experiments using impure Bap batches were performed. Impurities are only weakly visible on the gel running at around 70 kDa (**Figure 31**, inlay marked by black arrows).

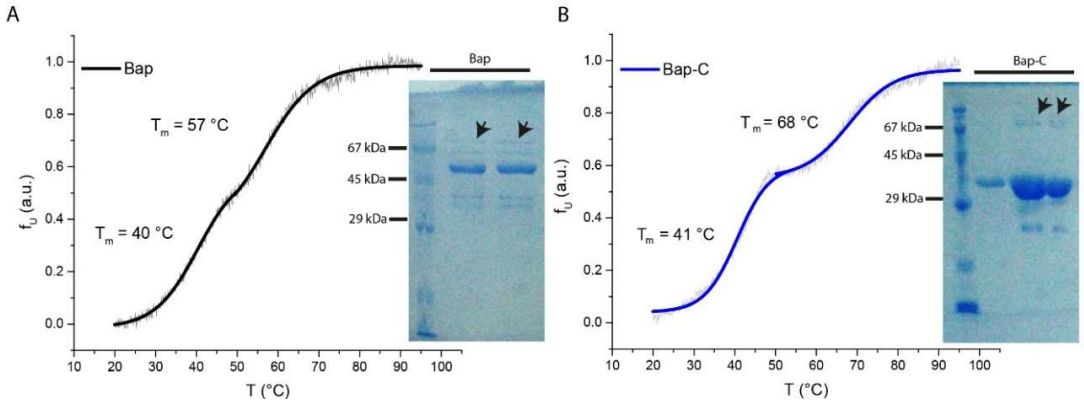

Figure 31: Bap with DnaK impurities shows differences in the thermal unfolding. Unfolding of A) Bap wt and B) Bap-C. The inlays show pictures of the SDS-PAGE gel of the purified proteins.

CD spectra using these batches showed no difference to the CD spectra in **Figure 16** A and are therefore comparable to the spectra with pure Bap. Thermal transition experiments, however, show a two-step denaturation of Bap and Bap-C (Figure 31). The melting points of Bap are 40 °C and 57 °C and the melting points for Bap-C are 41 °C and 68 °C which is similar to the thermal unfolding of the Hsp70 BiP in **Figure 15**.

Next, it was tested whether these impurities have an impact on the ATPase stimulation (**Figure 32**). It has already been shown that the intrinsic ATPase rate of DnaK is higher than that of BiP (**Figure 22**). Bap-C alone already seems to have an ATPase activity since higher concentrations of Bap-C lead to a stronger decrease in ATP (**Figure 32** A, purple bars). This is probably not due to Bap-C, but the contamination with DnaK. Addition of this Bap-C batch to BiP also shows a concentration-dependent stimulation of BiP's ATP hydrolysis with no saturation at concentrations of 10 µM Bap-C. This is in strong contrast to ATPase assays with pure Bap-C which show no stimulation of BiP's ATPase rate (**Figure 29** B).

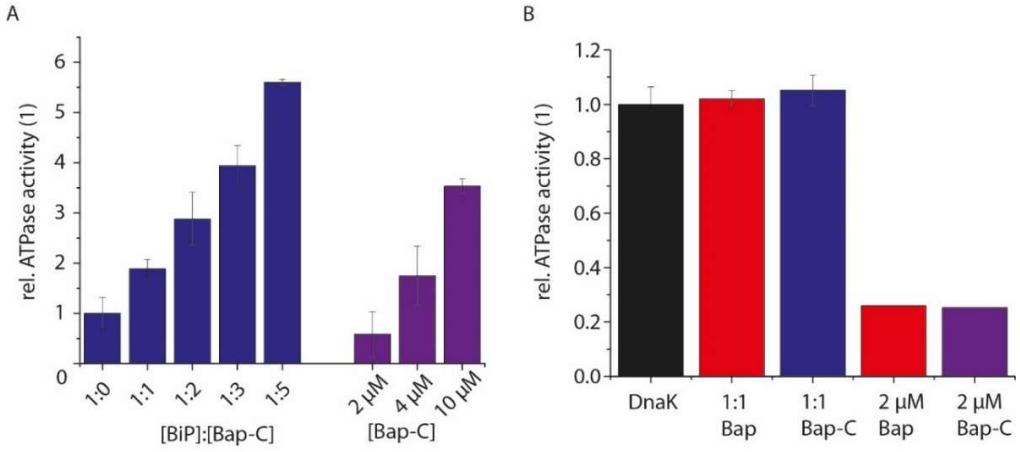

Figure 32: ATPase stimulation of A) BiP by Bap-C that is contaminated with DnaK (blue). In purple ATPase activity of only Bap-C is shown at different concentrations. ATPase stimulation of B) DnaK with pure Bap (red) or Bap-C (blue).

To test if this stimulation is only because more DnaK is added upon increasing the Bap-C amount in the assay, it was tested whether Bap or Bap-C is able to stimulate DnaK's ATPase rate. Bap is a human NEF for BiP and no homolog is known in the bacterial system that interacts with DnaK. The study of this interaction is therefore only relevant for *in vitro* studies of bacterially expressed and purified Hsp70 NEFs and to better define the potential "non-specific" background of this experimental system. For this experiment, Bap and Bap-C without DnaK impurities was used (**Figure 32**). As in the ATPase assays with BiP, the intrinsic ATPase activity of DnaK was set to 1 and no stimulation by Bap or Bap-C of the DnaK ATPase activity was detected. Bap and Bap-C have no intrinsic ATPase acitivity, which directly verifies the quality of the protein in this assay.

Role of the N-terminal domain of Bap

Structure of the N-terminal domain

The role of the N-terminal domain of Bap remained enigmatic to this point. This domain has been defined as the part of the protein that degrades when Bap is purified [114]. Also, it was found to be unnecessary for nucleotide exchange. In the CD spectra this domain seems to be mainly unfolded (**Figure 16** A). To get better insight in the structure, different structural prediction tools were used.

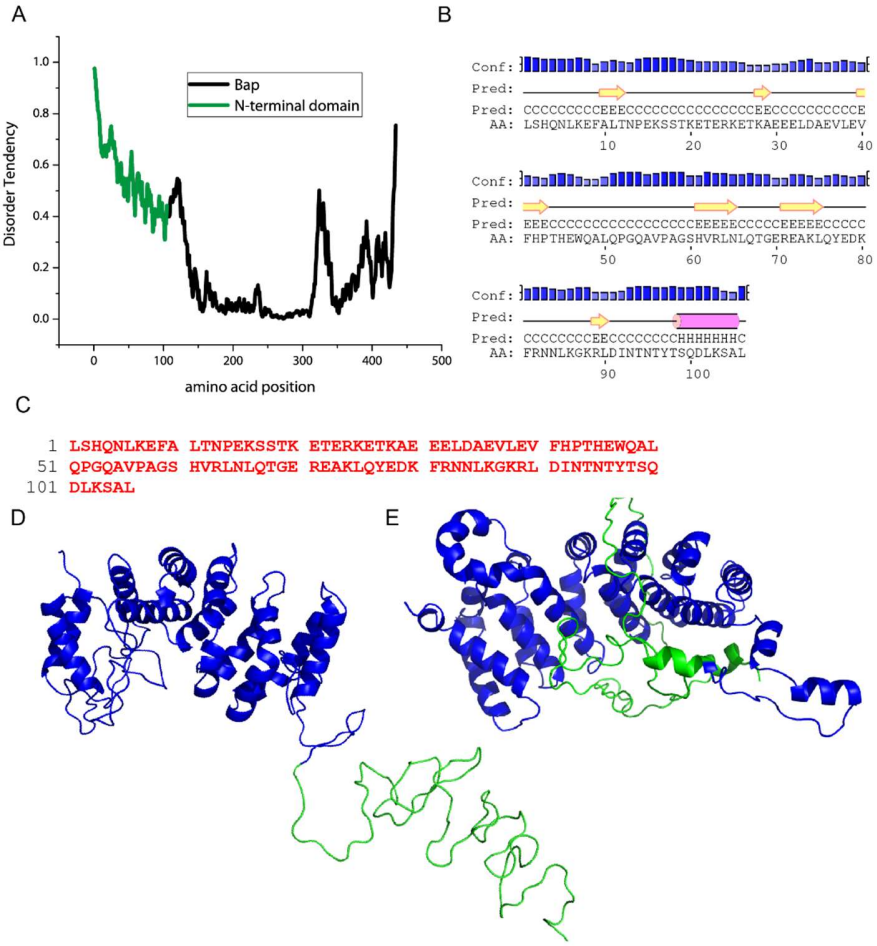

Figure 33: Structural characterization of Bap's N-terminal domain. A) Structural prediction using iupred showed a high disorder tendency for the N-terminal domain (green), whereas most of the core seems to be structured. B) Psipred analysis predicts mainly coiled structures (C, black line) for Bap-N with some possible β-sheets (E, yellow arrow) and a helical part (H, pink cylinder). C) Prediction with FoldIndex of the first 106 aa of Bap predicted a disordered segment (in red). D) Modelling the full-length hBap with Phyre2 resulted in a structure with the characteristic armadillo repeats at the core (Bap-C, blue), a small helical part in the N-terminal domain (green) and a mainly unfolded protein chain wrapping around the core. E) Modelling with MODELLER integrated in Chimera, based on the scSil1 structure (PDB-ID: 3QML). The core (Bap-C, blue) shows the armadillo repeats and Bap-N (green) is modelled as a long protein chain.

Looking at Bap-N alone, FoldIndex [146] suggests a completly unfolded structure. Prediction of the secondary structure using iupred [147] yields a similar result. Here, the first 105-120 aa show a high disorder tendency. Also using PsiPred [148,149], a similar result was obtained and except for a slight α-helical part, the protein consists mainly of random coil structure.

We tried modelling the N-terminal domain using Chimera MODELLER [46] and Phyre2. As can be seen in **Figure 33** D and E, this modeling suggests a compact form of the N-terminal domain around the Bap core in its unbound form. But Bap-N is very likely a flexible domain of Bap that can fulfill its function in the protein. However, this function is still enigmatic although ATPase assays suggest a role for Bap-N in ATP hydrolysis stimulation of BiP (**Figure 29**).

Bap-N and other substrates of BiP

In former studies, predicitons for BiP binding sites in substrate proteins were performed with an algorithm called BiPPred [71]. Chase anisotropy measurements with labelled peptides were performed to test different peptides for their ability to displace the peptide HTFPAVL (derived from the C_H1 antibody domain) from the BiP-SBD [57]. Ly-labeled HTFPAVLGSC was bound to BiP and then a 150-fold access of peptide was added. Results were compared to a chase with unlabeled HTFPAVL. The obtained kinetics for peptides derived from C_H1 can be seen in **Figure 34**.

The displacement efficiency was calculated by dividing the amplitude of the displacement against the amplitude of the binding of HTFPAVL-Ly to BiP. The binding and release of substrate was fitted with a single exponential fit and the obtained on and off rates can be seen in **Table 5**.

ATPase assays as well as structural analysis and binding predictions with BiPPred suggest that Bap-N might also be a substrate of BiP. Bap-N is unstructured with hydrophobic patches. In the modelled complex it is close to the SBD in BiP and its presence stimulates BiP's ATPase activity (**Figure 29**).

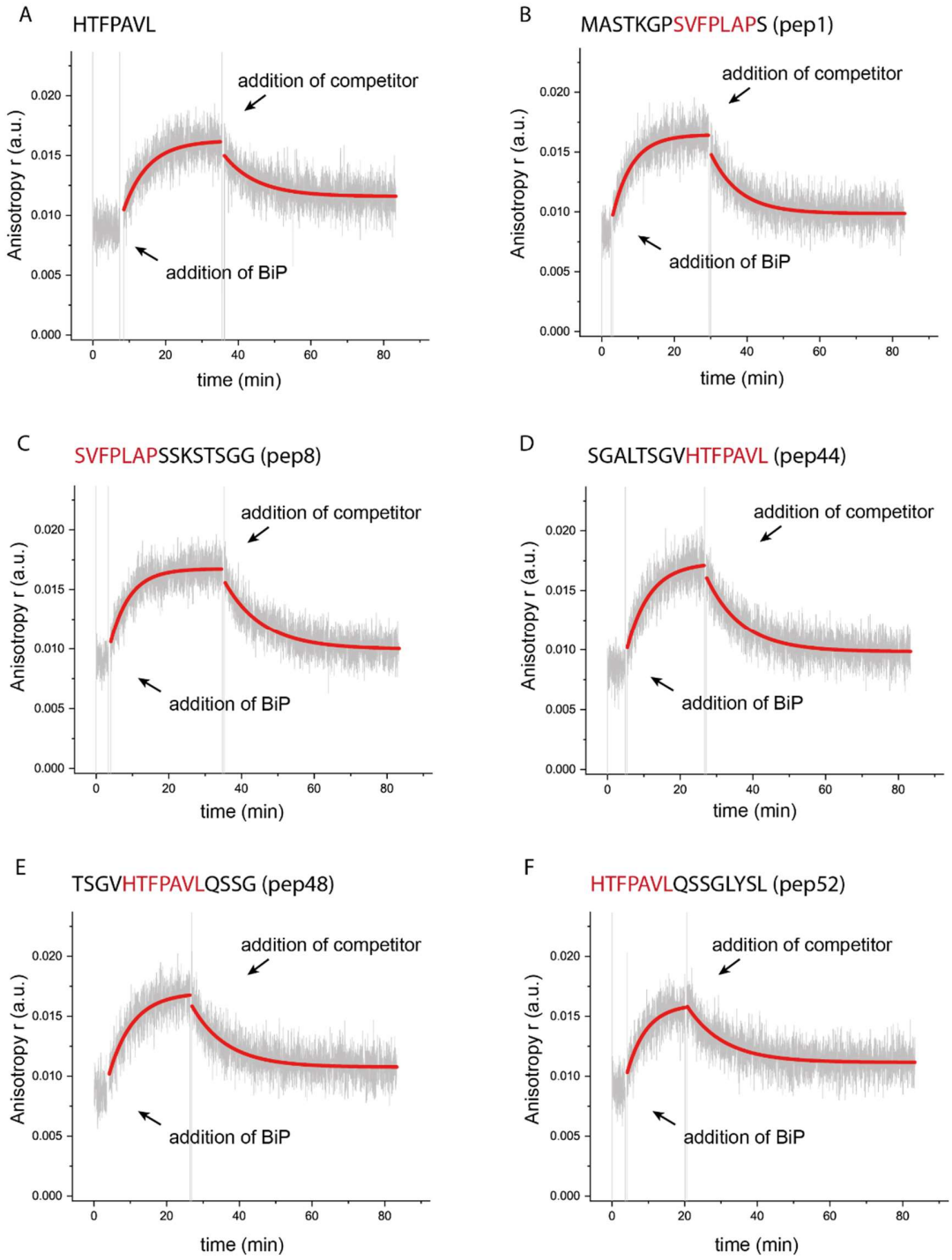

Figure 34: Anisotropy chase experiments of C_H1 peptides with BiP at 37 °C. Binding of 1µM HTFPAVL-Ly to 15 µM BiP was measured and then chased with 150 µM of different peptides from C_H1 which are A) HTFPAVL as a control, B) pep1 with the BiP binding motif SVFPLAP at the end, C) pep8 with SVFPLAP at the start, D) pep44 with HTFPAVL at the end, E) pep48 with HTFPAVL in the middle of the peptide and F) pep52 with HTFPAVL at the start.

Table 5: Results of anisotropy chase experiments performed with BiP and Ly-labeled HTFPAVL. In red peptides of C_H1 and in in green peptides of Bap are shown. Peptides that were easily solubilized are marked with a (+), the ones that were not completely solubilized are marked with a (-); n.d. for not determined. Green letters show good binders, blue letters moderate binders, orange letters weak binders and red letters non-binders as defined in 3.3.9.

Peptide ID (solubility)	Sequence	HTFPAVL-Ly λ_{on} (min^{-1})	Competitor λ_{off} (min^{-1})	Displacement efficiency (%)	Ratio $\lambda_{off}/\lambda_{on}$
HTFPAVL (+)	HTFPAVL	0.15	0.11	76	0.7
Pep1 (+)	MASTKGPSVFPLAPS	0.19	0.13	98	0.7
Pep8 (+)	SVFPLAPSSKSTSGG	0.19	0.10	111	0.5
Pep44 (+)	SGALTSGVHTFPAVL	0.16	0.10	105	0.6
Pep48 (+)	TSGVHTFPAVLQSSG	0.15	0.10	93	0.7
Pep52 (-)	HTFPAVLQSSGLYSL	0.18	0.10	85	0.5
9>S3 (+)	KEFALTN	0.17	0.10	84	0.6
10>S5 (+)	FALTNPE	0.21	0.11	80	0.5
11>S9 (+)	LTNPEKS	0.15	0.19	62	1.3
Pep5 (-)	HVRLNLQ	0.19	n.d.	n.d.	n.d.
NB1 (-)	SSTKETE	0.18	n.d.	29	n.d.
Pep8new (+)	GQAVPAG	0.22	n.d.	59	n.d.
HTFPAVL (20x) (+)	HTFPAVL	0.21	0.12	64	0.6
Bap (20x)	Bap	0.20	0.11	82	0.6
Bap-N (20x)	Bap-N	0.16	n.d.	67	n.d.
Bap-N (100x)	Bap-N	0.15	1.80	54	12.2
Bap-C (20x)	Bap-C	0.17	0.41	76	2.4
MSS1	Bap-MSS1	0.21	0.04	67	0.2
MSS2	Bap-MSS2	0.20	n.d.	n.d.	n.d.
MSS3	Bap-MSS3	0.21	n.d.	6	n.d.

To test the hypothesis that regions in Bap-N can act as pseudo substrates, the anisotropy chase experiments were performed with peptides derived from Bap-N. The results are depicted in **Figure 35**.

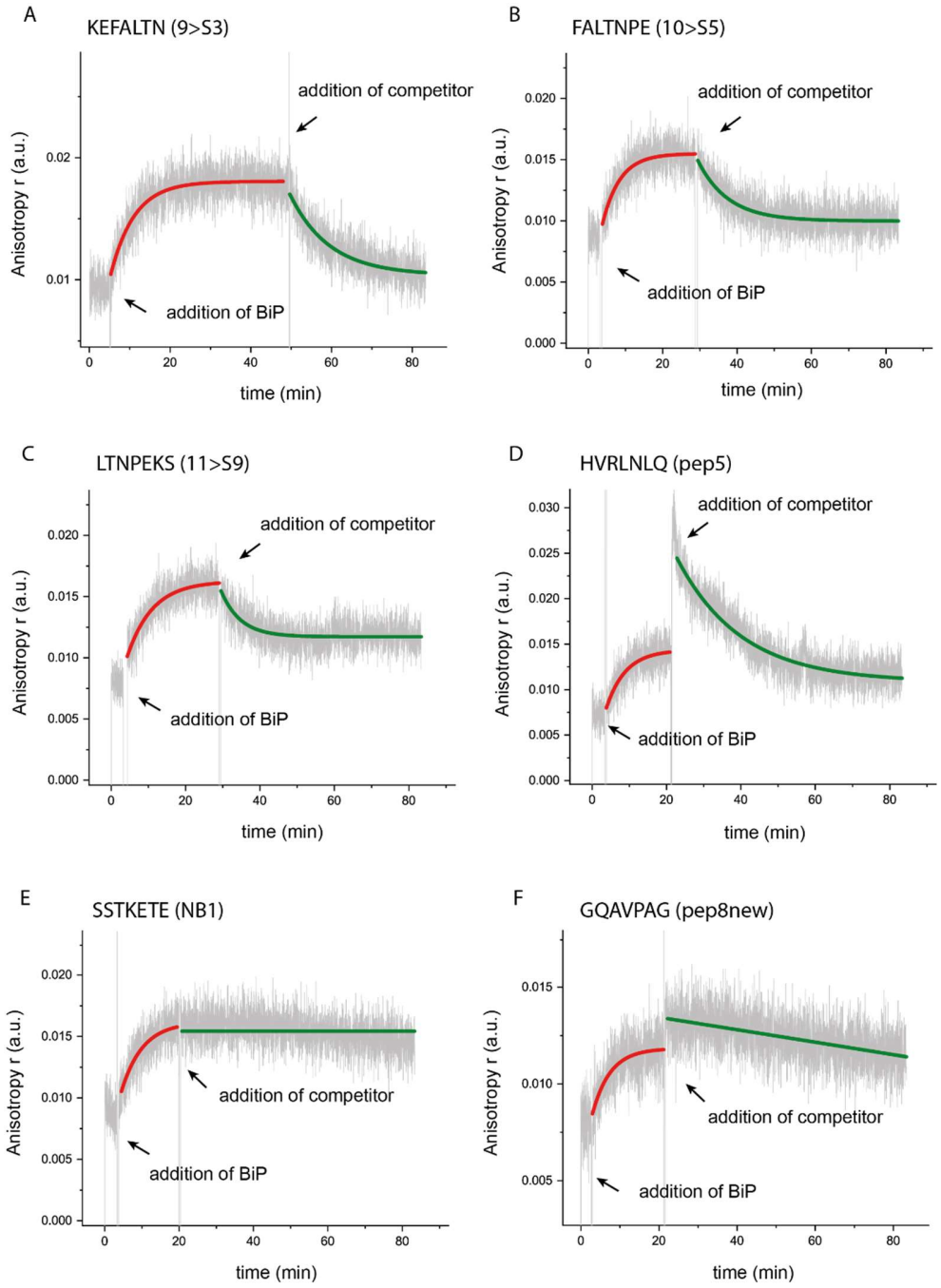

Figure 35: Anisotropy chase experiments of Bap peptides with BiP at 37 °C. Binding of 1µM HTFPAVL-Ly to 15 µM BiP was measured and then chased with 150 µM of different peptides from Bap, which are A) KEFALTN, B) FALTNPE, C) LTNPEKS, D) HVRLNLQ, which was badly dissolved, E) SSTKETE as a predicted non-binder and F) GQAVAPAG.

Pep5 and NB1 were partly dissolved and especially for pep5 this leads to a sharp signal spike that was also described by Mathias Rosam [123]. The results are summarized in **Table 5**. The anisotropy chase experiments were repeated with purified Bap, Bap-C and Bap-N (**Figure 36** and **Figure 37**).

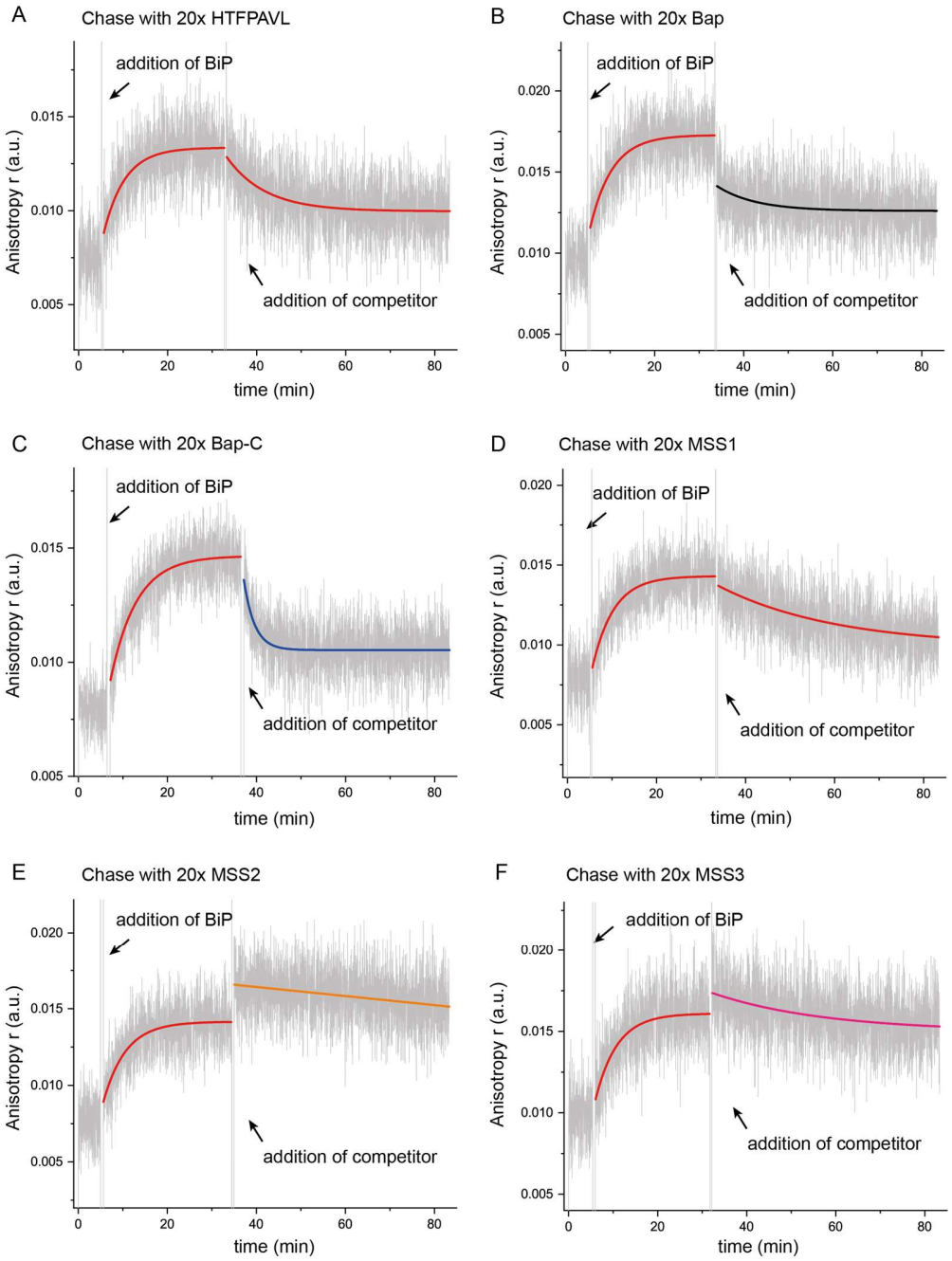

Figure 36: Anisotropy chase experiments of Bap proteins with BiPat 37 °C. Binding of 1µM HTFPAVL-Ly to 15 µM BiP was measured and then chased with 20 µM of different Bap mutants and can be compared to A) HTFPAVL. B) Chase with Bap wt, C) Bap-C, D) MSS1, E) MSS2 and F) MSS3.

Due to concentration limitations, a 20-fold excess of the proteins to HTFPAVL-Ly were used in **Figure 36** and **Figure 37**. Release of HTFPAVL upon addition of Bap-N was so efficient that the temperature was decreased to 30 °C for the experiments (**Figure 37**).

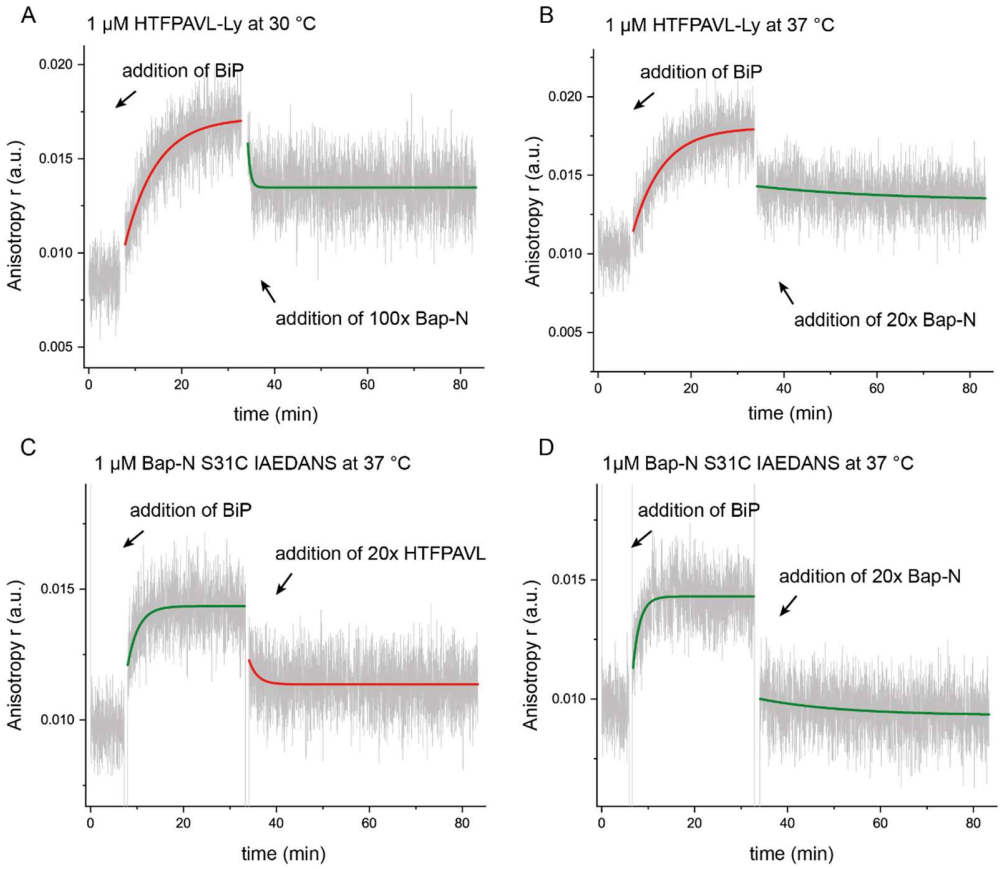

Figure 37: Anisotropy binding and chase experiments of Bap-N with BiP. A) and B) Binding of 1 µM HTFPAVL-Ly to 15 µM BiP was measured and then chased with A) 100 µM of Bap-N at 30 °C or B) 20 µM Bap-N at 37 °C. C) and D) 1 µM IAEDANS-labeled Bap-N S31C binding to 15 µM BiP and then chased with A) 20 µM HTFPAVL or B) 20 µM Bap-N.

To test the direct binding of Bap-N to BiP, a cysteine mutation of Bap-N was cloned, purified and labeled with IAEDANS (Bap-N S31C IAEDANS). Binding of Bap-N to BiP was again monitored in anisotropy assays and chase experiments were performed with HTFPAVL and unlabeled Bap-N (Figure 37). The calculated on-rates from the single exponential fit for IAEDANS-labeled Bap-N is much faster than for HTFPAVL-Ly with a k_{on} of 0.4 - 0.7 min^{-1}. The off-rates for HTFPAVL were around 0.5 min^{-1}, which is also faster than for the experiments with bound HTFPAVL-Ly. It was not possible to determine the k_{off} for chase experiments with Bap-N, since the reaction was too fast to monitor in our assay. Also, displacement efficiencies were difficult to calculate, but it can be seen in the graphs (**Figure 37**) that a 20-fold excess of HTFPAVL leads to an almost complete displacement. Even more pronounced is the displacement for Bap-N as a competitor, where the displacement seems to be complete.

MSS mutants

The rare autosomal-recessive disease Marinesco-Sjögren Syndrom (MSS) is linked to mutations in Bap [122]. Several mutations in different exons of the SIL1 gene encoding Bap are described in literature.

Table 6: MSS mutations chosen for this thesis. The name refers to the name of the mutation in this thesis and the publication where it has been described. "Mutation protein" indicates the position of the mutation on the protein level (amino acid numbering according to UniProt ID: Q9H173), column 3 gives the gene locus of the mutation (numbering according to NM_022464.4), column 4 provides a short description of the phenotype, column 5 the type of mutation.

Name (Source)	Mutation protein	Mutation gene	Phenotype	Mutation type
MSS1[121]	V231_l232del	Exon 7 691_696del GTGATC	Reduced Bap levels, hypotonia, strabismus, ataxia, dysarthria, cerebellar atrophy, delayed motor milestones and others	In-frame deletion of hydrophobic residues
MSS2[121]	G312R	Exon 9 934G>A	Reduced Bap levels, Cataracts, strabismus, hypotonia, delayed motor milestones, ataxia, dysarthria, cerebellar atrophy and others	Missense mutation, introduction of charged residue
MSS3[150]	Q438X	Exon 10 1312C>T	delayed motor milestones, hypotonia, Cataracts, cerebellar atrophy, no ataxia detected and others	Early stop codon, lack of ER retention sequence KNDEL

Three of these mutations were chosen to be investigated in more detail *in vitro*. These mutations are depicted in **Table 6** and can be seen in **Figure 10** and **Figure 38**. The mutations were numbered MSS1-

3. All chosen mutations show a clinical phenotype with delayed physical development, hypotonia, muscle weakness and other patient specific symptoms. The obtained results are also part of the Master thesis of Vanessa Gilg [151].

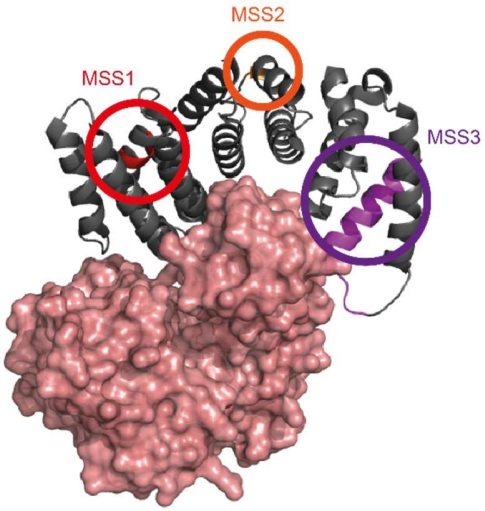

Figure 38: Position of the MSS mutation on the crystal structure of Sil1 on Kar2 with the MSS mutations mapped on the yeast protein.

The proteins were cloned in a pSUMO vector and purified as described for Bap wt. MSS2 and MSS3 still showed some DnaK impurities after purification. **Figure 39** shows the structural characterization of the mutant proteins compared to Bap wt by CD spectroscopy.

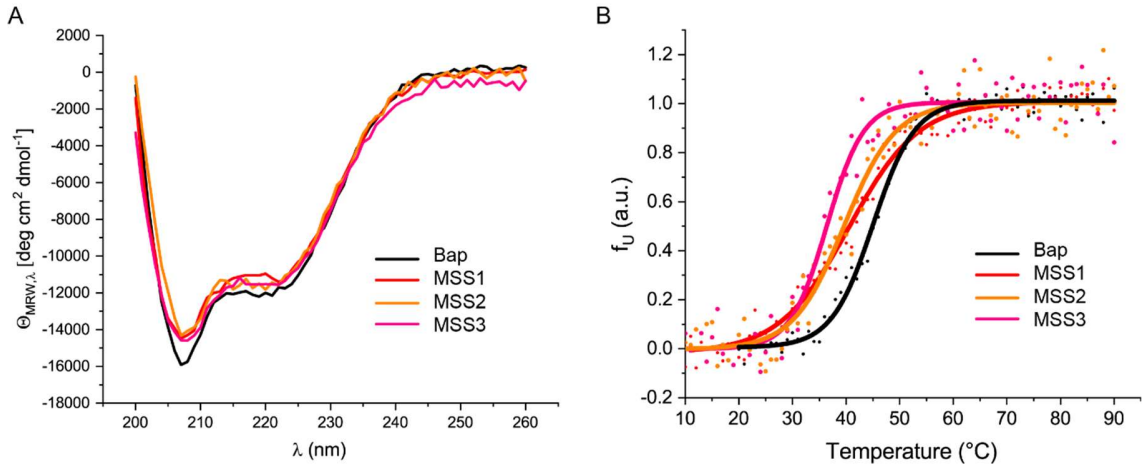

Figure 39: CD data of Bap and MSS1-3. A) FUV-CD spectra of Bap wt and MSS mutants and B) thermal denaturation of Bap and the investigated MSS mutants at 25 °C in a 0.5 mm cuvette with concentrations of 0.5 mg/ml.

All mutants show a folded FUV CD spectra (**Figure 39** A) with two minima at 208 nm and 222 nm. The first minimum at 208 nm is more pronounced as it can be also seen for the wt protein (black line). Thermal unfolding experiments at 222 nm showed a decreased stability of all MSS mutant proteins compared to the T_m of Bap with T_m = 45 °C ± 1 (**Figure 39** B). All show a one- step unfolding. The least stable mutant is MSS3 with a T_m = 36 °C ± 1, followed by MSS2 with a T_m = 40 °C ± 1 and MSS1 with a T_m = 41 °C ± 1.

To test the oligomerization state and interaction with BiP, the proteins were further analyzed using SEC-HPLC and AUC. Results for MSS1 are depicted in **Figure 40**. The SEC-HPLC results show that MSS1 mainly elutes as a monomer with the same retention time as Bap wt (**Figure 40** A). Compared to Bap, MSS1 shows some undefined higher molecular aggregates eluting from t =22 min. Binding to BiP was tested in AUC with Atto488-labeled BiP without nucleotide as described (**Figure 40** B). BiP alone shows the monomer peak at around 3.8 S and a dimer peak at around 6.2 S. Addition of a 10-fold excess of MSS1 leads to a peak shift to 4.8 S, which is a complex of BiP with MSS1. A small shoulder referring to the BiP monomer is still visible, so not all BiP is in a complex with MSS1.

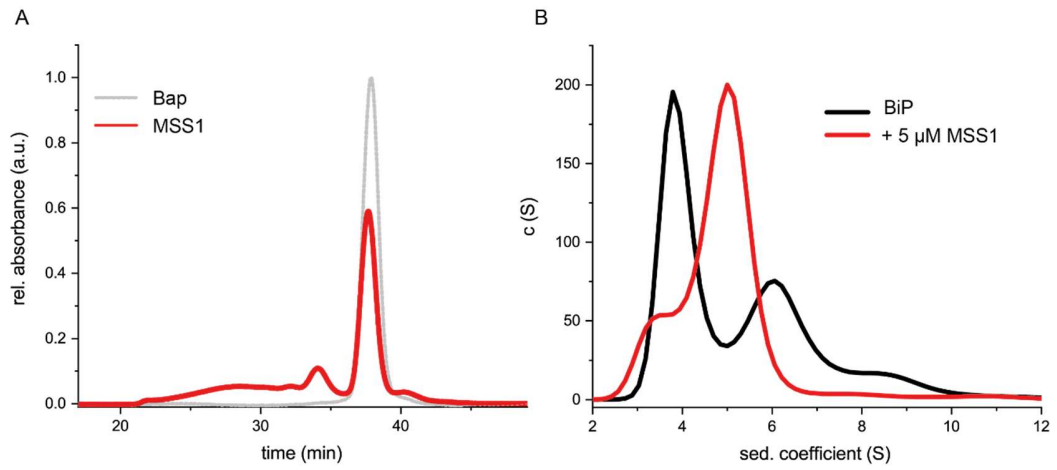

Figure 40: HPLC and AUC data of MSS1. A) HPLC of 1 mg/ml Bap (grey) and MSS1 (red) on a Superdex 200 increase column in HKM. B) AUC run with 0.6 µM Atto488-labeled BiP (167C) and 5 µM MSS1 in the apo state.

To further analyze this interaction AUC titration experiments were performed and can be seen in **Figure 41** in comparison to Bap wt. For better evaluation, the decrease of BiP monomer peak at 3.8 S

(**Figure 41** A for Bap and C for MSS1) was plotted against the concentration (**Figure 41** B for Bap and D for MSS1).

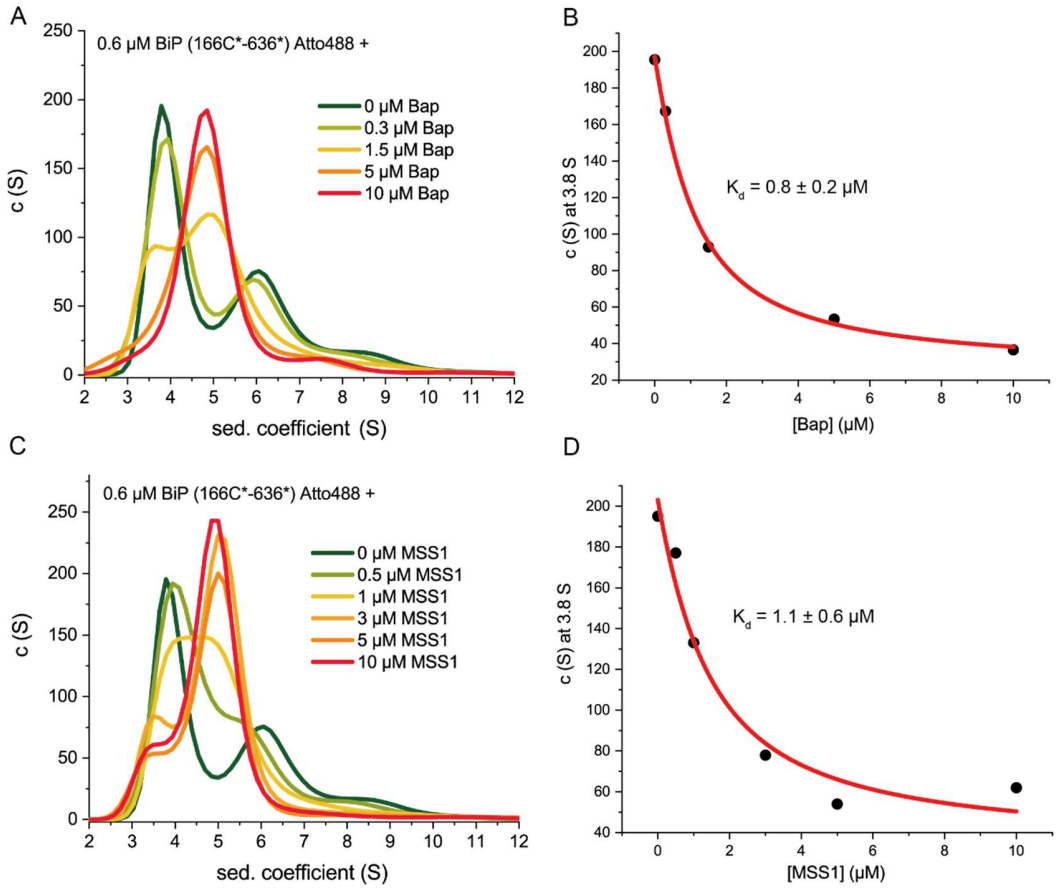

Figure 41: AUC titration of Atto488-labeled BiP (167C) and Bap/MSS1 without nucleotide. A) Addition of Bap in increasing concentrations (green to red). C(S) value at 3.8 S lead to B) measurement points for measuring the K_d of the interaction. C) Addition of MSS1 in increasing concentrations (green to red). C(S) value at 3.8 S lead to D) measurement points for measuring the K_d of the interaction.

The complex peak of BiP and Bap or MSS1 is detectable at 3.8 S while the monomer and dimer peak decreases. The K_d of the interaction is similar for wildtype and MSS1 and is for Bap K_d = 0.8 µM and for MSS1 K_d = 1.1 µM. These K_ds are also comparable to the K_d measured before for Bap (**Figure 24** B and D). MSS2 was also investigated by SEC-HPLC (**Figure 42** A). Different from Bap or MSS1 it does not elute in a single peak but rather shows a broad distribution pattern with only a small amount at the expected retention time of a monomer.

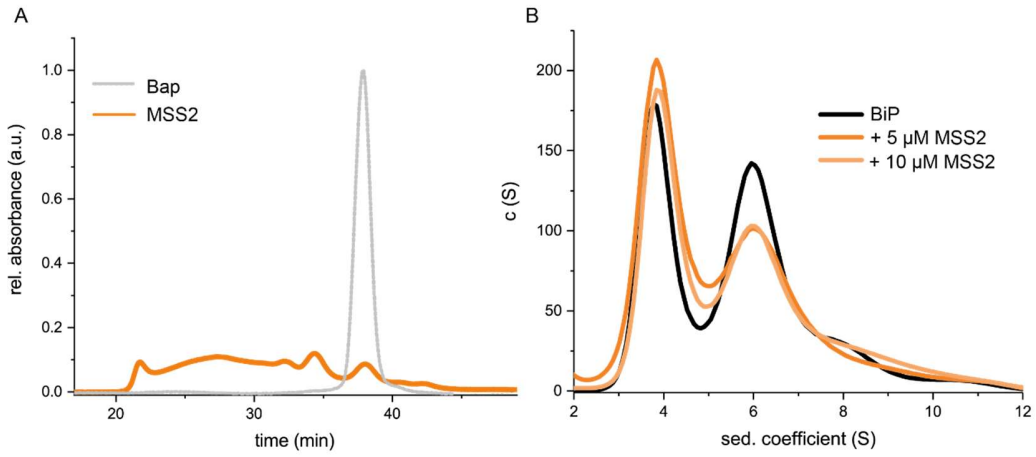

Figure 42: HPLC and AUC data of MSS2. A) HPLC of 1 mg/ml Bap (grey) and MSS2 (orange) on a Superdex200 increase in HKM. B) AUC run with 0.6 µM Atto488-labeled BiP (167C) and 5 µM or 10 µM MSS2 in the apo state.

This leads to the conclusion that MSS2 is present in a disperse distribution from high molecular oligomers to degradation products. In AUC experiments with labeled BiP, it was not possible to detect binding of MSS2 to BiP in neither 10- nor 20-fold excess (**Figure 42** B).

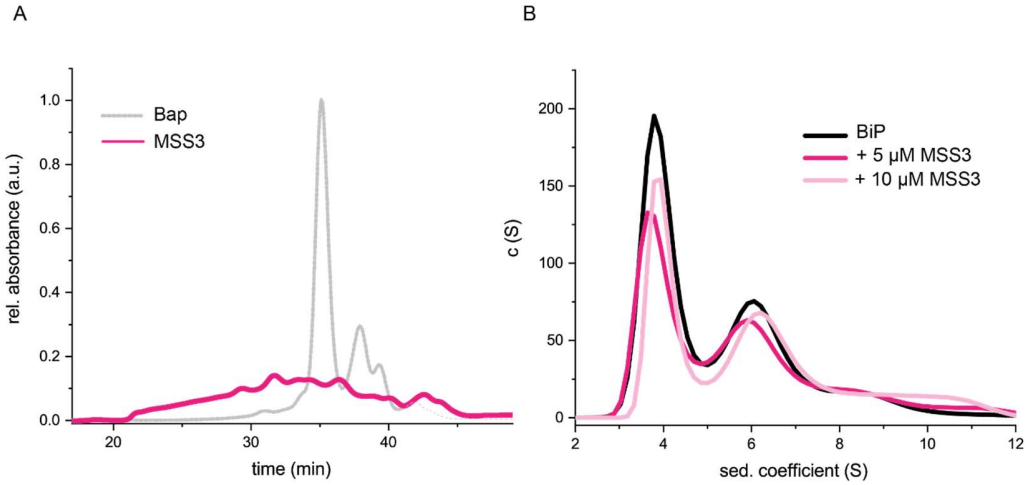

Figure 43: HPLC and AUC data of MSS3. A) HPLC of 1 mg/ml Bap (grey) and MSS3 (magenta) on a Superdex200 increase in HKM. B) AUC run with 0.6 µM Atto488-labeled BiP (167C) and 5 µM or 10 µM MSS3 in the apo state.

Next, we assessed the behavior of MSS3 in SEC-HPLC and upon interaction with BiP (**Figure 43**). Similar to MSS2, MSS3 did not elute in a single peak but rather showed a broad elution starting at t = 22 min and eluting until t = 46 min (**Figure 43** A). AUC runs were performed as described for MSS1, but no binding of MSS3 to BiP at 5 or 10 µM was detectable (**Figure 43** B).

In single molecule FRET experiments (performed by Ganesh Agam at the institute of Don Lamb) using the set-up described before [76,131], the effect of co-chaperones on the BiP structure can be investigated. Using the NBD- and Lid-sensor described in **Figure 4**, conformational changes in the distance of the domains can be measured. It has been shown that Bap can transiently bind to BiP in the ATP state indicated by a low FRET species that increases with increasing Bap concentrations [131]. To see if the MSS mutants also bind to BiP in the ATP state and are able to induce the conformational change upon binding. SmFRET was performed with 1 µM BiP and 1 mM ATP (**Figure 44**).

Addition of MSS2 or MSS3 did not lead to a change in the FRET distribution pattern with a medium FRET efficiency of around 0.6 as for BiP alone. Addition of MSS1 gave a low FRET peak of 0.25 (**Figure 44**, black arrow). This is similar to the addition of Bap or small peptide substrates as HTFPAVL [131].

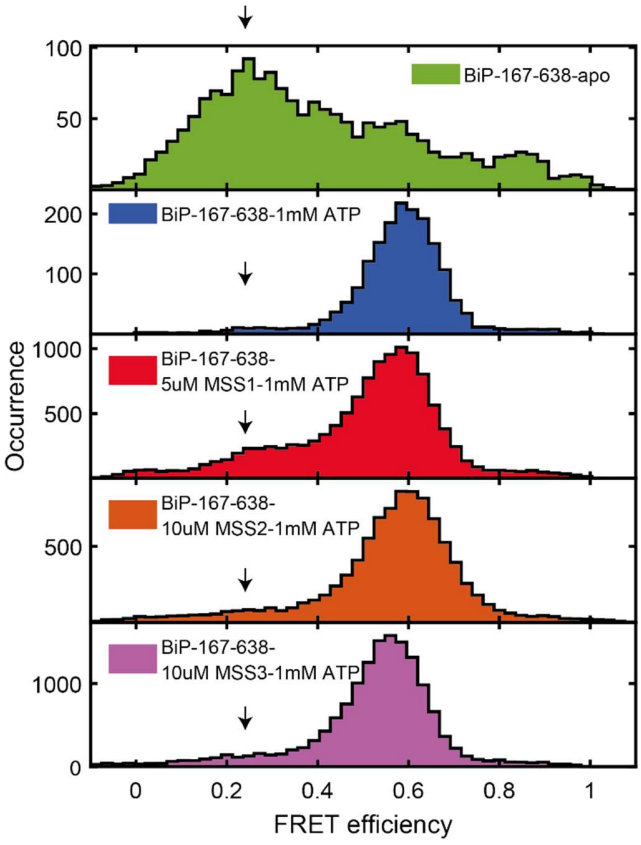

Figure 44: SmFRET histogram of 1 µM Atto488-labeled BiP (167C-638C) in absence of nucleotide (green) or in presence of 1 mM ATP (blue). Addition of 5 µM MSS1 (red), 10 µM MSS2 (orange) and 10 µM MSS3 (purple) to BiP in presence of 1 mM ATP.

3.3.6. ERdj3 interacts with BiP

ERdj3 is a tetramer in solution. To obtain more information about ERdj3 in complex with BiP, AUC titrations were performed. Unfortunately, the results obtained did not allow proper evaluation, since no single species complex was formed. In addition, only four different concentrations were used to determine the K_d. The obtained K_d was around 1 µM and it was determined by calculating the area under the BiP monomer peak from 2.9 S to 5.2 S and divide it by the area between 3 S and 9 S. To verify the K_d and get more trustworthy results, SEC-HPLC titrations with 2 µM Atto488-labeled BiP 167C were performed and the fluorescence signal was detected (**Figure 45**).

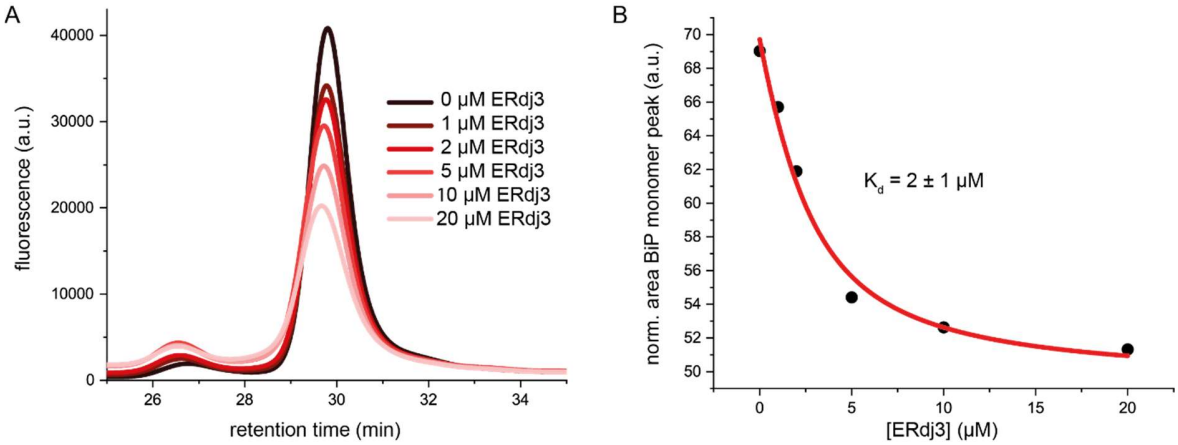

Figure 45: HPLC titration of ERdj3 to 2 µM Atto488-labeled BiP (167C). A) Elution profile of BiP monomer peak with 1 mM ATP upon addition of increasing amounts of ERdj3. B) Decrease of the peak area under the monomer peak in A) and K_d fit.

The run was performed with 1 mM ATP. The peak at 30 min is the monomer peak of BiP. Upon increasing the ERdj3 concentration, the peak intensity decreases. To calculate a K_d from this SEC-HPLC run, the area under the peak area starting at 28.5 min until 31.4 min was divided by the area from 0-60 min (**Figure 45** B).The obtained K_d of around 2 µM is similar to the one obtained by AUC titration.

3.3.7. ERdj3 stimulates ATPase rate but slows down nucleotide exchange

It is known that JDPs stimulate the ATP hydrolysis in BiP [82,84,133]. ERdj3 purified according to the protocol described in this thesis was tested with regard to its stimulating activity on the BiP ATP hydrolysis rate in a steady state ATPase assay (**Figure 46**).

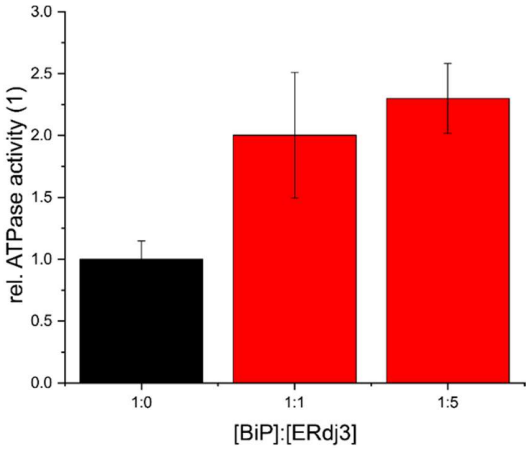

Figure 46: Steady state ATPase stimulation assay of 2 µM BiP by 2 µM ERdj3 (1:1) or 10 µM ERdj3 (1:5).

ERdj3 was able to stimulate BiP's ATPase activity to comparable levels as observed in previous analyses [76]. Stimulation was concentration-dependent and in a 1:5 ratio (2 µM BiP and 10 µM ERdj3) stimulation was about 2.5-fold.

To test the effect of ERdj3 and Bap on the ADP release of BiP, MABA-ADP release was measured in stopped flow experiments (**Figure 47**). It was already shown that Bap and Bap-C stimulate ADP release in a concentration-dependent manner as expected from a NEF. When ERdj3 is pre-bound to BiP, ADP release from BiP is slowed down by about one third (**Figure 47** B, **Table 4**). However, Bap is still able to accelerate ADP release from BiP and ERdj3 in a concentration-dependent manner (**Figure 47** A).

Direct comparison of the stimulation by Bap in the presence or absence of ERdj3 shows that the whole release is slowed down when ERdj3 is present (**Figure 47** B). In the presence of ERdj3, the nucleotide dissociates almost 4 times slower than with BiP alone. The data can be fitted by a single exponential fit with a linear slope and the off-rate is shown in **Figure 48**.

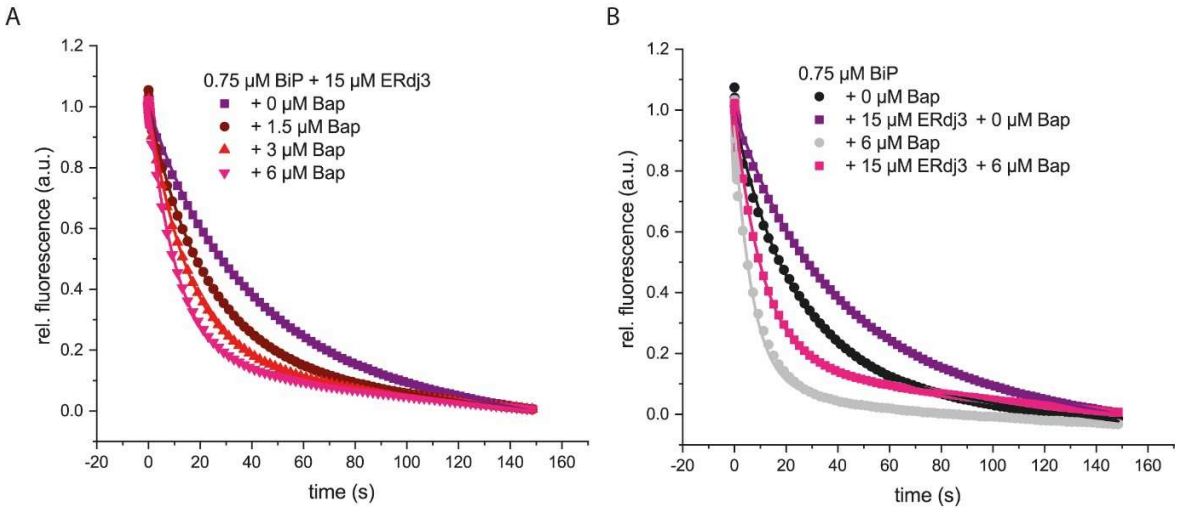

Figure 47: Nucleotide release from BiP in presence of Bap and ERdj3 A) in the presence of increasing Bap concentrations. B) Direct comparison of nucleotide exchange rate in presence or absence of ERdj3 and Bap.

A much steeper slope corresponding to off rates with BiP and Bap alone can be determined compared to the values obtained with when BiP is pre-bound to ERdj3. The values for the slope m of the experiment with BiP and Bap alone is 0.012 whereas the slope is 0.007 when 15 µM ERdj3 are present.

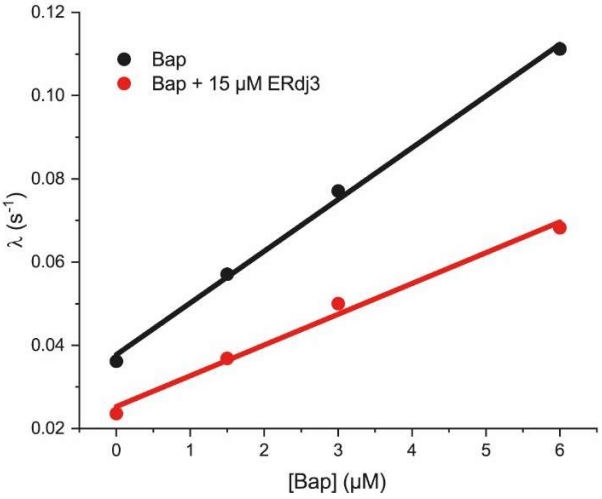

Figure 48: Rate constants λ of nucleotide release from Figure 47 where plotted against Bap concentrations.

3.3.8. ERdj3 and its role in protein homeostasis

It has been suggested that ERdj3 is involved in protein folding and binding to unfolded protein. ERdj3 has also been shown to be secreted [30]. This leads to the assumption that ERdj3 is also secreted while bound to substrate proteins. Unpublished results by Pamina Kazman (Technische Universität München, Germany) also suggest a role of ERdj3 in protein homeostasis by preventing the formation of amyloid fibrils of the V_L domain of antibodies.

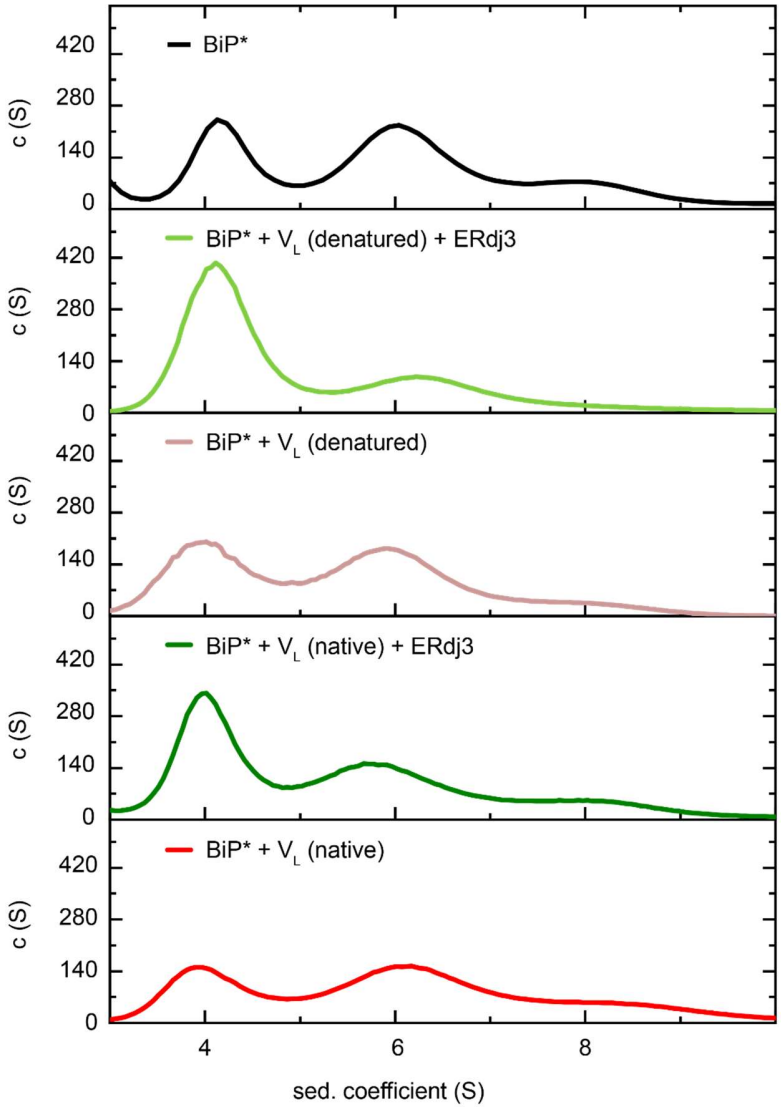

Figure 49: AUC data obtained with Atto488-labeled BiP-167C in presence of antibody light chain V_L domain and ERdj3.

To test the interaction of ERdj3 and V_L with BiP, AUC runs with Atto488 labeled BiP-167C were performed (**Figure 49**). The experiments were performed in the apo state and compared to BiP alone (black curve), which shows an equal distribution of monomer and dimer and some higher oligomers in the apo state at S values of about 4 S (monomer), 6 S (dimer) and 8 S (trimer or higher oligomers). It has been shown that addition of substrate to BiP disturbs the oligomerization, shifts the monomer:dimer ratio and therefore leads to more monomeric BiP [69,131,152]. Addition of V_L showed a distribution with a higher peak at around 4.2 S, which is similar to the monomer peak (light and dark green curve) which can be due to the previously described substrate binding. Addition of ERdj3 and V_L lead to a similar picture as BiP alone (dark and light red curve). Whether V_L is in its native or heat-denatured form does not change the results.

3.3.9. Discussion

The nucleotide exchange factors of BiP

Grp170 is a NEF of BiP and belongs to the Hsp110 family. It has a structure similar to Hsp70 proteins with an extended SBD [103]. It is heavily glycosylated but we were able to purifiy Grp170 from *E.coli* expression. This has been reported before and Grp170 is supposed to fulfill at least some functions when purified from *E.coli*, like stimulating ADP release from BiP but not DnaK [52]. Here, Grp170 shows a mainly α-helical FUV-CD spectra and a thermal unfolding in three steps, which is probably correlated to its different domains unfolding at different temperatures. In SEC-HPLC experiments, no dimers or higher oligomers of Grp170 were detected. Grp170 interacts with BiP. Since BiP is almost completely shifted to a species at 6.4 S, it can be concluded that the K_d for the interaction is in the low micromolar range. However, it remains unclear, why the complex peak of BiP and Grp170 sediments at 6.4 S, which is approximately the same sedimentation coefficient of the BiP dimer. The complex of Grp170 and BiP is supposed to be much bigger with around 240 kDa. Since no crystal structure of Grp170 or the complex with BiP exists, the shape of the complex is unknown. Thus, this can lead to inaccuracies when evaluating the AUC data.

Bap was the first NEF described for BiP. Previously it has been shown by AUC experiments that BiP is able to interact with Bap in the ADP and apo state but not in the ATP state. Also, interaction of Bap-

C with BiP was detected in a nucleotide-dependent manner [123]. In AUC titration experiments (**Figure 24**), the interaction with BiP was detected and a K_d for this interaction was determined to be in the low micromolar range (0.3 µM) in the apo state. To exclude an effect of the labeling position, the experiment was repeated with labels at different positions and resulted in a similar K_d. This is as expected from previous results where the K_d was measured in the AMP-PNP state [123]. It was also shown that interaction with Bap leads to an increase in nucleotide exchange as expected from a NEF (**Table 4**). The Bap-C part of the protein is sufficient to release the nucleotide from BiP with an even higher efficiency (**Figure 28**) whereas Bap-N alone does not lead to a nucleotide release. BiP-NBD alone has a weaker release rate of nucleotide but can be stimulated by both Bap and Bap-C to a similar extent. This leads to the conclusion that the N-terminal part of Bap is not necessary to fulfil the NEF function of Bap and that the SBD of BiP plays a role of the intrinsic nucleotide release by BiP.

Another function for Bap

The role of the N-terminal domain of Bap remained enigmatic, since it is not necessary for Baps function as a NEF but it has been shown that it is important for protein homeostasis, since mutations in Bap can cause MSS [118,122,153]. This domain seems to be unstructured as can be seen by CD measurements and structural prediction. In H/DX experiments (**Figure 25**) it can be seen that the N-terminal segment is more accessible for deuterium exchange. Other parts of Bap that show a strong hydrogen exchange over time are mainly located in the armadillo-like repeats. Overall, H/DX and limited proteolysis show that Bap is a protein that is unstable and can easily be degraded by proteases. To further investigate the role of the N-terminal domain, refolding assays or aggregation assays can be performed. Here, a functional role might also be detected as it has been shown for p23 that the C-terminal region is important for the chaperone activity, although it has been shown to be unstructured [154].

In steady state ATPase assays a hint of Bap's functions other than nucleotide exchange was obtained. Bap is able to stimulate the intrinsic ATPase activity but only when the N-terminal segment is present. This excludes the idea that the ATPase rate is only stimulated due to a quicker nucleotide release, since Bap-C is sufficient for nucleotide release in BiP (**Figure 28**). Also, the SBD of BiP, especially the lid, seem to be important for this stimulation, which is in accordance with the fact, that the lid of yeast BiP Kar2 is critical for cell growth [155]. Bap-N alone is unable to stimulate the ATPase rate, however, it might be

possible that binding of Bap is necessary to locate the N-terminal domain into proximity of the BiP-SBD. This effect is not seen with DnaK, where Bap is unable to stimulate ATP hydrolysis (**Figure 32** B). However, direct binding of Bap to DnaK with SEC-HPLC or AUC was not tested in this thesis.

In the crystal structure of the Bap and BiP complex and also when modelling the N-terminal domain, Baps N-terminal domain and the BiP-lid are in close proximity and may even interact. Unstructured, hydrophobic patches are substrates of BiP and peptides in the N-terminal domain of Bap have been predicted to be good substrates by the BiPPred algorithm by Markus Schneider and Iris Antes [71]. Anisotropy chase experiments verified the predicted data and showed that the peptides of Bap-N as well as Bap-N itself are able to bind to BiP and release a known substrate (HTFPAVL from C_H1) from BiP-SBD. Substrates of BiP are known to modulate BiP's ATPase activity [64,69]. Therefore it is suggested that Bap is not only acting as a NEF for BiP in the cell but also has an additional function in regulating the chaperone cycle of BiP by interacting with the SBD as a pseudo-substrate and stimulates its ATP hydrolysis.

To test the substrate hypothesis, peptides of C_H1 and Bap as well as the whole protein were tested in anisotropy chase experiments. To make a reasonable statement about the effect on HTFPAVL displacement from BiP, different values were compared. First, only data which showed a similar binding of HTFPAVL-Ly to BiP was evaluated. Only experiments with on-rates ranging from 0.15-0.22 min^{-1} were used.

The displacement efficiency was calculated and gives an idea of the affinity of the peptide to BiP compared to HTFPAVL. This value shows, if the peptide in the concentration used is able to bind to Bip and replace HTFPAVL from its position on BiP and to what extent (completely or just partially). Complete displacement of HTFPAVL-Ly is 90-100% for peptides pep8, pep44, pep48 and pep1. These peptides contain the sequence SVFPLAP or at the end a HTFPAVL.

A moderate displacement can be seen with values of 75-90% as for peptides HTFPAVL and pep52, which also contain the HTFPAVL sequence as well as the Bap peptides KEFALTN and FALTNP, Bap wt and Bap-C.

A weak displacement of 50-75% is in the peptide LTNPEKS, pep8new HTFPAVL in a 20-fold excess, MSS1 and Bap-N. No displacement can be seen in pep5, NB1, MSS2 and MSS3. The displacement efficiency does not show the thermodynamics of this displacement and how quick this happens. Here, a second value was used, which is the ratio between the on and off rates. Values of 0.5-1 are taken as an expected value, since they are comparable to a displacement by HTFPAVL itself. Values <0.5 show a very slow replacement of the bound species, as it can be seen in MSS1. Values >1 show a very fast displacement of the bound HTFPAVL although this does not necessarily mean that the whole peptide is replaced.

Indeed, the equilibrium between binding and release of HTFPAVL-Ly is often reached very fast but with a weak to moderate displacement efficiency. This is especially the case for Bap-N and Bap-C as well as LTNPEKS. Notably, Bap-N shows the fastest off rate measured in all experiments performed even at lower temperatures, which cannot be properly detected in the experimental setup used. These experiments as well as the evaluation can be used to evaluate if peptides are BiP substrates and how strong and fast they bind compared to a known binder, namely HTFPAVL.

Nevertheless, this method is only an indirect way of evaluating the binding. Therefore, IAEDANS-labeled Bap-N S31C was used to detect the direct binding. Unfortunately, the data obtained was more noisy than in the other experiments. It can be seen that Bap-N is able to bind BiP and that it gets released by addition of the peptide HTFPAVL (**Figure 37** C, D). It can be assumed that Bap-N binds to the SBD of BiP. Also, it can be concluded that Bap is able to release bound peptide from BiP and that, although both domains of Bap are able to do so, Bap-N is a very fast release factor for BiP substrates.

Role of protein purity for in vitro experiments

BiP has a low intirinsic ATPase activity with a k_{cat} of approximately 0.2 min^{-1} (**Table 3**)[64]. This is much lower than the ATPase rate of other Hsp70s like DnaK. BiP lacking the lid or BiP's NBD alone have increased ATPase activity. This leads to the conclusion that the SBD of BiP seems to have a regulating effect on the ATP hydrolysis of BiP. This is also in line with published data [76]. However, Bap is not able to stimulate DnaK's ATPase activity. It is not clear how and if Bap interacts with DnaK in the set up of our *in vitro* experiments. However, the results obtained suggest that Bap is interacting more as a substrate of DnaK than a co-factor. Further analysis in SEC-HPLC and AUC need to be performed to

elucidate this issue. It is essential, that the co-factors are not contaminated with DnaK, since this has a strong effect on the results obtained. Even small amounts of DnaK lead to a strong increase in ATPase activity, due to the fast ATP hydrolysis by DnaK (**Figure 22**). DnaK also stabilizes Bap as can be seen in thermal transition experiments. Only when DnaK denatures at around 70 °C, Bap is fully unfolded. This protection of Bap can also be seen upon interaction with BiP. BiP or BiP-SBD show this stabilizing effect when a two-step denaturation is seen in thermal transition experiments. This can be due to the unfolding of the single domains but can also be explained due to a partial stabilization of the protein by the SBD. In limited proteolysis experiments we were able to also see a stabilization of Bap by BiP (**Figure 27**). Furthermore, HDX experiments showed that Bap is less flexible when interacting with BiP (**Figure 25**).

Erdj3 and its role in protein homeostasis

Soluble expressed ERdj3 is able to stimulate BiP's ATPase activity (**Figure 46**) to an extent expected from previous publications [76]. Binding of ERdj3 to BiP can be detected in AUC and SEC-HPLC experiments although it was difficult to determine a K_d, which seems to be in the low micromolar range. We were unable to establish a labeling protocol for ERdj3. Cysteine labeling is not possible due to the formation of disulfide bridges in ERdj3. Also labeling of lysins leads to a strong decrease in protein stability.

Looking at the interplay of BiP, Bap and ERdj3 shows that ERdj3 decelerates nucleotide release of BiP (**Figure 48**). The reason for this deceleration might be in the function of ERdj3. Maybe binding of ERdj3 leads to a steric hindrance of ADP release or Bap binding. Interestingly, when both, Bap and ERdj3 are present, Baps NEF effect is much weaker than in the absence of ERdj3. This might be due to a replacement of Bap by ERdj3. It needs to be further investigated if both Bap and ERdj3 are able to bind to BiP. It has been shown that ERdj3 induces conformational changes in BiP that are not only related to its J domain [68,76]. These changes are independent of its ability to stimulate ATP hydrolysis, since also ERdj3-QPD, a mutant that is unable to stimulate ATP hydrolysis, leads to a conformational change in BiP [76]. Therefore, it is assumed that ERdj3 can stabilize BiP in the state similar to the substrate-bound state (**Figure 50**).

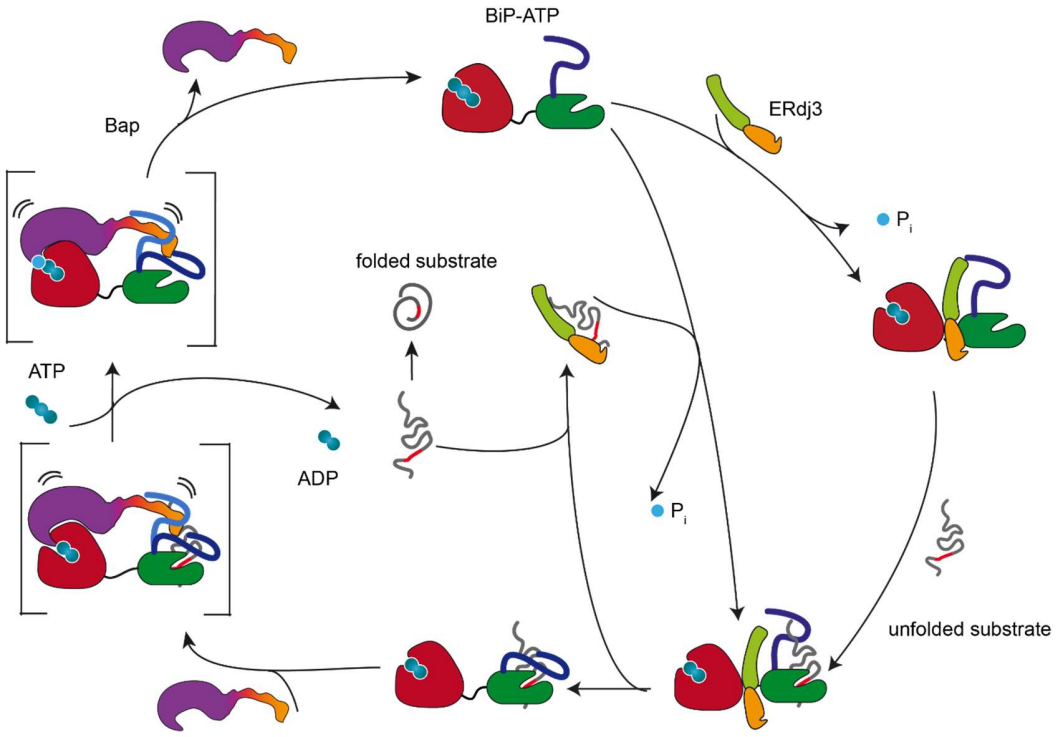

Figure 50: Functional cycle of BiP with ERdj3 and Bap. In the ATP state ERdj3 can bind to BiP and keep it in a substrate like state (XX) or it can transport unfolded substrate protein to BiP. In the ADP state the substrate is bound and ERdj3 gets released and the lid closes. Now the NEF Bap can bind transiently in the substrate-bound state and extrude the substrate and ADP. Upon ATP binding BiP dissociates and a new cycle can start.

Another exciting aspect of ERdj3 is its extracellular function [156,157]. Unpublished results show that ERdj3 alone and in complex with BiP can decelerate fibril formation in antibody light chain V_L domains. Direct binding of V_L to ERdj3 was not detected in our experiments. Also, no binding of ERdj3 and V_L to BiP was detectable. V_L is too small to show a detectable shift in our AUC experiments. However, in the absence of ERdj3, V_L seems to bind to BiP indicated by a higher amount of monomer in the AUC experiment. This can be seen when substrate binds to BiP [69,131]. In the presence of ERdj3 this effect is not visible. Here no binding can be detected, neither of ERdj3 nor of V_L. One possible explanation for this observation is that V_L is bound by ERdj3 and only in the absence of the latter, V_L is also bound by BiP. A similar mechanism has been described for HTFPAVL peptide binding to BiP, where bound peptide is released from BiP in presence of ERdj3 [76]. Of course, it needs to be taken into account, that the effect observed is rather weak and other experiments need to be performed to further calrify the results. Therefore ERdj3-QPD mutants can be used in the assays or labeling mutants of ERdj3 for example with unnatural amino acids can be a valuable tool.

MSS mutations

Mutations of Bap can lead to the disease MSS. The purified and analyzed MSS mutants in this work have all been clinically described before (**Table 6**). Since the phenotype and severity of the disease is different from individual to individual [158], it is interesting to see if the mutations also show differences on the protein level. MSS2 and 3 showed a similar behavior in all experiments. The proteins were probably misfolded as aggregates, oligomers and degradation products were visible in SEC-HPLC runs (**Figure 43**). These oligomers seem to have a defined secondary structure (**Figure 39**). The stabilities of the mutants are lower than that of wildtype Bap. Especially in the case of MSS3, where the 24 aa of the C terminus of Bap is missing, an unstable protein was expected, as the deletion of the last 6 aa has been proven to be important for Bap stability [117]. Both mutants were not able to bind to BiP in the concentrations tested in the AUC experiments. Therefore, these proteins are expected to be dysfunctional. It can be concluded that mutations leading to MSS2 or MSS3 result in defective proteins which are possibly not able to fulfil their functions in the cell. A different picture can be seen for MSS1. Here the protein is less stable then Bap wt but it seems to be correctly folded and elutes as a monomer in SEC-HPLC (**Figure 39**, **Figure 40**). Few higher oligomeric species in the elution profile can give a hint on the decreased stability. In agreement with this notion, limited proteolysis experiments showed that MSS1 is less stable than Bap wt [151]. MSS1 can be stabilized by BiP to a similar extent as Bap. MSS1 also binds to BiP and the K_d is in the low micromolar range (**Figure 41**) as the Bap wt. Exons 6 and 9 in the SIL1 gene encode for the regions that are important for BiP binding. As the MSS1 mutation is located in Exon 7, unaltered binding to BiP was expected. However, while BiP is completely in a complex with Bap at a 10-fold excess, a 20-fold excess of MSS1 over BiP is not sufficient to shift BiP completely in the complex peak. Considering that Bap levels in patients with the MSS1 mutation are reduced [121], this might give a hint on the basis of the observed disease phenotype. In smFRET experiments, MSS1 behaved similar to Bap and a low FRET species suggesting a transient interaction was visible. MSS2 and MSS3 however, were unable to do this, which leads to the conclusion, that they might not bind to BiP at all. For MSS2, two possible explanations exist. The mutation leading to MSS2 is located in exon 9, a region encoding for a protein structure that is important for BiP interaction. Besides the strongly aggregated protein is probably not able to bind to BiP at all as can also be seen for MSS3. The small part that might be correctly folded (**Figure 42**) is probably not enough to induce a visible shift in the AUC experiment.

Therefore, even higher concentrations of MSS2 are necessary in the experiment. Both MSS2 and 3 also show no change on the oligomerization behavior of BiP. This can usually be seen, if substrate (peptides, Bap-N, C_H1) bind to BiP [131]. To obtain more insight on why the MSS mutations leads to the disease phenotype, anisotropy chase experiments were performed. MSS2 and MSS3 behaved like the bad binders. A spike upon addition of the competitor correlates with the assumption that both proteins are unstable and show aggregates. In addition, they were not able to displace the bound HTFPAVL-Ly and therefore it can be concluded, that MSS2 and 3 both do not bind to BiP neither on its NBD nor as a substrate. MSS1 was able to displace HTFPAVL but the off rate was slowed down compared to Bap. The displacement efficiency was weak and comparable to Bap-N. Since hydrophobic patches are known to be recognized as BiP substrates, the MSS1 mutation might lead to a loss of BiP binding site and therefore to a weaker displacement and displacement efficiency. If MSS1 is still able to perform nucleotide exchange in BiP should be tested in the near future. This is an interesting aspect, since the deletion of the hydrophobic residues Val and Ile in MSS1 lie in the first armadillo repeat probably in helix 4 if modeled on the ScBap structure. The armadillo repeats are known to play an important role in the nucleotide exchange activity of Bap. Thus, MSS1 might not only be less stable and abundant in patients but also have a reduced nucleotide exchange activity.

4. Summary and Perspective

This thesis provides a new insight into the interaction of BiP with its co-chaperones. To investigate BiP and its co-factors *in vitro*, purification protocols of tagless proteins were established or improved. This led to the reproducible purifications of BiP and its co-chaperones in good yields and the optimization of storage buffers that can be directly used in experiments. It is essential that purity, integrity and concentration of the proteins purified are controlled and can be reproduced [159]. Here, it was shown that the purity of the proteins is essential for the experiments since the contamination with certain proteins can bias the results. This was shown for DnaK as an example. DnaK as the major Hsp70 in *E. coli* is a frequently encountered contamination of recombinantly expressed proteins [160,161]. Slight contaminations of less than 5 % can already lead to completely different results as it can be seen in thermal unfolding experiments or ATPase assays (**Figure 32**). Here, it was also shown that the interaction of Bap can distinguish between BiP and other Hsp70 proteins, as it is not able to stimulate ATP hydrolysis in DnaK.

The purified co-factors Bap and ERdj3 have been investigated before [123,135], but this thesis characterizes the proteins in detail regarding their stability and structure as well as interaction with BiP. The JDP ERdj3, which was previously purified from inclusion bodies and afterwards refolded [135], was natively expressed and purified. It behaves similar to the proteins that were purified by refolding and is able to stimulate BiP's ATPase rate by a factor of around 2.5. It was shown, that ERdj3 is a tetramer when purified *in vitro* as it has recently been published [93]. The ERdj3 interaction with BiP was monitored using AUC titration experiments and SEC-HPLC with labeled BiP. In the presence of ATP, the interaction seems to be in a low micromolar range as it was previously expected. It is known that ERdj3 is mainly retained in the ER by interaction with BiP and not because of an intrinsic retention signal [157]. ERdj3 can therefore be secreted from cells and might fulfil important functions in protein homeostasis also outside the ER and independent of BiP [88,162]. Unpublished results suggest a stabilization of instable V_L domains by ERdj3. Indeed, SEC-HPLC experiments indicate a strong interaction of V_L with ERdj3 compared to BiP (**Figure 49**). It is of high importance to understand the role of ERdj3 in protein homeostasis independent of BiP. Other JDPs have been shown to have chaperone activity, as for example DnaJ [163]. Also, it is very interesting to investigate the structure of ERdj3 by SAXS, NMR or crystallography. For

NMR, this is difficult, because of the size of the tetramer and since the expression yields of ERdj3 in the native purification are still low. Also, the protein can only be stored in buffer containing high salt or glycerol concentrations; otherwise it precipitates. This is especially difficult when the protein structure is analyzed via SAXS or crystallography. A possible way to analyze the three-dimensional structure of ERdj3 can be electron microscopy, although some problems with protein stability and salt concentrations are also likely to occur. So far only a 19 Å resolution negative stain EM structure is available [93]. It remains unclear if ERdj3 interacts with BiP or substrate as a monomer or in a dimer or even in a tetramer. It has already been shown, that the ability to form dimers is essential for the interaction with substrate [90] although this interaction is independent of the interaction with BiP as mentioned above.

The two NEFs of BiP, Grp170 and Bap, were also investigated. For Grp170 we were able to purify the protein and characterize its structure as mainly α-helical, which is in line with structural data of other Hsp110 [104]. Interestingly it shows a three-fold thermal transition profile. Grp170 is monomeric in the apo and ATP state and even at low concentrations only one peak can be detected. Many open questions remain concerning the functionality and tasks of Grp170. Therefore, ATPase assays need to be performed and smFRET analysis can give an indication of its interaction and influence of BiP.

The NEF Bap was investigated in more detail. For a long time, it was assumed that the C-terminal domain of Bap might be sufficient to fulfil the functions of the protein *in vivo*. It has been shown that ScBap-C alone is sufficient bind and to promote nucleotide release from ScBiP/Kar2 [114]. However, mutations leading to the disease MSS suggested, that the N-terminal domain of Bap also plays an important role for the cells. Bap, Bap-C and Bap-N were analyzed in this thesis regarding their structure and stability. Here, Bap and Bap-C behaved very similar whereas Bap-N was mainly unstructured after purification. Both, Bap and Bap-C, were able to bind BiP in a low micromolar range in the apo state. The nucleotide exchange of BiP was enhanced when either Bap or Bap-C were present with Bap-C being more potent in nucleotide exchange than the wt. Bap-N again showed no function in nucleotide exchange. A first hint of the importance of the N-terminal domain occurred when ATPase assays were performed. It has already been shown that Bap stimulates ATP hydrolysis by BiP [115]. Indeed, only full-length Bap was able to stimulate the hydrolysis in full length BiP. Lack of the C-terminal lid in BiP or the N-terminal domain of Bap prevent stimulation of BiP's ATPase activity. Since substrates of BiP are known to also

enhance the intrinsic ATPase rate of BiP, it was tested whether the N-terminal domain functions as a substrate for BiP. Single molecule FRET results support this hypothesis [131] and anisotropy chase experiments show a fast release of already bound substrate from BiP upon addition of Bap-N or peptides derived from Bap-N (**Table 5**). Therefore, it can be suggested that Baps N-terminal domain fulfills an important function in triggering substrate release from BiP. This leads to an improved model of the chaperone cycle of BiP (**Figure 51**). Bap can bind at a defined stage in the chaperone cycle and promotes not only the ADP release, but also releases the substrate to prepare BiP for a new chaperone cycle. A flexible N-terminal region as a release domain has also been described for the Sil1 homologs Fes1 and HspBP1 [164]. A similar function has been also described for the *E. coli* NEF GrpE [165] although the mechanism is completely different from the one observed in Bap. Although the NEFs evolved independently [109], there seems to be a conserved function in Hsp70 NEFs in the release of substrate proteins.

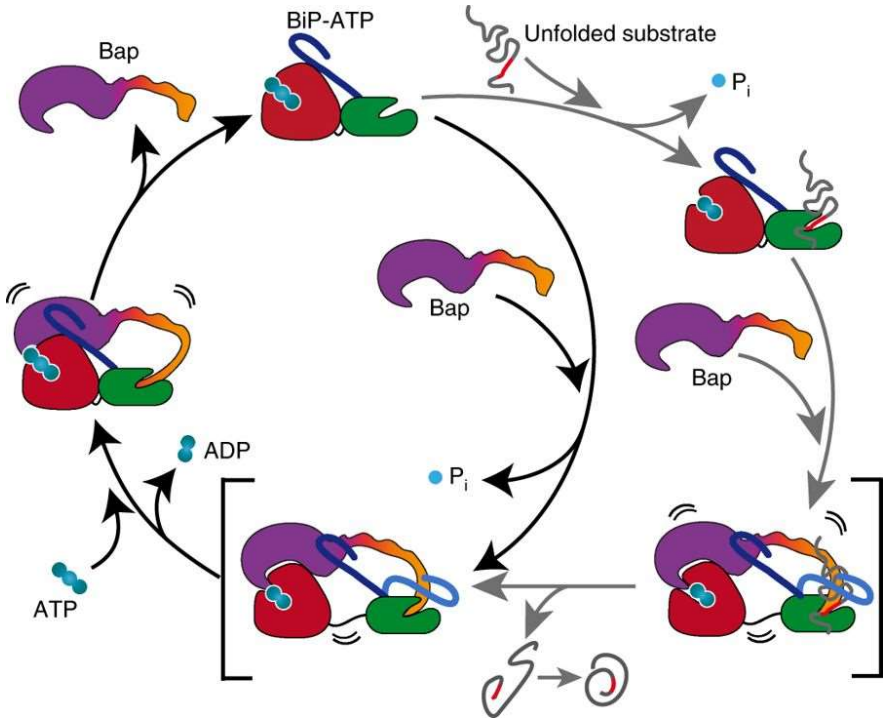

Figure 51: Model for the Bap-regulated chaperone cycle of BiP [131]**.** In BiP-ATP state, substrate is bound and ATP is hydrolyzed. Bap is also able to bind transiently to BiP in the ATP state. In the ADP conformation, Bap binds to BiP and promotes the release of substrate and ADP. Bap-N can bind as a pseudo-substrate and also affect the lid conformation.

The Bap mutants investigated in this thesis can lead to MSS. The different mutations investigated were found to have different impact on Bap and therefore the disease phenotype is probably not linked to a failure of one function of Bap, but more likely a higher order problem. It is unlikely that loss of Bap directly leads to MSS, but it has been suggested that the whole proteostasis in the ER is out of balance which leads to ER stress. Therefore the disease can better be described as a ER dysfunction in protein biosynthesis or processing [122]. This is further endorsed by the finding, that some patients with MSS do not have identifyiable mutations in Bap. However, it has also been suggested, that the common screening method for mutations in the SIL1 gene might be not able to find all mutations [166]. A distorted Hsp70 cycle might therefore lead to the symptoms linked to the MSS phenotype. Interestingly complete disruption of Bap is not lethal in mice or reduces the lifespan drastically [118,167] and not all tissues and organs are equally affected by MSS [121], although Bap is ubiquitously expressed [115]. One reason might be, that other NEFs compensate for the function of Bap. Also, it was shown that knockout of the NEF structurally different Bag2 in *C. elegans* has a huge effect on muscle functionality [168]. Interestingly the phenotype can be rescued by overexpression of a JDP. This also leads to an interesting approach in rescuing the MSS phenotype. Further investigations of MSS mutantions need to be performed for a better understanding of the disease. An interesting mutant is a double mutant investigated in a French-Canadian family [169]. The single mutation A247V or Q261H does not lead to MSS, whereas the double mutants results in a disease phenotype. These results provide a general overview on characteristics of several MSS mutations in Bap. They support the argument that MSS is a disorder of protein folding in the ER [122].

Taken together this thesis allows a better understanding of the function and interplay of BiP's co-chaperones ERdj3, Bap and Grp170 and suggest a role for Bap not only in nucleotide exchange but also in substrate release.

5. References

1. Anfinsen, C. B. The formation and stabilization of protein structure. *Biochem. J.* **128**, 737–749 (1972).
2. Anfinsen, C. B. Principles that Govern the Folding of Protein Chains. *Science* **181**, 223–230 (1973).
3. Levinthal, C. How to Fold Graciously. in (eds. Debrunnder, J. & Munck, E.) 22–24 (University of Illinois Press, 1969).
4. Dobson, C. M., Šali, A. & Karplus, M. Protein Folding: A Perspective from Theory and Experiment. *Angew. Chem. Int. Ed.* **37**, 868–893 (1998).
5. Hartl, F. U. & Hayer-Hartl, M. Converging concepts of protein folding *in vitro* and *in vivo*. *Nat. Struct. Mol. Biol.* **16**, 574–581 (2009).
6. Zimmerman, S. B. & Trach, S. O. Estimation of macromolecule concentrations and excluded volume effects for the cytoplasm of Escherichia coli. *J. Mol. Biol.* **222**, 599–620 (1991).
7. Hartl, F. U. Molecular chaperones in cellular protein folding. *Nature* **381**, 571–580 (1996).
8. Seckler, R. & Jaenicke, R. Protein folding and protein refolding. *FASEB J.* **6**, 2545–2552 (1992).
9. Walter, S. & Buchner, J. Molecular Chaperones—Cellular Machines for Protein Folding. *Angew. Chem. Int. Ed.* **41**, 1098–1113 (2002).
10. Goeckeler, J. L. & Brodsky, J. L. Molecular chaperones and substrate ubiquitination control the efficiency of endoplasmic reticulum-associated degradation. *Diabetes Obes. Metab.* **12**, 32–38 (2010).
11. Richter, K., Haslbeck, M. & Buchner, J. The Heat Shock Response: Life on the Verge of Death. *Mol. Cell* **40**, 253–266 (2010).

12. Schiene-Fischer, C., Habazettl, J., Schmid, F. X. & Fischer, G. The hsp70 chaperone DnaK is a secondary amide peptide bond *cis-trans* isomerase. *Nat. Struct. Mol. Biol.* **9**, 419–424 (2002).

13. Bocian-Ostrzycka, K. M. *et al.* Functional and evolutionary analyses of Helicobacter pylori HP0231 (DsbK) protein with strong oxidative and chaperone activity characterized by a highly diverged dimerization domain. *Front. Microbiol.* **6**, (2015).

14. Haslbeck, M., Weinkauf, S. & Buchner, J. Small heat shock proteins: Simplicity meets complexity. *J. Biol. Chem.* **294**, 2121–2132 (2019).

15. Horwich, A. L. & Fenton, W. A. Chaperonin-mediated protein folding: using a central cavity to kinetically assist polypeptide chain folding. *Q. Rev. Biophys.* **42**, 83–116 (2009).

16. Young, J. C., Agashe, V. R., Siegers, K. & Hartl, F. U. Pathways of chaperone-mediated protein folding in the cytosol. *Nat. Rev. Mol. Cell Biol.* **5**, 781–791 (2004).

17. Buck, T. M., Wright, C. M. & Brodsky, J. L. The activities and function of molecular chaperones in the endoplasmic reticulum. *Semin. Cell Dev. Biol.* **18**, 751–761 (2007).

18. Jomaa, A. *et al.* Structure of the quaternary complex between SRP, SR, and translocon bound to the translating ribosome. *Nat. Commun.* **8**, 15470 (2017).

19. Stornaiuolo, M. *et al.* KDEL and KKXX Retrieval Signals Appended to the Same Reporter Protein Determine Different Trafficking between Endoplasmic Reticulum, Intermediate Compartment, and Golgi Complex. *Mol. Biol. Cell* **14**, 889–902 (2002).

20. Hammond, C., Braakman, I. & Helenius, A. Role of N-linked oligosaccharide recognition, glucose trimming, and calnexin in glycoprotein folding and quality control. *Proc. Natl. Acad. Sci.* **91**, 913–917 (1994).

21. Benham, A. M. Endoplasmic Reticulum redox pathways: in sickness and in health. *FEBS J.* **286**, 311–321 (2019).

22. Melnyk, A., Rieger, H. & Zimmermann, R. Co-chaperones of the Mammalian Endoplasmic Reticulum. in *The Networking of Chaperones by Co-chaperones: Control of Cellular Protein Homeostasis* (eds. Blatch, G. L. & Edkins, A. L.) 179–200 (Springer International Publishing, 2015). doi:10.1007/978-3-319-11731-7_9

23. Walter, P. & Ron, D. The Unfolded Protein Response: From Stress Pathway to Homeostatic Regulation. *Science* **334**, 1081–1086 (2011).

24. Acosta-Alvear, D. *et al.* The unfolded protein response and endoplasmic reticulum protein targeting machineries converge on the stress sensor IRE1. *eLife* **7**, e43036 (2018).

25. Cox, J. S., Shamu, C. E. & Walter, P. Transcriptional induction of genes encoding endoplasmic reticulum resident proteins requires a transmembrane protein kinase. *Cell* **73**, 1197–1206 (1993).

26. Calfon, M. *et al.* IRE1 couples endoplasmic reticulum load to secretory capacity by processing the XBP-1 mRNA. *Nature* **415**, 92 (2002).

27. Shamu, C. E. & Walter, P. Oligomerization and phosphorylation of the Ire1p kinase during intracellular signaling from the endoplasmic reticulum to the nucleus. *EMBO J.* **15**, 3028–3039 (1996).

28. Shoulders, M. D. *et al.* Stress-Independent Activation of XBP1s and/or ATF6 Reveals Three Functionally Diverse ER Proteostasis Environments. *Cell Rep.* **3**, 1279–1292 (2013).

29. Amin-Wetzel, N. *et al.* A J-Protein Co-chaperone Recruits BiP to Monomerize IRE1 and Repress the Unfolded Protein Response. *Cell* **171**, 1625-1637.e13 (2017).

30. Plate, L. & Wiseman, R. L. Regulating Secretory Proteostasis Through the Unfolded Protein Response: From Function to Therapy. *Trends Cell Biol.* **27**, 722–737 (2017).

31. Credle, J. J., Finer-Moore, J. S., Papa, F. R., Stroud, R. M. & Walter, P. On the mechanism of sensing unfolded protein in the endoplasmic reticulum. *Proc. Natl. Acad. Sci.* **102**, 18773–18784 (2005).

32. Zhou, J. *et al.* The crystal structure of human IRE1 luminal domain reveals a conserved dimerization interface required for activation of the unfolded protein response. *Proc. Natl. Acad. Sci.* **103**, 14343–14348 (2006).

33. Karagöz, G. E. *et al.* An unfolded protein-induced conformational switch activates mammalian IRE1. *eLife* **6**, e30700 (2017).

34. Lemus, L. & Goder, V. Regulation of Endoplasmic Reticulum-Associated Protein Degradation (ERAD) by Ubiquitin. *Cells* **3**, 824–847 (2014).

35. Meusser, B., Hirsch, C., Jarosch, E. & Sommer, T. ERAD: the long road to destruction. *Nat. Cell Biol.* **7**, 766–772 (2005).

36. Sun, Z. & Brodsky, J. L. Guardians of the ERAD Galaxy. *Cell* **171**, 267–268 (2017).

37. Bauer, D. *et al.* A folding nucleus and minimal ATP binding domain of Hsp70 identified by single-molecule force spectroscopy. *Proc. Natl. Acad. Sci.* **115**, 4666–4671 (2018).

38. Haas, I. G. & Wabl, M. Immunoglobulin heavy chain binding protein. *Nature* **306**, 387–389 (1983).

39. Pouysségur, J., Shiu, R. P. C. & Pastan, I. Induction of two transformation-sensitive membrane polypeptides in normal fibroblasts by a block in glycoprotein synthesis or glucose deprivation. *Cell* **11**, 941–947 (1977).

40. Hamman, B. D., Hendershot, L. M. & Johnson, A. E. BiP Maintains the Permeability Barrier of the ER Membrane by Sealing the Lumenal End of the Translocon Pore before and Early in Translocation. *Cell* **92**, 747–758 (1998).

41. Schäuble, N. *et al.* BiP-mediated closing of the Sec61 channel limits Ca2+ leakage from the ER. *EMBO J.* **31**, 3282–3296 (2012).

42. Lee, K. *et al.* IRE1-mediated unconventional mRNA splicing and S2P-mediated ATF6 cleavage merge to regulate XBP1 in signaling the unfolded protein response. *Genes Dev.* **16**, 452–466 (2002).

43. Urano, F., Bertolotti, A. & Ron, D. IRE1 and efferent signaling from the endoplasmic reticulum. *J. Cell Sci.* **113**, 3697–3702 (2000).

44. Yang, J., Nune, M., Zong, Y., Zhou, L. & Liu, Q. Close and Allosteric Opening of the Polypeptide-Binding Site in a Human Hsp70 Chaperone BiP. *Structure* **23**, 2191–2203 (2015).

45. Pettersen, E. F. *et al.* UCSF Chimera—A visualization system for exploratory research and analysis. *J. Comput. Chem.* **25**, 1605–1612 (2004).

46. Šali, A. & Blundell, T. L. Comparative Protein Modelling by Satisfaction of Spatial Restraints. *J. Mol. Biol.* **234**, 779–815 (1993).

47. Carlsson, L. & Lazarides, E. ADP-ribosylation of the Mr 83,000 stress-inducible and glucose-regulated protein in avian and mammalian cells: modulation by heat shock and glucose starvation. *Proc. Natl. Acad. Sci.* **80**, 4664–4668 (1983).

48. Chambers, J. E., Petrova, K., Tomba, G., Vendruscolo, M. & Ron, D. ADP ribosylation adapts an ER chaperone response to short-term fluctuations in unfolded protein load. *J Cell Biol* **198**, 371–385 (2012).

49. Hendershot, L. M., Ting, J. & Lee, A. S. Identity of the immunoglobulin heavy-chain-binding protein with the 78,000-dalton glucose-regulated protein and the role of posttranslational modifications in its binding function. *Mol. Cell. Biol.* **8**, 4250–4256 (1988).

50. Preissler, S. *et al.* AMPylation matches BiP activity to client protein load in the endoplasmic reticulum. *eLife* e12621 (2015). doi:10.7554/eLife.12621

51. Preissler, S., Rato, C., Perera, L., Saudek, V. & Ron, D. FICD acts bi-functionally to AMPylate and de-AMPylate the endoplasmic reticulum chaperone BiP. *bioRxiv* 071332 (2016). doi:10.1101/071332

52. Preissler, S. *et al.* AMPylation targets the rate-limiting step of BiP's ATPase cycle for its functional inactivation. *eLife* **6**, e29428 (2017).

53. Freiden, P. J., Gaut, J. R. & Hendershot, L. M. Interconversion of three differentially modified and assembled forms of BiP. *EMBO J.* **11**, 63–70 (1992).

54. Gething, M.-J. Role and regulation of the ER chaperone BiP. *Semin. Cell Dev. Biol.* **10**, 465–472 (1999).

55. Flynn, G. C., Chappell, T. G. & Rothman, J. E. Peptide binding and release by proteins implicated as catalysts of protein assembly. *Science* **245**, 385–390 (1989).

56. Kassenbrock, C. K. & Kelly, R. B. Interaction of heavy chain binding protein (BiP/GRP78) with adenine nucleotides. *EMBO J.* **8**, 1461–1467 (1989).

57. Marcinowski, M. *et al.* Conformational Selection in Substrate Recognition by Hsp70 Chaperones. *J. Mol. Biol.* **425**, 466–474 (2013).

58. Macias, A. T. *et al.* Adenosine-Derived Inhibitors of 78 kDa Glucose Regulated Protein (Grp78) ATPase: Insights into Isoform Selectivity. *J. Med. Chem.* **54**, 4034–4041 (2011).

59. Wisniewska, M. *et al.* Crystal Structures of the ATPase Domains of Four Human Hsp70 Isoforms: HSPA1L/Hsp70-hom, HSPA2/Hsp70-2, HSPA6/Hsp70B', and HSPA5/BiP/GRP78. *PLOS ONE* **5**, e8625 (2010).

60. Rist, W., Graf, C., Bukau, B. & Mayer, M. P. Amide Hydrogen Exchange Reveals Conformational Changes in Hsp70 Chaperones Important for Allosteric Regulation. *J. Biol. Chem.* **281**, 16493–16501 (2006).

61. Swain, J. F. *et al.* Hsp70 Chaperone Ligands Control Domain Association via an Allosteric Mechanism Mediated by the Interdomain Linker. *Mol. Cell* **26**, 27–39 (2007).

62. Vogel, M., Mayer, M. P. & Bukau, B. Allosteric Regulation of Hsp70 Chaperones Involves a Conserved Interdomain Linker. *J. Biol. Chem.* **281**, 38705–38711 (2006).

63. Mayer, M. P. & Gierasch, L. M. Recent advances in the structural and mechanistic aspects of Hsp70 molecular chaperones. *J. Biol. Chem.* **294**, 2085–2097 (2019).

64. Mayer, M., Reinstein, J. & Buchner, J. Modulation of the ATPase Cycle of BiP by Peptides and Proteins. *J. Mol. Biol.* **330**, 137–144 (2003).

65. Wei, J. & Hendershot, L. M. Characterization of the Nucleotide Binding Properties and ATPase Activity of Recombinant Hamster BiP Purified from Bacteria. *J. Biol. Chem.* **270**, 26670–26676 (1995).

66. Flynn, G. C., Pohl, J., Flocco, M. T. & Rothman, J. E. Peptide-binding specificity of the molecular chaperone BiP. *Nature* **353**, 726 (1991).

67. Wei, J., Gaut, J. R. & Hendershot, L. M. In Vitro Dissociation of BiP-Peptide Complexes Requires a Conformational Change in BiP after ATP Binding but Does Not Require ATP Hydrolysis. *J. Biol. Chem.* **270**, 26677–26682 (1995).

68. Behnke, J., Mann, M. J., Scruggs, F.-L., Feige, M. J. & Hendershot, L. M. Members of the Hsp70 Family Recognize Distinct Types of Sequences to Execute ER Quality Control. *Mol. Cell* **63**, 739–752 (2016).

69. Blond-Elguindi, S., Fourie, A. M., Sambrook, J. F. & Gething, M. J. Peptide-dependent stimulation of the ATPase activity of the molecular chaperone BiP is the result of conversion of oligomers to active monomers. *J. Biol. Chem.* **268**, 12730–12735 (1993).

70. Knarr, G., Gething, M.-J., Modrow, S. & Buchner, J. BiP Binding Sequences in Antibodies. *J. Biol. Chem.* **270**, 27589–27594 (1995).

71. Schneider, M. *et al.* BiPPred: Combined sequence- and structure-based prediction of peptide binding to the Hsp70 chaperone BiP. *Proteins Struct. Funct. Bioinforma.* **84**, 1390–1407 (2016).

72. Rüdiger, S., Buchberger, A. & Bukau, B. Interaction of Hsp70 chaperones with substrates. *Nat. Struct. Biol.* **4**, 342 (1997).

73. Knarr, G., Modrow, S., Todd, A., Gething, M.-J. & Buchner, J. BiP-binding Sequences in HIV gp160 IMPLICATIONS FOR THE BINDING SPECIFICITY OF BiP. *J. Biol. Chem.* **274**, 29850–29857 (1999).

74. Rüdiger, S., Germeroth, L., Schneider-Mergener, J. & Bukau, B. Substrate specificity of the DnaK chaperone determined by screening cellulose-bound peptide libraries. *EMBO J.* **16**, 1501–1507 (1997).

75. Gething, M.-J. Molecular chaperones: Clasping the prize. *Curr. Biol.* **6**, 1573–1576 (1996).

76. Marcinowski, M. *et al.* Substrate discrimination of the chaperone BiP by autonomous and cochaperone-regulated conformational transitions. *Nat. Struct. Mol. Biol.* **18**, 150–158 (2011).

77. Kampinga, H. H. & Craig, E. A. The HSP70 chaperone machinery: J proteins as drivers of functional specificity. *Nat. Rev. Mol. Cell Biol.* **11**, 579–592 (2010).

78. Ajit Tamadaddi, C. & Sahi, C. J domain independent functions of J proteins. *Cell Stress Chaperones* **21**, 563–570 (2016).

79. Bies, C. *et al.* A Scj1p Homolog and Folding Catalysts Present in Dog Pancreas Microsomes. *Biol. Chem.* **380**, (1999).

80. Weitzmann, A., Baldes, C., Dudek, J. & Zimmermann, R. The heat shock protein 70 molecular chaperone network in the pancreatic endoplasmic reticulum – a quantitative approach. *FEBS J.* **274**, 5175–5187 (2007).

81. Zahedi, R. P. *et al.* Analysis of the membrane proteome of canine pancreatic rough microsomes identifies a novel Hsp40, termed ERj7. *PROTEOMICS* **9**, 3463–3473 (2009).

82. Shen, Y. & Hendershot, L. M. ERdj3, a Stress-inducible Endoplasmic Reticulum DnaJ Homologue, Serves as a CoFactor for BiP's Interactions with Unfolded Substrates. *Mol. Biol. Cell* **16**, 40–50 (2005).

83. Shen, Y., Meunier, L. & Hendershot, L. M. Identification and Characterization of a Novel Endoplasmic Reticulum (ER) DnaJ Homologue, Which Stimulates ATPase Activity of BiP in Vitro and Is Induced by ER Stress. *J. Biol. Chem.* **277**, 15947–15956 (2002).

84. Jin, Y., Awad, W., Petrova, K. & Hendershot, L. M. Regulated release of ERdj3 from unfolded proteins by BiP. *EMBO J.* **27**, 2873–2882 (2008).

85. Mapa, K. *et al.* The Conformational Dynamics of the Mitochondrial Hsp70 Chaperone. *Mol. Cell* **38**, 89–100 (2010).

86. Dejgaard, K. *et al.* Organization of the Sec61 Translocon, Studied by High Resolution Native Electrophoresis. *J. Proteome Res.* **9**, 1763–1771 (2010).

87. Schorr, S. *et al.* Co-chaperone Specificity in Gating of the Polypeptide Conducting Channel in the Membrane of the Human Endoplasmic Reticulum. *J. Biol. Chem.* **290**, 18621–18635 (2015).

88. Genereux, J. C. *et al.* Unfolded protein response-induced ERdj3 secretion links ER stress to extracellular proteostasis. *EMBO J.* **34**, 4–19 (2015).

89. Genereux, J. C. & Wiseman, R. L. Regulating extracellular proteostasis capacity through the unfolded protein response. *Prion* **9**, 10–21 (2015).

90. Otero, J. H., Lizák, B., Feige, M. J. & Hendershot, L. M. Dissection of Structural and Functional Requirements That Underlie the Interaction of ERdj3 Protein with Substrates in the Endoplasmic Reticulum. *J. Biol. Chem.* **289**, 27504–27512 (2014).

91. Nillegoda, N. B. *et al.* Crucial HSP70 co-chaperone complex unlocks metazoan protein disaggregation. *Nature* **524**, 247–251 (2015).

92. Kelley, L. A., Mezulis, S., Yates, C. M., Wass, M. N. & Sternberg, M. J. E. The Phyre2 web portal for protein modeling, prediction and analysis. *Nat. Protoc.* **10**, 845 (2015).

93. Chen, K.-C. *et al.* The endoplasmic reticulum HSP40 co-chaperone ERdj3/DNAJB11 assembles and functions as a tetramer. *EMBO J.* **36**, 2296–2309 (2017).

94. Alderson, T. R., Kim, J. H. & Markley, J. L. Dynamical Structures of Hsp70 and Hsp70-Hsp40 Complexes. *Structure* **24**, 1014–1030 (2016).

95. Ang, D. & Georgopoulos, C. The heat-shock-regulated grpE gene of Escherichia coli is required for bacterial growth at all temperatures but is dispensable in certain mutant backgrounds. *J. Bacteriol.* **171**, 2748–2755 (1989).

96. Melero, R. *et al.* Modulation of the Chaperone DnaK Allosterism by the Nucleotide Exchange Factor GrpE. *J. Biol. Chem.* **290**, 10083–10092 (2015).

97. Höhfeld, J. & Jentsch, S. GrpE-like regulation of the Hsc70 chaperone by the anti-apoptotic protein BAG-1. *EMBO J.* **16**, 6209–6216 (1997).

98. Takayama, S. & Reed, J. C. Molecular chaperone targeting and regulation by BAG family proteins. *Nat. Cell Biol.* **3**, E237–E241 (2001).

99. Takayama, S., Xie, Z. & Reed, J. C. An Evolutionarily Conserved Family of Hsp70/Hsc70 Molecular Chaperone Regulators. *J. Biol. Chem.* **274**, 781–786 (1999).

100. Behnke, J., Feige, M. J. & Hendershot, L. M. BiP and Its Nucleotide Exchange Factors Grp170 and Sil1: Mechanisms of Action and Biological Functions. *J. Mol. Biol.* **427**, 1589–1608 (2015).

101. Tyson, J. R. & Stirling, C. J. LHS1 and SIL1 provide a lumenal function that is essential for protein translocation into the endoplasmic reticulum. *EMBO J.* **19**, 6440–6452 (2000).

102. Andréasson, C., Rampelt, H., Fiaux, J., Druffel-Augustin, S. & Bukau, B. The Endoplasmic Reticulum Grp170 Acts as a Nucleotide Exchange Factor of Hsp70 via a Mechanism Similar to That of the Cytosolic Hsp110. *J. Biol. Chem.* **285**, 12445–12453 (2010).

103. Liu, Q. & Hendrickson, W. A. Insights into Hsp70 Chaperone Activity from a Crystal Structure of the Yeast Hsp110 Sse1. *Cell* **131**, 106–120 (2007).

104. Polier, S., Dragovic, Z., Hartl, F. U. & Bracher, A. Structural Basis for the Cooperation of Hsp70 and Hsp110 Chaperones in Protein Folding. *Cell* **133**, 1068–1079 (2008).

105. Schuermann, J. P. *et al.* Structure of the Hsp110:Hsc70 Nucleotide Exchange Machine. *Mol. Cell* **31**, 232–243 (2008).

106. Hale, S. J., Lovell, S. C., Keyzer, J. de & Stirling, C. J. Interactions between Kar2p and Its Nucleotide Exchange Factors Sil1p and Lhs1p Are Mechanistically Distinct. *J. Biol. Chem.* **285**, 21600–21606 (2010).

107. Chen, X. *et al.* The 170 kDa glucose regulated stress protein is a large HSP70- HSP110-like protein of the endoplasmic reticulum. *FEBS Lett.* **380**, 68–72 (1996).

108. Easton, D. P., Kaneko, Y. & Subjeck, J. R. The Hsp110 and Grp170 stress proteins: newly recognized relatives of the Hsp70s. *Cell Stress Chaperones* **5**, 276 (2000).

109. Bracher, A. & Verghese, J. The nucleotide exchange factors of Hsp70 molecular chaperones. *Front. Mol. Biosci.* **2**, (2015).

110. Dierks, T. *et al.* A microsomal ATP-binding protein involved in efficient protein transport into the mammalian endoplasmic reticulum. *EMBO J.* **15**, 6931–6942 (1996).

111. Behnke, J. & Hendershot, L. M. The Large Hsp70 Grp170 Binds to Unfolded Protein Substrates in Vivo with a Regulation Distinct from Conventional Hsp70s. *J. Biol. Chem.* **289**, 2899–2907 (2014).

112. Park, J. *et al.* The Chaperoning Properties of Mouse Grp170, a Member of the Third Family of Hsp70 Related Proteins†. *Biochemistry* **42**, 14893–14902 (2003).

113. Spee, P., Subjeck, J. & Neefjes, J. Identification of Novel Peptide Binding Proteins in the Endoplasmic Reticulum: ERp72, Calnexin, and grp170. *Biochemistry* **38**, 10559–10566 (1999).

114. Yan, M., Li, J. & Sha, B. Structural analysis of the Sil1–Bip complex reveals the mechanism for Sil1 to function as a nucleotide-exchange factor. *Biochem. J.* **438**, 447–455 (2011).

115. Chung, K. T., Shen, Y. & Hendershot, L. M. BAP, a Mammalian BiP-associated Protein, Is a Nucleotide Exchange Factor That Regulates the ATPase Activity of BiP. *J. Biol. Chem.* **277**, 47557–47563 (2002).

116. Shomura, Y. *et al.* Regulation of Hsp70 Function by HspBP1: Structural Analysis Reveals an Alternate Mechanism for Hsp70 Nucleotide Exchange. *Mol. Cell* **17**, 367–379 (2005).

117. Howes, J., Shimizu, Y., Feige, M. J. & Hendershot, L. M. C-terminal Mutations Destabilize SIL1/BAP and Can Cause Marinesco-Sjögren Syndrome. *J. Biol. Chem.* **287**, 8552–8560 (2012).

118. Anttonen, A.-K. *et al.* The gene disrupted in Marinesco-Sjögren syndrome encodes SIL1, an HSPA5 cochaperone. *Nat. Genet.* **37**, 1309–1311 (2005).

119. Marinesco, G. Novelle maladie familiale caracterisee pare une cataracte congenitale et un arret du development somato-neurophysique. *Encephale* **26**, 97–109 (1931).

120. Sjogren, T. Hereditary congenital spinocerebellar ataxia accompanied by congenital cataract and oligophrenia; a genetic and clinical investigation. *Confin. Neurol.* **10**, 293–308 (1950).

121. Krieger, M. *et al.* SIL1 mutations and clinical spectrum in patients with Marinesco-Sjögren syndrome. *Brain* **136**, 3634–3644 (2013).

122. Senderek, J. *et al.* Mutations in SIL1 cause Marinesco-Sjögren syndrome, a cerebellar ataxia with cataract and myopathy. *Nat. Genet.* **37**, 1312–1314 (2005).

123. Rosam, M. Substrate recognition and regulation of conformations of the molecular chaperone BiP. (Technische Universität, 2015).

124. Laemmli, U. K. Cleavage of structural proteins during the assembly of the head of bacteriophage T4. *Nature* **227**, 680–685 (1970).

125. Hochmair, J. Investigation of the molecular chaperone BiP and its co-factors. (Technische Universität, 2017).

126. Ellman, G. L. A colorimetric method for determining low concentrations of mercaptans. *Arch. Biochem. Biophys.* **74**, 443–450 (1958).

127. Ellman, G. L. Tissue sulfhydryl groups. *Arch. Biochem. Biophys.* **82**, 70–77 (1959).

128. Kelly, S. M., Jess, T. J. & Price, N. C. How to study proteins by circular dichroism. *Biochim. Biophys. Acta BBA - Proteins Proteomics* **1751**, 119–139 (2005).

129. Schuck, P. Size-distribution analysis of macromolecules by sedimentation velocity ultracentrifugation and lamm equation modeling. *Biophys. J.* **78**, 1606–1619 (2000).

130. Schuck, P. Sedimentation analysis of noninteracting and self-associating solutes using numerical solutions to the Lamm equation. *Biophys. J.* **75**, 1503–1512 (1998).

131. Rosam, M. *et al.* Bap (Sil1) regulates the molecular chaperone BiP by coupling release of nucleotide and substrate. *Nat. Struct. Mol. Biol.* **25**, 90–100 (2018).

132. Nørby, J. G. Coupled assay of Na+,K+-ATPase activity. *Methods Enzymol.* **156**, 116–119 (1988).

133. Jin, Y., Zhuang, M. & Hendershot, L. M. ERdj3, a Luminal ER DnaJ Homologue, Binds Directly to Unfolded Proteins in the Mammalian ER: Identification of Critical Residues. *Biochemistry* **48**, 41–49 (2009).

134. Marcus, N. Y., Marcus, R. A., Schmidt, B. Z. & Haslam, D. B. Contribution of the HEDJ/ERdj3 cysteine-rich domain to substrate interactions. *Arch. Biochem. Biophys.* **468**, 147–158 (2007).

135. Marcinowski, M. D. Functional conformations of the molecular chaperone BiP. (Technische Universität, 2011).

136. Lobstein, J. *et al.* SHuffle, a novel Escherichia coli protein expression strain capable of correctly folding disulfide bonded proteins in its cytoplasm. *Microb. Cell Factories* **11**, 56 (2012).

137. Andrade, M. A., Chacón, P., Merelo, J. J. & Morán, F. Evaluation of secondary structure of proteins from UV circular dichroism spectra using an unsupervised learning neural network. *Protein Eng.* **6**, 383–390 (1993).

138. Whitmore, L. & Wallace, B. A. Protein secondary structure analyses from circular dichroism spectroscopy: Methods and reference databases. *Biopolymers* **89**, 392–400 (2008).

139. Whitmore, L. & Wallace, B. A. DICHROWEB, an online server for protein secondary structure analyses from circular dichroism spectroscopic data. *Nucleic Acids Res.* **32**, W668–W673 (2004).

140. Qi, R. *et al.* Allosteric opening of the polypeptide-binding site when an Hsp70 binds ATP. *Nat. Struct. Mol. Biol.* **20**, 900–907 (2013).

141. Preissler, S. *et al.* Physiological modulation of BiP activity by trans-protomer engagement of the interdomain linker. *eLife* **4**, e08961 (2015).

142. Barends, T. R. M. *et al.* Combining crystallography and EPR: crystal and solution structures of the multidomain cochaperone DnaJ. *Acta Crystallogr. D Biol. Crystallogr.* **69**, 1540–1552 (2013).

143. Hu, J. *et al.* The crystal structure of the putative peptide-binding fragment from the human Hsp40 protein Hdj1. *BMC Struct. Biol.* **8**, 3 (2008).

144. Adams, C. J., Kopp, M. C., Larburu, N., Nowak, P. R. & Ali, M. M. U. Structure and Molecular Mechanism of ER Stress Signaling by the Unfolded Protein Response Signal Activator IRE1. *Front. Mol. Biosci.* **6**, (2019).

145. Mayer, M. P. & Bukau, B. Hsp70 chaperones: Cellular functions and molecular mechanism. *Cell. Mol. Life Sci.* **62**, 670 (2005).

146. Prilusky, J. *et al.* FoldIndex©: a simple tool to predict whether a given protein sequence is intrinsically unfolded. *Bioinformatics* **21**, 3435–3438 (2005).

147. Mészáros, B., Erdős, G. & Dosztányi, Z. IUPred2A: context-dependent prediction of protein disorder as a function of redox state and protein binding. *Nucleic Acids Res.* **46**, W329–W337 (2018).

148. Buchan, D. W. A., Minneci, F., Nugent, T. C. O., Bryson, K. & Jones, D. T. Scalable web services for the PSIPRED Protein Analysis Workbench. *Nucleic Acids Res.* **41**, W349–W357 (2013).

149. Jones, D. T. Protein secondary structure prediction based on position-specific scoring matrices11Edited by G. Von Heijne. *J. Mol. Biol.* **292**, 195–202 (1999).

150. Karim, M. A. *et al.* A novel mutation in BAP/SIL1 gene causes Marinesco–Sjögren syndrome in an extended pedigree. *Clin. Genet.* **70**, 420–423 (2006).

151. Gilg, V. Investigation of Bap mutants associated with the Marinesco-Sjögren syndrom. (Technische Universität, 2019).

152. Chevalier, M. *et al.* Substrate Binding Induces Depolymerization of the C-terminal Peptide Binding Domain of Murine GRP78/BiP. *J. Biol. Chem.* **273**, 26827–26835 (1998).

153. Riazuddin, S. A. *et al.* Novel SIL1 mutations in consanguineous Pakistani families mapping to chromosomes 5q31. (2009). Available at: http://www.molvis.org/molvis/v15/a111/. (Accessed: 15th March 2019)

154. Weikl, T., Abelmann, K. & Buchner, J. An unstructured C-terminal region of the hsp90 co-chaperone p23 is important for its chaperone function11Edited by R. Huber. *J. Mol. Biol.* **293**, 685–691 (1999).

155. Tokunaga, M., Kato, S., Kawamura-Watabe, A., Tanaka, R. & Tokunaga, H. Characterization of deletion mutations in the carboxy-terminal peptide-binding domain of the Kar2 protein in Saccharomyces cerevisiae. *Yeast* **14**, 1285–1295 (1998).

156. Deng, J. *et al.* Neurons Export Extracellular Vesicles Enriched in Cysteine String Protein and Misfolded Protein Cargo. *Sci. Rep.* **7**, 956 (2017).

157. Pobre, K. F. R., Poet, G. J. & Hendershot, L. M. The endoplasmic reticulum (ER) chaperone BiP is a master regulator of ER functions: Getting by with a little help from ERdj friends. *J. Biol. Chem.* **294**, 2098–2108 (2019).

158. Karras, G. I. *et al.* HSP90 Shapes the Consequences of Human Genetic Variation. *Cell* **168**, 856-866.e12 (2017).

159. Raynal, B., Lenormand, P., Baron, B., Hoos, S. & England, P. Quality assessment and optimization of purified protein samples: why and how? *Microb. Cell Factories* **13**, 180 (2014).

160. Gamer, J., Bujard, H. & Bukau, B. Physical interaction between heat shock proteins DnaK, DnaJ, and GrpE and the bacterial heat shock transcription factor σ32. *Cell* **69**, 833–842 (1992).

161. Hellebust, H., Uhlén, M. & Enfors, S. O. Interaction between heat shock protein DnaK and recombinant staphylococcal protein A. *J. Bacteriol.* **172**, 5030–5034 (1990).

162. Nishikawa, S., Brodsky, J. L. & Nakatsukasa, K. Roles of Molecular Chaperones in Endoplasmic Reticulum (ER) Quality Control and ER-Associated Degradation (ERAD). *J. Biochem. (Tokyo)* **137**, 551–555 (2005).

163. Hendrick, J. P., Langer, T., Davis, T. A., Hartl, F. U. & Wiedmann, M. Control of folding and membrane translocation by binding of the chaperone DnaJ to nascent polypeptides. *Proc. Natl. Acad. Sci. U. S. A.* **90**, 10216–10220 (1993).

164. Gowda, N. K. C. *et al.* Nucleotide exchange factors Fes1 and HspBP1 mimic substrate to release misfolded proteins from Hsp70. *Nat. Struct. Mol. Biol.* **25**, 83–89 (2018).

165. Brehmer, D., Gässler, C., Rist, W., Mayer, M. P. & Bukau, B. Influence of GrpE on DnaK-Substrate Interactions. *J. Biol. Chem.* **279**, 27957–27964 (2004).

166. Takahata, T. *et al.* Novel mutations in the *SIL1* gene in a Japanese pedigree with the Marinesco–Sjögren syndrome. *J. Hum. Genet.* **55**, 142–146 (2010).

167. Zhao, L., Longo-Guess, C., Harris, B. S., Lee, J.-W. & Ackerman, S. L. Protein accumulation and neurodegeneration in the woozy mutant mouse is caused by disruption of SIL1, a cochaperone of BiP. *Nat. Genet.* **37**, 974–979 (2005).

168. Papsdorf, K., Sacherl, J. & Richter, K. The Balanced Regulation of Hsc70 by DNJ-13 and UNC-23 Is Required for Muscle Functionality. *J. Biol. Chem.* **289**, 25250–25261 (2014).

169. Noreau, A. *et al.* Novel SIL1 mutations cause cerebellar ataxia and atrophy in a French-Canadian family. *neurogenetics* **16**, 315–318 (2015).

Danksagung

Ich danke meinem Doktorvater Johannes Buchner für die Bereitstellung meines Themas und den Mitteln um hier meine Doktorarbeit zu machen. Ich danke Ihm für den fachlichen Austausch und die Unterstützung, die ich jederzeit während meiner Arbeit erfahren habe. Ich danke der Studienstiftung des deutschen Volkes für die finanzielle und ideelle Unterstützung.

Ich danke Margot Rubinstein, die mir oft eine große Hilfe im Formularchaos war. Ich möchte mich bei Natalia Sarmiento und Mathias Rosam bedanken, die mir thematisch und praktisch viel beigebracht haben. Vielen Dank an Marina, Katrin und Christine, Patzi, Priyanka und Bine sowie Mareike, Moritz und Pamina. Ohne euch hätte ich es hier bestimmt nicht geschafft – zumindest wäre es aber nicht so lustig gewesen. Ein Dank gilt Philipp und Pamina für die AUC Messungen und die Hilfe bei Computerproblemen. Ein spezieller Dank gilt auch an Benedikt Weber, für Kaffee, Hilfe, Bier und Lachen. Ich danke dem ganzen aktuellen und ehemaligen Lehrstuhl Biotechnologie, auch dafür, dass ihr mich so gut unterstützt habt und mir oft geholfen habt. Thank you Frank for having a look at my thesis! Danke auch an die Arbeitsgruppe von Don Lamb, speziell an Daniela und Ganesh. Ich danke Inga und Lisi für die schöne Zeit in München.

Ein großer Dank gilt meinen vielen Praktikanten die ich während meiner Zeit am Lehrstuhl betreut habe. Ihr habt mir oft einen neuen Blickwinkel auf mein Thema ermöglicht. Speziell möchte ich mich noch bei meinen Masterstudenten bedanken. Janine, du hast mit deiner lustigen und positiven Art für tolle Stimmung gesorgt und mich vor allem während der Schwangerschaft bei meiner Arbeit extrem unterstützt. Vanessa, dir danke ich vor allem für die Unterstützung nach meiner Elternzeit und dass du das MSS Thema endlich etwas vorangebracht hast.

Ich danke meinem Sohn Jonas, der mir immer wieder zeigt, was eigentlich wichtig ist. Ich danke meinen Eltern für wirklich alles. Zuletzt möchte ich meinem Mann Jens danken. Du hast mich immer unterstützt und bei vielen Fragen geholfen und oft den Frust abbekommen. Danke, dass du immer zu mir gehalten hast.

Eidesstattliche Erklärung

Hiermit erkläre ich, Christina Utta Nickels, an Eides statt, dass ich die vorliegende Arbeit selbstständig verfasst und keine anderen als die angegebenen Quellen und Hilfsmittel verwendet habe. Aus fremden Quellen übernommene Gedanken sind als solche kenntlich gemacht. Die vorliegende Arbeit wurde noch keiner anderen Prüfungsbehörde vorgelegt. Teile dieser Arbeit werden in einem wissenschaftlichen Journal veröffentlicht.

Hereby I, Christina Utta Nickels, declare that this thesis was prepared by me using only references and resources stated here. The work has not been submitted to any audit commission. Parts of this work will be published in scientific journals.

_____

Datum, Christina Utta Nickels

Liste der Vorveröffentlichungen

Bap (Sil1) regulates the molecular chaperone BiP by coupling release of nucleotide and substrate

DOI: 10.1038/s41594-017-0012-6

Nature Structural & Molecular Biology; volume 25, pages 90–100 (2018